SYNTHESIS AND MICROSCOPY STUDIES OF CARBON NANOSHEETS BY PYROLYSIS OF PHTHALAZINIUM BETAINES

by

BARIŞ GÜZEL

THESIS SUBMITTED TO

THE GRADUATE SCHOOL OF NATURAL AND APPLIED SCIENCES

OF

THE ABANT IZZET BAYSAL UNIVERSITY

IN PARTIAL FULLFILLMENT OF THE REQUIREMENTS

FOR THE DEGREE OF MASTER OF SCIENCE

IN THE DEPARTMENT OF CHEMISTRY

JUNE 2014

Approval of the Graduate School of Natural and Applied Sciences.

Prof. Dr. Yaşar DÜRÜST

Director

I certify that this thesis satisfies all the requirements as a thesis for the degree of Master of Science.

Prof. Dr. Nedime DÜRÜST

Head of Department

This is to certify that we have read this thesis and that in our opinion it is fully adequate, in scope and quality, as a thesis for the degree of Master of Science

Prof. Dr. Nihat ÇELEBİ

Supervisor

Examining Committee Members

1- Prof. Dr. Nihat ÇELEBİ .....

2- Prof. Dr. Özdemir ÖZARSLAN .....

3- Asst. Prof. Dr. Gürcan YILDIRIM .....

ABSTRACT

SYNTHESIS AND MICROSCOPY STUDIES OF CARBON NANOSHEETS BY PYROLYSIS OF PHTHALAZINIUM BETAINES

GÜZEL, Barış

M.Sc. , Department of Chemistry

Supervisor : Prof.Dr. Nihat ÇELEBİ

JUNE 2014, 97 pages

In the first part of this study, the phenylphthalazinium betaine, azomethine imine, that had been synthesized previously by Katritzky[4] was synthesized. The synthesis of azomethine imine was achived by starting with phthalic anhydride and phenylhydrazine and proceeding in four foregoing steps. In particular steps of azomethine imine (betaine) synthesis reaction, products were separated purely from the reaction mixture by recrystallization technique using ethanol as the solvent and purification of them was controlled by preparative thin layer chromatography. The structure of this organic compound was characterized using FT/IR spectroscopy and some physical characteristics such as melting point determination, the retardation factor (R_f) value.

In the second part of this work, the studies of the synthesis of carbon nanosheets, which are the new in the literature by solid-state air pyrolysis of betaine at four different temperatures and by pyrolysis of betaine in nitrogen gas atmosphere at 350 °C were described. On the basis of the most recent literature survey, the synthesis and characterization of carbon nanosheets from this betaine have been performed. In the characterization of carbon nanoheets, FT/IR Spectroscopy for characteristic bond analysis, X-Ray Diffractometer for structural analysis and Scanning Electron Microscopy for the surface morphology were used.

Keywords: Betaine, azomethine imine, nanotechnology, nanochemistry, carbon materials, carbon based nanomaterials, carbon nanosheets and pyrolysis.

ÖZET

KARBON NANOPLAKALARIN FITALAZİNYUM BETAİNLERİN PİROLİZİ İLE SENTEZLENMESİ VE MİKROSKOPİK ÇALIŞMALARI

GÜZEL, Barış

Yüksek Lisans Tezi, Kimya Bölümü

Tez Danışma : Prof.Dr. Nihat ÇELEBİ

Haziran 2014, 97 sayfa

Bu çalışmanın ilk bölümünde, literatürde Katritzky[4] tarafından daha önce sentezlenmiş olan "fenilfıtalazinyum betain"in, azometin imin'in sentezi gerçekleştirilmiştir. Bu azometin imin dört aşamada ftalik anhidrit ve fenilhidrazin ile başlanarak elde edilmektedir. Azometin imin (betain) sentezinin bazı aşamalarında, ürünlerin tepkime karışımından çözücü olarak etanol kullanarak yeniden kristallendirme tekniği ile saf olarak ayrılmaları sağlandı ve saflıkları preparatif ince tabaka kromatografisi ile kontrol edildi. Bu organik bileşiğin yapısı FT/IR spektroskopisi ve erime noktası belirleme işlemi, R_f değeri gibi bazı fiziksel özellikleri kullanılarak belirlendi.

Bu çalışmanın ikinci bölümünde, literatürde yeni olarak, betain'den hava pirolizi ile dört farklı sıcaklıkta ve azot gazı atmosferindeki pirolizi ile sadece 350°C'de elde edilen karbon nanoplakaların sentezinin çalışmaları tanımlanmaktadır. En son literatür çalışmaları baz alınarak bu betainden karbon nanosheets sentezleri ve

karakterizasyonları gerçekleştirilmiştir. Karbon nanoplakaların karakterizasyonunda, karakteristik bağ analizi için FT/IR spektroskopisi, yapısal analiz için X-Ray Difraktometresi ve yüzey morfolojisi için Taramalı Elektron Mikroskopisi kullanılmıştır.

Anahtar Kelimeler: Betain, azometin imin, nanoteknoloji, nanokimya, karbon materyaller, karbon temelli nanomateryaller, karbon nanoplakar ve piroliz.

TO MY PARENTS

ACKNOWLEDGEMENTS

I would like to express my deep gratitude to my supervisor, Prof. Dr. Nihat ÇELEBİ for his understanding, his guidance and encouragements at every stage of this study and writing up. He took his time to educate and instruct me with all his efforts and for that I will always be grateful. He always encouraged me to put my very best into the scientific research. It has been a great concession and pleasure to work for him. I gained very valuable experience from himself.

I would like to express my special thanks to Asst. Prof. Dr. Gürcan YILDIRIM and Asst. Prof. Dr. Erhan BUDAK for their endless guidance, advice, criticism, encouragements and insight especially throughout evaluation of X-Ray and SEM analysis for the synthesis of carbon nanosheet part.

I am grateful to the Administration of Chemistry Department of A.İ.B.U. and for providing me the necessary opportunities and chemicals for the completion of my research topic.

I would like to thank to Dr. Asaf Tolga ÜLGEN for his helps throughout my research and, of course, Glass Technician Metin ALKAN for their support whenever and whatever I need about glass equipments. Also, I would like to special thank to my friend Elif YILDIZ for always with me and she felt me strong support and advice.

I would like to thank to Dr.Seda TANYILDIZI for the TGA/DTA analysis of the compound and she showed me all the time strong support and encouragement.

My most heartfelt thanks and words of gratitude are reserved Dr. Nevin SOYLU for the XRD analysis and especially SEM analysis. We have spent countless hours talking about science, good and bad, applicable and not in SEM analysis times. I would like to express to thank to herself for endless patience and support.

Now, Dear my family, it is not possible to explain with the words your place in my life. However, I would like to say a few special thing about this research time for my family. My sincere appreciation and gratitude are devoted to my family especially for their endless patience, encouragement, support, and love whenever I needed throughout this research.

Consequently, I have met so many fantastic people in my university, A.I.B.U, and I will always look back on my time with fondness. I cannot forget you and I will remember all the time wonderful. Thank you to A.I.B.U and BOLU, I love you so much.

TABLE OF CONTENTS

FORMULAE

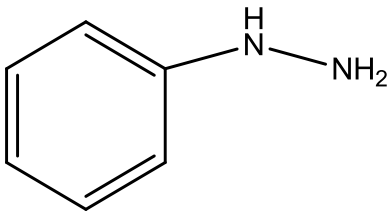

(1a)

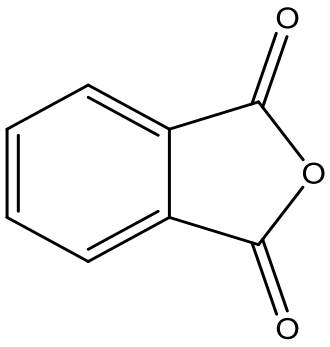

(1b)

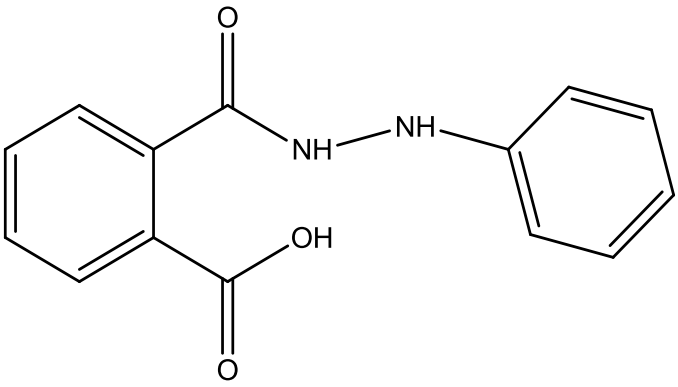

(1c)

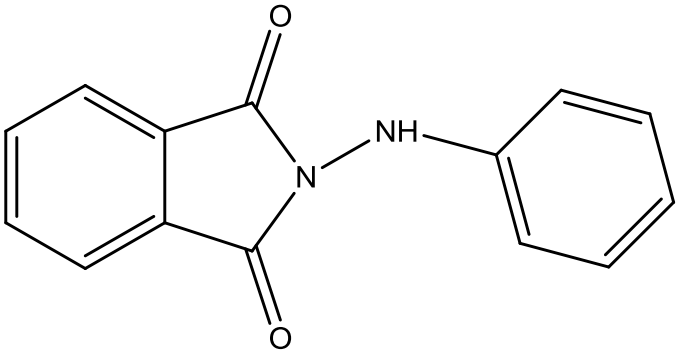

(1d)

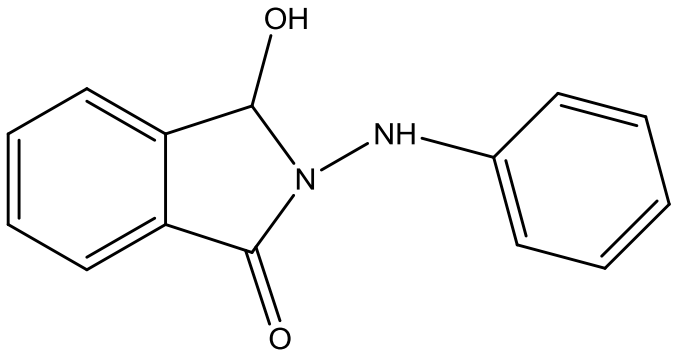

(1e)

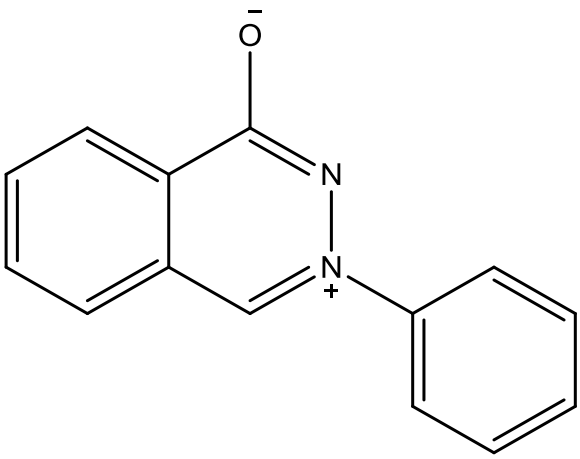

(1f)

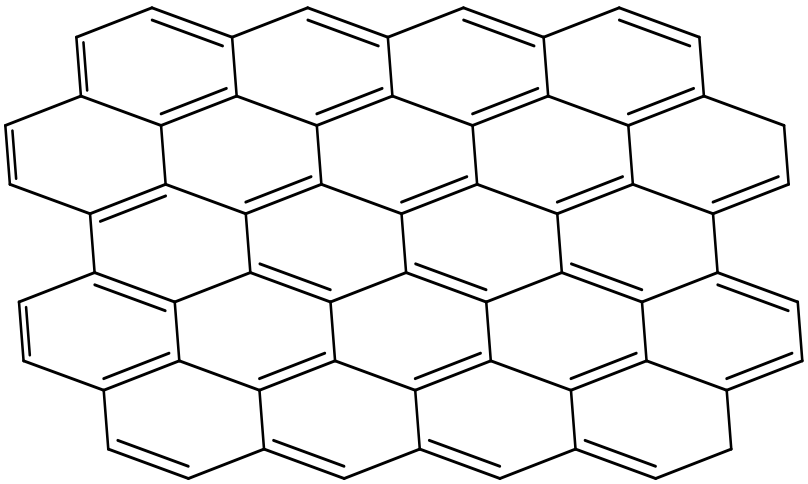

(1g)

LIST OF TABLES

LIST OF FIGURES

LIST OF SCHEMES

LIST OF SYMBOLS AND ABBREVIATIONS

Δ	Heat
DC	Dipolar Cycloaddition
Å	Angström
0-D	Zero Dimensional
1-D	One Dimensional
2-D	Two Dimensional
3-D	Three Dimensional
***a*-C**	Amorphous Carbon
DLC	Diamond-Like Carbon
GLC	Glass-Like Carbon
IUPAC	International Union of Pure and Applied Chemistry
CVD	Chemical Vapor Deposition
CBNs	Carbon based nanomaterials
CNTs	Carbon Nanotubes
SWCNTs	Single-Walled Carbon Nanotubes
MWCNTs	Multi-Walled Carbon Nanotubes
FLG	Few-Layer Graphene
CNSs	Carbon Nanosheets
SEM	Scanning Electron Microscopy

RF-PECVD	RF plasma enhanced chemical vapour deposition
Rs	Sheet Resistance
FT/IR	Fourier Transform Infrared
TLC	Thin Layer Chromatography
EDS	Energy Dispersive X-Ray Spectrometer
TGA	Thermal Gravimetric Analysis
XRD	X-Ray Diffraction
MB	Mesomeric Betaine
IR	Infra Red
GO	Graphene Oxide
NMR	Nuclear Magnetic Resonance

1. INTRODUCTION

1. 1. CHAPTER I

This chapter covers the general aspects of organic compounds that we used for synthesis of nanosheets.

Genarally organic synthesis is a way of obtaining somewhat complex organic compounds from simple starting compounds by a series of chemical reactions. In nature, of course, the compounds synthesized by this way are called natural products [1].

The synthesis of organic molecules is the most important part of the organic chemistry. The total synthesis and methodology are two main areas of research in the field of organic synthesis. A total synthesis is the complete chemical synthesis of complex organic molecules from simple, commercially available or natural precursors. Methodology usually includes the following stages; firstly discovery of a new way on the knowledge of the known ways, secondly optimization of the works handled and thirdly the study of scope and limitations. All of these stages require a cumulative experience on the corresponding areas [1].

1. 1. 1. Betaines

Betaines are zwitterion type compounds having positive and negative charges on the corresponding heteroatoms. Betaines can also be treated as 1,3-dipoles depending on the sequences of the heteroatoms. For example, 2-phenylphthalazin-2-

ium-4-olates or phenylphthalazinium betaines fall into that kind of compounds. They also undergo 1,3-dipolar cycloaddition reactions[2,3] as having 4π moiety. On the other hand, if the opposite charges developed on both heteroatom and carbon atoms then the species are called as ylides. Some examples of them can be seen on the following scheme:

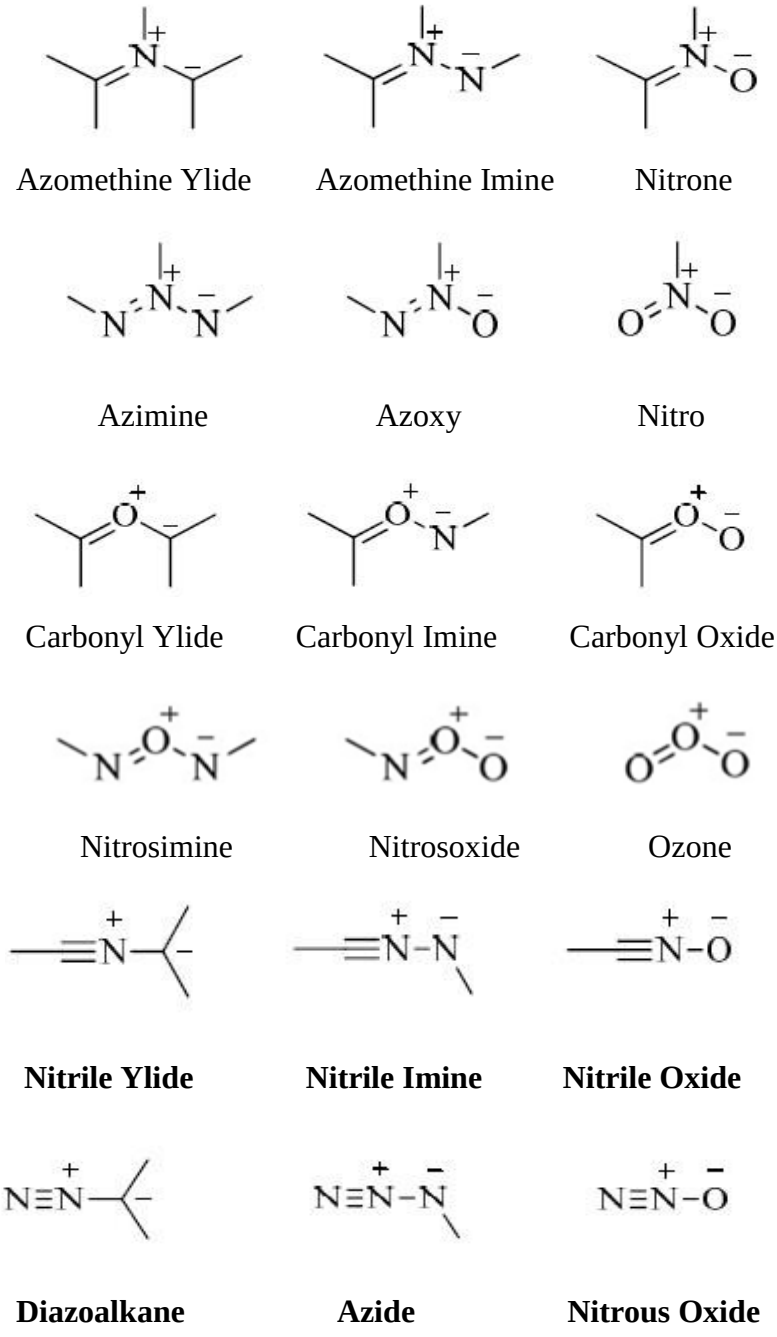

Scheme 1.1. Some 1,3-dipoles appearing as either betaines or ylides.

1. 1. 2. Azomethine Imines

The compounds containing C=N double bond obtained in reactions of aldehydes and ketones with amines are referred to as Schiff bases, imines, or azomethines. Azomethine imines are 1,3-dipoles without a double bond but with internal octet stabilization [2].

Phenylphthalazinium betaines were worked previously by Katritzky A.R. and his coworkers[4] are azomethine imine type compounds that they classified generally betaines.

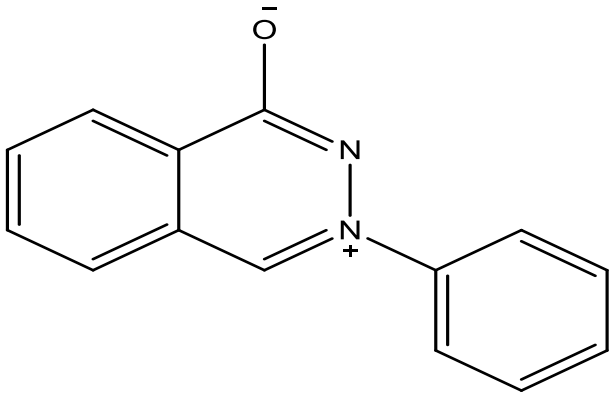

Scheme 1.2. Phenylphthalazinium betaine (2-phenylphthalazin-2-ium-4-olate)**.**

Although phenylphthalazinium betaines and their derivatives were explicitly and largely studied in detail [4] there couldn't be found any nanosheet preparation studies, such as pyrolysis works.

Further informations were handled in the experimental part.

1. 2. CHAPTER II

It was not so long ago in the world of molecules and materials that 1 nm (1 nm = 10 Å) was considered large in chemistry while 1μm (1μm = 1000 nm =10000 Å) was considered small in engineering physics. Matter residing in the ‘’fuzzy interface’’ between these large and small extremes of length scales emerged as the science nanoscale materials and has grown into one of the most exciting and vibrant fields of endeavor, showing all the signs of having a revolutionary impact on materials as we know them today. Nanomaterials characteristically exhibit physical and chemical properties different from the bulk as a consequence of having at least one spatial dimension in the size range of 1-1000 nm [5].

It is the synthesis, manipulation and imaging of materials having nanoscale dimensions, the study of exploitation of the differences between bulk and nanoscale materials, and understanding and utilization of nanomaterials scaling laws by interdisciplinary scientists, which drive contemporary endeavors in nanoscience and nanotechnology. The field of nanotechnology is related to the length scale of a nanometer, with one nanometer being defined as a meter being divided into one billion equally spaced divisions ($1x10^{-9}$ m). Although it is impossible to imagine how small a nanometer is, one can kind of approximate this length scale as being approximately equal to 1/75,000 of the thickness of a human hair [5].

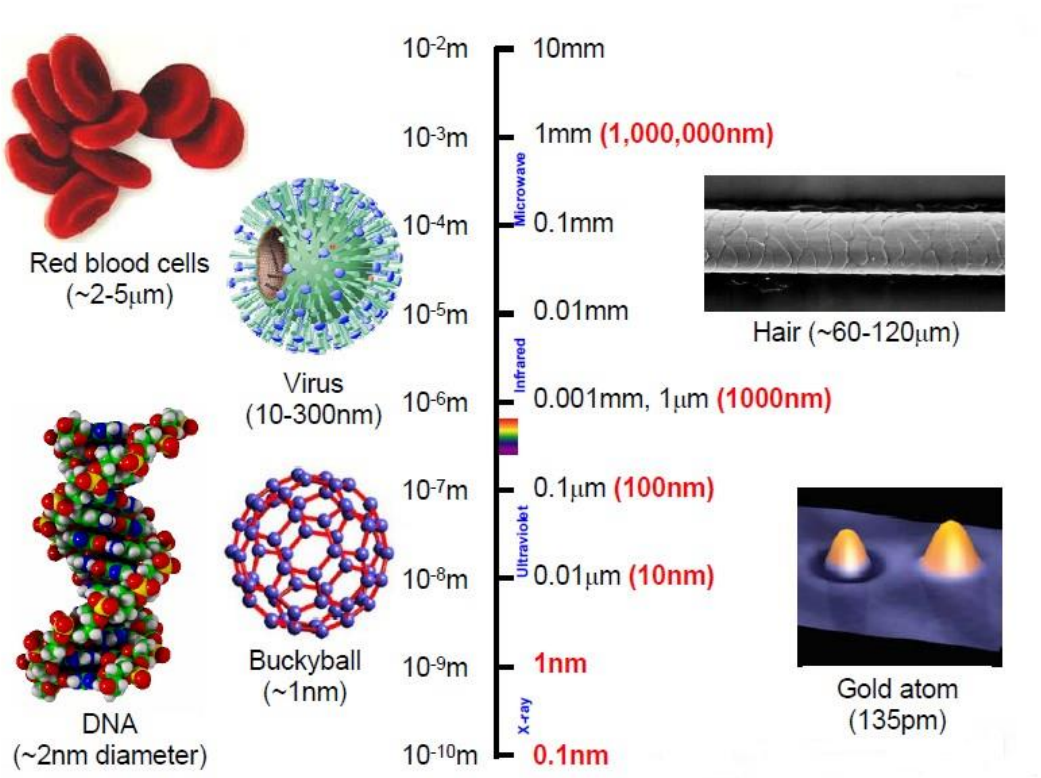

Figure 1.1. The Examples of Some Nanoscale Substances

1. 2. 1. Nanotechnology and Nanochemistry

The term nanotechnology was created to represent the multidisciplinary field of science where nanoscale particles and devices with interesting properties are created by scaling functional materials down to the nanometer size scale. These particles and devices are considered nanoscale materials when the length, width, and thickness of the material are on the size scale of a few 10's of nanometers up to approximately 100 nm [6]. It introduces nanometer-scale (nanoscale) synthesis and nanometer-scale materials, functional devices, switches and sensor arrays. These chemical topics form the discipline of nanochemistry, a sub-field closely related to nanotechnology [7].

The defining feature of nanochemistry is the utilization of synthetic chemistry to make nanoscale building blocks of different size and shape, composition and surface structure, charge and functionality. These building blocks may be useful in their own right or in a self-assembly construction process, spontaneous, directed by templates or guided by chemically or lithographically defined surface patterns, they may form architectures that perform an intelligent function and portend a particular use. When thinking about self-assembly of a targeted structure from the spontaneous organization of building blocks with dimensions that are beyond the sub-nanometer scale of most molecules or macromolecules, there are five promient principles that need to be taken into consideration. There are:

i. Building blocks, scale, shape, surface structure,
ii. Attractive and repulsive interactions between building blocks, equilibrium seperation,
iii. Reversible association-dissociation and/or adaptable motion of building blocks in assembly, lowest energy structure,
iv. Building blocks interactions with solvents, interfaces and templates,
v. Building-blocks dynamics, mass transport and agitation.

A challenge for perfecting structures made by this kind of self-assembly chemistry is to find ways of synthesizing (bottom-up) or fabricating (top-down) building blocks not only with the right composition but also having the same size and shape [21]. The top-down approach is the use of microfabrication techniques that reduce bulk material into smaller componenets to form nanoscale features or objects. The bottom-up approach is the synthesis of nanoscale structures and devices by chemically building up from the molecular level and forms the foundations of nanochemistry [7].

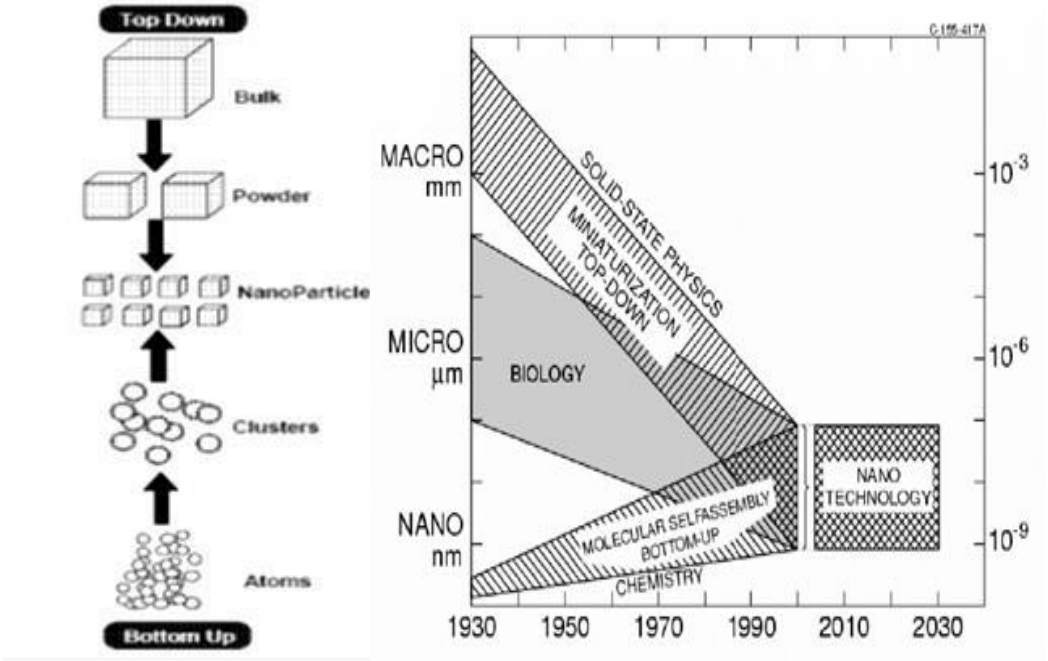

Figure 1.2. The Preparation of nanoparticle by using the bottom-up approach and the top-down approach and graphical representation of these two approaches

No matter which way building blocks are made they are never truly monodisperse, unless they happen to be single atoms or molecules. There always exists a degree of polydispersity in their size ande shape, which is manifest in the achievable degree of structural perfection of the assembly and the nature and population of defects in the assembled system. Equally demanding is to make building blocks with a particular surface structure, charge and functionality. Surface properties will control the interactions between building blocks as well as with their enviroment, which ultimately determines the geometry and the distances at which building blocks come to equilibrium in a self-assembled system. Relative motion between building blocks facilitates collisions between them, whilst energetically allowed aggregation-deaggregation processes and corrective movements of the self-assembled structure will allow it to attain the most stable form. Providing the building blocks are not too strongly bound in the assembly it will be able to adjust to

an orderly structure. If on the other hand the building blocks in the assembly are too strongly interacting, they will be unable to adjust their relative positions within the assembly and a less ordered structure will result [5].

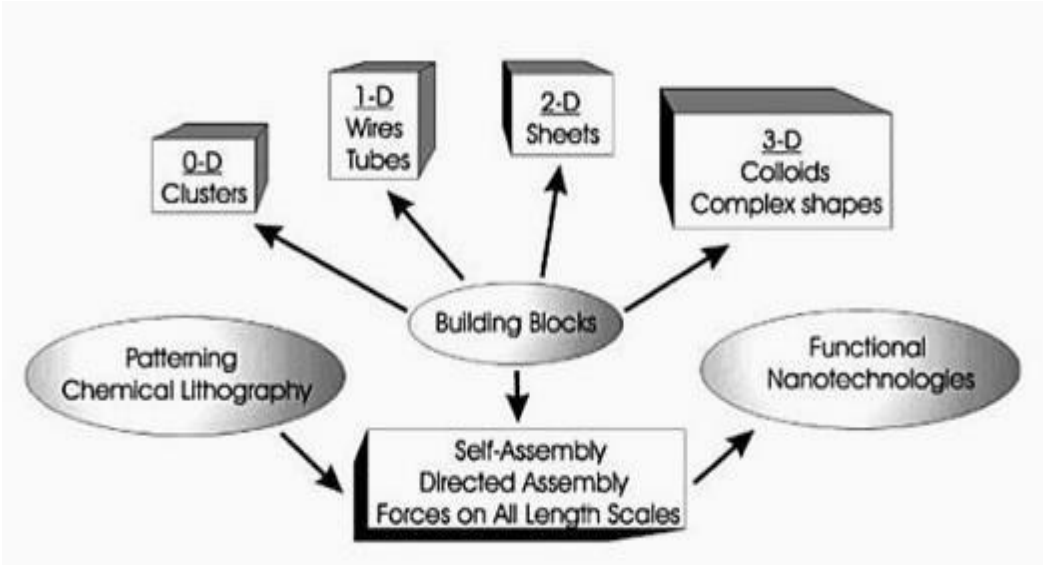

Figure 1.3. A Flowchart delineating the factors that must be considered when approaching the self-assembly of a nanoscale system

Building blocks can be made out of most known organic, inorganic, polymeric, and hybrid materials. Creative ways of making spheres and cubes, sheets, and discs, wires and tubes, rings and spirals, with nm to cm dimensions, abound in the materials self-assembly literature. They provide the basic construction modules for materials self-assemnly over all scales, a new way of synthesizing electronic, optical, photonic, magnetic materials with hierarchical structures and complex form. A flowchart describing these main ideas is shown in Figure 1.3 [5].

1. 2. 2. Carbon Materials

Carbon is a fascinating chemical element with unique properties. It is one of the few elements known and used since antiquity. The name comes from Latin language word “carbo” which means coal. No other element in the periodic table occurs in so many different forms [8]. Coal, soot, graphite, and diamond are all nearly pure forms of carbon. While graphite is soft enough to be used in pencils, diamond ranks among the hardest materials known. Carbon has been used from ancient times, in charcoal form for bronze production or as candle soot mixed with olive oil for writing. Some of the earliest cave paintings, at Lascaux or Altamira, were realized using a mixture of charcoal and soot [9,10]. Carbon based nanomaterials refer to solid carbon materials with structural units on a nanometer scale in at least one direction. These materials have a large surface to volume ratio reflected in their unique and remarkable properties. Carbon is accepted to be as important for nanotechnology as silicon is for electronics [11]. The morphology of carbon nanomaterials ranges from fullerenes to carbon nanotubes, from graphene to nanocones or nanodiamonds. Carbon, the common element of these materials, continues to arouse the interest and attention of researchers all over the world. This chapter is a review of the most important aspects of the carbon materials, carbon nanomaterials.

1. 2. 2. 1. Electronic Structure of A Single Carbon Atom

Carbon is the chemical element with symbol C, atomic number 6. It is found in the periodic table as a member of group 14. A carbon atom has six electrons with a $1s^2 2s^2 2p^2$ electronic ground state configuration. The two electrons contained in the 1s

orbital are strongly bound electrons and are called core electrons. The other four electrons which occupy the $2s^2 2p^2$ orbitals, are weakly bound electrons, and are called valence electrons (Figure 1.4a). The actual location of electrons in a carbon atom cannot be determined with certainty and the diagram can be misleading. A better way to look at the carbon atom is by using an energy level chart shown in Figure 1.4b [12].

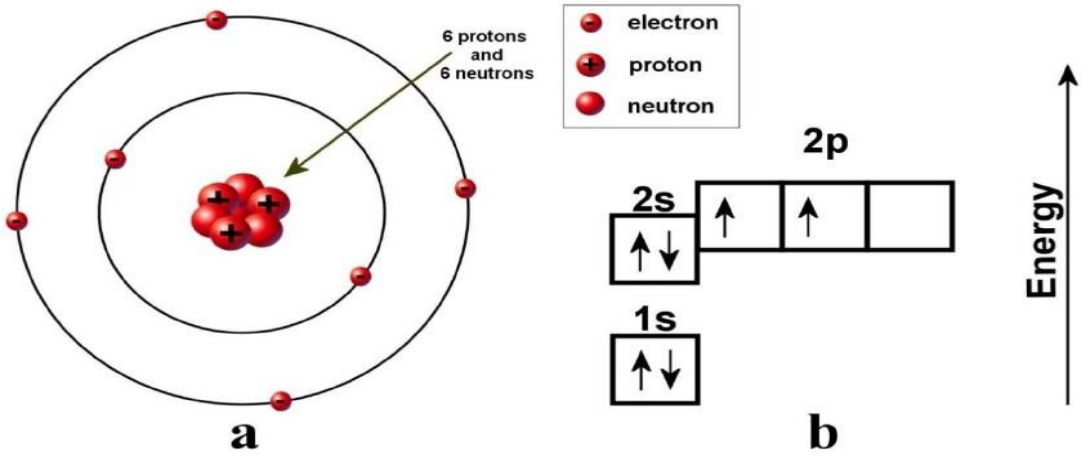

Figure 1.4. Diagram of the electronic structure of the carbon atom in (a) the ground state and (b) the energy level chart.

The electrons are represented by arrows while the direction of the arrow represents the spin of the electron. Two electrons are found in the 1s orbital close to the nucleus. These two electrons, which spin in opposite directions, have the lowest possible energy. They fill the K shell or first shell as principal quantum number; K (n=1). Being filled, the K shell is completely stable and its two electrons do not take part in any bonding. The four electrons belong to the L shell; L (n=2). The L-shell has two different sub-shells, s and p. Two electrons fill the 2s orbital and have opposite spin. The last two electrons partially fill the 2p orbital and have parallel spin. The 2s and the 2p electrons have different energy levels. The 2p electrons

located in the outer orbital are the only electrons available for bonding to other atoms. These electrons are the valence electrons [12].

In this state carbon is divalent because only two electrons are available for bonding. Divalent carbon is found in carbene, a class of highly reactive molecules. In contrast, carbon allotropes and polymorphs are tetravalent and four valence electrons are present for bonding the carbon atoms. The description of how carbon electron valence is increased to form carbon allotropes is outlined below [12].

1. 2. 2. 2. Hybridization of Carbon Atoms

The electron configuration of the carbon atom has to be modified in order to allow carbon atoms to combine themselves. The configuration of the carbon atom must be altered to a state with four instead of two valence electrons. This modification implies mixing the orbitals of the outer shell of the atom in the ground state and, consequently, forming new hybrid atomic orbitals. The concept is called hybridization. For carbon, one 2s electron is promoted into the 2p orbital. The remaining 2s orbital is spherically symmetrical while the formed three 2p orbitals are oriented along the three axes perpendicular to each other. The way of combining these different orbitals gives different carbon hybridization types [12].

1. 2. 2. 2. 1. *sp* Hybridization

In *sp* hybridization one s and one p (2px) orbital from the outer shell are altered to form two equivalent orbitals called '*sp*' hybrid orbitals directed towards the 'x' axis. This hybridization is often known as diagonal hybridization as the two sp orbitals are at 180^{o} due to mutual repulsion of their electron clouds. The remaining $2p_y$ and $2p_z$ orbitals do not take part in hybridization and are directed along the 'y' and

'z' axes, perpendicular to the two sp orbitals (Figure 1.5). The linear orientation of the sp orbitals is available to form high strength sigma (σ) bonds while the non-hybridized p orbitals are available to form pi (π) bonds. Carbon, in its *sp* hybridization, forms carbine or polyyne [12].

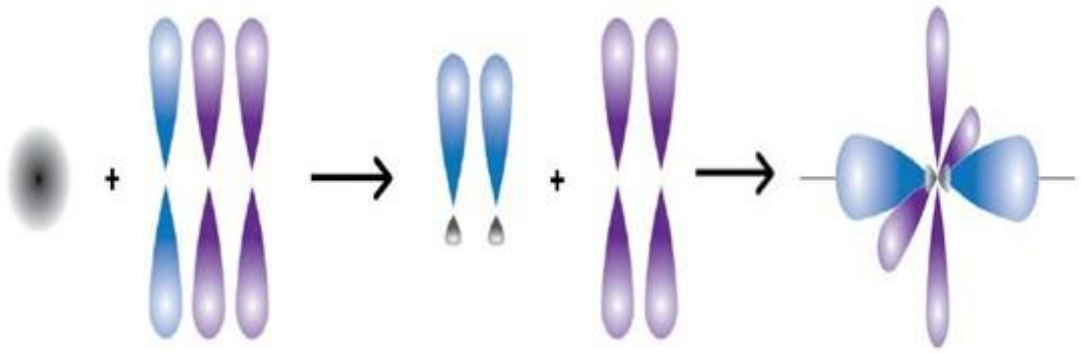

Figure 1.5. *sp* hybridization of carbon.

1. 2. 2. 2. 2. sp^2 Hybridization

In this type of hybridization, one s and two p orbitals ($2p_x$ and $2p_y$) get hybridized to form three equivalent orbitals called 'sp^2' hybrid orbitals. These identical orbitals are in the same plane and their orientation is at 120^o angle (Figure 1.6) [12].

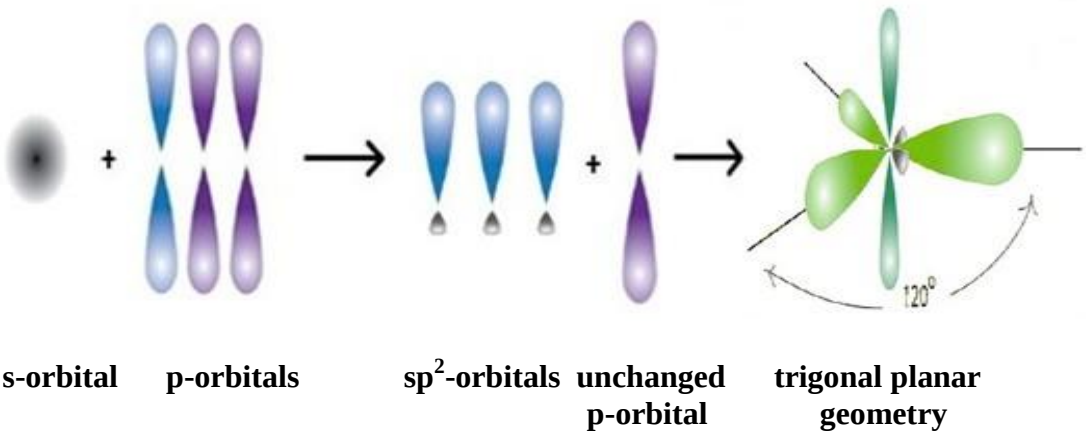

Figure 1.6. sp^2 hybridization of carbon.

Graphite is the typical structure for sp^2 hybridization of carbon. The planar orientation of the sp^2 orbitals is available to form σ bonds with three other sp^2-hybridized carbon atoms. The un-hybridized orbital $2p_z$ of carbon is oriented in a plane perpendicular to the plane containing the three hybridized orbitals and is available to form π bonds [12].

1. 2. 2. 2. 3. sp^3 Hybridization

In the sp^3 hybridization, the carbon atom has four sp^3 orbitals of equivalent energies formed from one s orbital and three p orbitals. These orbitals, due to mutual repulsion of the electron clouds, are directed towards the four corners of a regular tetrahedron with the carbon atom in the center. The angle between the hybrid orbitals is approximately 109.5^o. This structure is the basis of the diamond crystal. The four sp^3 valence electrons of the hybrid carbon atom, in combination with the small size of the atom, cause strong covalent σ bonds. Each tetrahedron of the hybridized carbon atom (shown in Figure 1.7) combines with other four hybridized carbon atoms to form a three dimensional lattice structure [12].

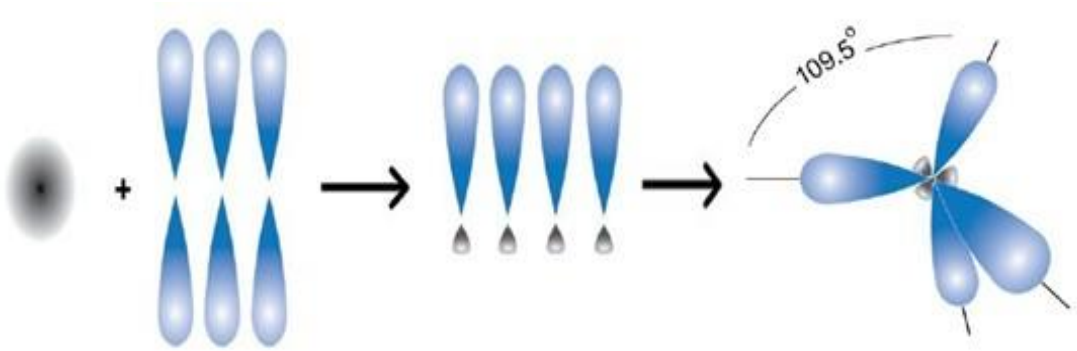

s-orbital **p-orbitals** **sp^3-orbitals** **tetrahedral geometry**

Figure 1.7. sp^3 hybridization of carbon.

1. 2. 2. 3. Carbon Allotropes

Carbon is one of the most abundant elements in nature. It forms many allotropes, depending on its specific hybridization, and bonding to surrounding atoms. Carbon with sp^3 hybridization will form a tetrahedral lattice, thus giving rise to diamond. Carbon with sp^2 hybridization will form either graphite (arranged in hexagonal sheets), buckminsterfullerene (60 carbon atoms forming a sphere), or carbon nanotubes (long hollow tubes of carbon) depending on the conditions in which it is formed [13].

Carbon has three main allotropes: diamond, graphite, and carbyne. These forms represent the three types of carbon hybridization: sp, sp^2, and sp^3 [14]. Carbon's abundance and versatility makes it one of the most studied materials in nanotechnology research, and its allotropes have a wide range of useful properties, such as high tensile strength, thermal and electric conductivity and high melting points [13].

1. 2. 2. 3. 1. Carbyne

Elemental carbon exists in three bonding states according to its hybridization. Each type of hybridization should correspond to a certain form of carbon. Only two forms of carbon related to the sp^2 and sp^3 hybridization were known up to 1960: graphite and diamond. Therefore, it was reasonable to assume the existence of a material with one-dimensional structure formed by carbon atoms sp hybridized [15]. This form was labeled carbyne from the Latin word “carboneum” (carbon) and the suffix “yne” used in organic chemistry to designate an acetylenic bond. Carbyne occurs in two forms: polyyne and cumulene. Polyyne is a linear chain-like form of

alternating single and triple bonds $(–C\equiv C–)_n$, while cumulene contains double bonds of carbon atoms $(=C=C=)_n$ [16]. Carbyne was found as a natural mineral in 1968 in the Ries meteorite crater (Germany) and was named "chaoite" in the honor of the respected scientist E. Chao. Carbynes have drawn considerable interest in nanotechnology as its Young's modulus is forty times that of diamond [17].

1. 2. 2. 3. 2. Graphite

Graphite, the sp^2 hybridized form of carbon, was named in 1789 from the Greek word "graphein" (to draw, to write) [18]. In graphite, sp^2 hybridization takes place, where each atom is connected evenly to three carbons (120°) in the {xy}-plane, and a weak π-bond is present along the z-axis. The C–C sp^2 bond length is 0.142 nm. The sp^2 set forms a hexagonal lattice (honeycomb) typical of a sheet of graphite with $P6_3/mmc$ space group. The p_z orbital is responsible for a weak Van der Waals bond, between the sheets. The spacing between these carbon layers is 0.335 nm. The free electrons in the p_z orbital move within this cloud and are no longer local to a single carbon atom (i.e. they are delocalized) giving graphite the electrical conductivity property [19]. Two forms of graphite are known, hexagonal and rhombohedral. Although these have graphene layers which stack differently, they have similar physical properties. The thermodynamically stable form of graphite is hexagonal graphite with an ABAB stacking sequence of the graphene layers (Figure 1.8). The unit cell dimensions are a=0.2456 nm and c=0.6708 nm [20]. Hexagonal graphite is thermodynamically stable below approximately 2600 K and 6 GPa [21]. The rhombohedral graphite is thermodynamically unstable with an ABCABC stacking sequence of the layers. The unit cell constants are a=0.2566 nm and c=1.0062 nm [22]. This form has not been isolated in pure form. It is always mixed

with the hexagonal form in variable amounts which can be increased up to 40% of rhombohedral content. Heating to above 1600 K progressively transforms rhombohedral graphite to hexagonal graphite, which shows that the hexagonal phase is thermodynamically more stable [23].

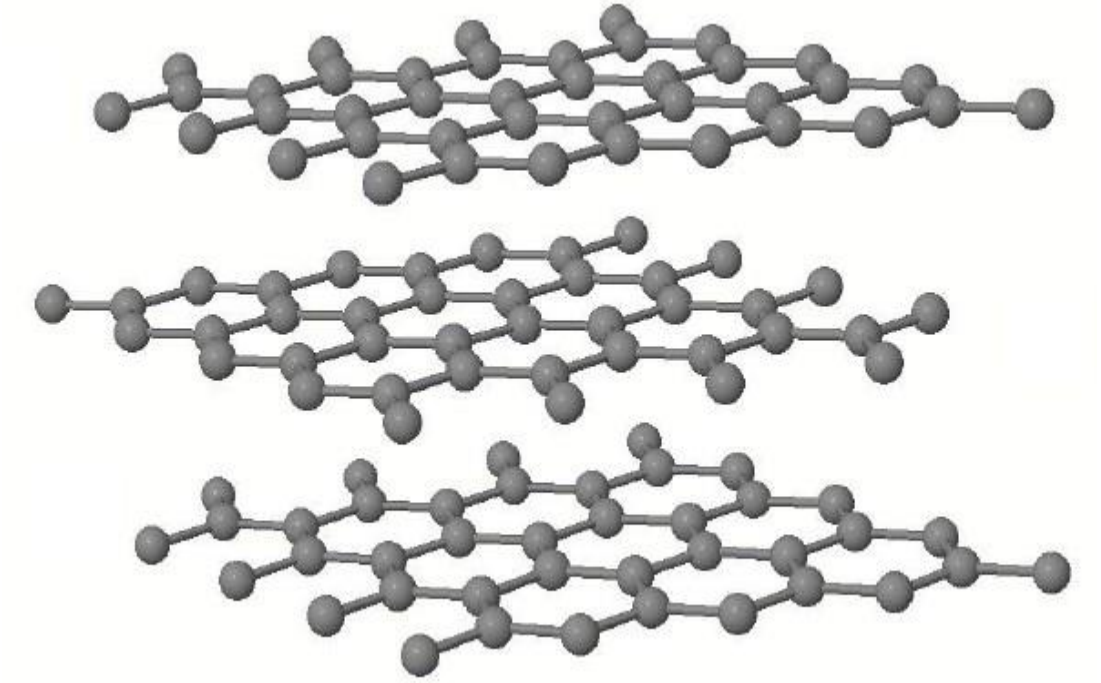

Figure 1.8. The hexagonal form of graphite.

Pure pyrolytic graphite, where the layers are all arranged in the same plane, is an extremely strong, heat-resistant material used in high-stress, high-temperature environments. Graphite can be used as a moderator for nuclear reactors. Graphitisation is the process that coke and similar irregular carbon structures or carbon based molecules take through to become more ordered into graphite. This could be either a series of artificial treatments, or a lengthy natural process within the earths crust involving pressure and heat. For catalysis applications, it is possible to find high surface area graphite, that allows good dispersion of the active phase [24].

1. 2. 2. 3. 3. Diamond

Diamond is one of the most well-known allotropes of carbon, and is both one of the hardest known natural minerals; it has the highest heat conductivity [25]. It is the hardest naturally occurring mineral and ranks among the rarest materials known. Most natural diamonds are formed at high-pressure and high-temperature conditions in the Earth mantle and are brought close to the surface through volcanic eruptions. Diamonds can also be produced synthetically by processes which simulates the conditions in the Earth mantle or by chemical vapour deposition [26]. Despite its hardness, the chemical bonds that hold together the carbon atoms are weaker in diamond than in graphite. The difference is that in diamond the covalent bonding between the carbon atoms has sp^3 hybridization and forms an inflexible and strong three-dimensional lattice. In graphite, the atoms are strongly bonded in sheets, but the sheets are weakly bonded and slide easily [27]. Two forms of diamond are known with cubic and hexagonal crystal structure. Frequently, diamond is found in the cubic form which is thermodynamically stable at pressures above 6 GPa at room temperature and metastable at atmospheric pressure. At low pressures cubic diamond converts rapidly to graphite at temperature above 1900 K in an inert atmosphere [28].

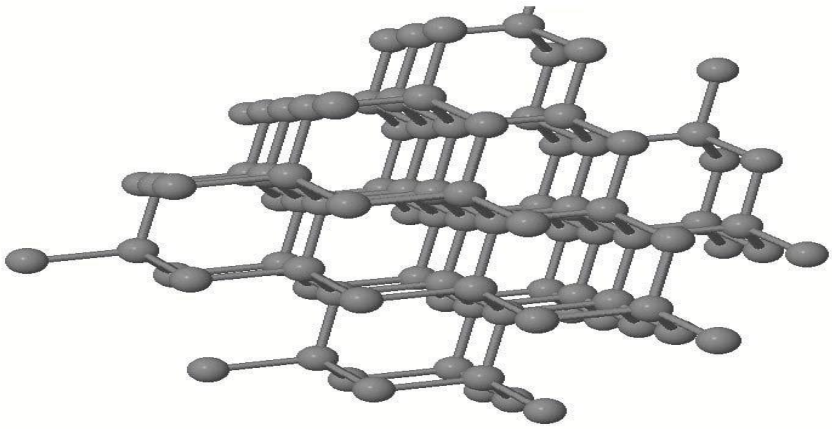

Figure 1.9. The cubic form of diamond.

In the cubic form, the bond length between two carbon atoms is 0.154 nm [29]. Pure diamond transmits visible light and appears as a clear colourless crystal. The other form of diamond is called hexagonal diamond. It is thought to occur when meteoric graphite falls to Earth [30].

1. 2. 2. 4. Other Forms of Carbon

1. 2. 2. 4. 1. Amorphous Carbon

Amorphous carbon is a carbon material without long-range crystalline order. Short-range order exists and it is related to the graphite and diamond lattices [31]. Amorphous carbon, like most glasses has no organized crystal structure (Figure 1.10). This carbon form is visually highly disordered and lacks structural integrity. The disorder allows it to have many available bonds and is responsible for building more complex carbon based molecules [32].

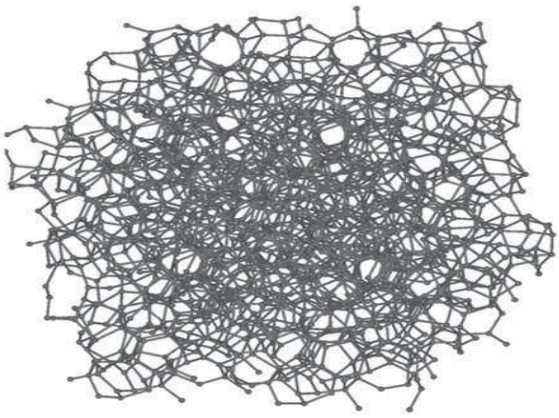

Figure 1.10. Coke (disordered carbon)

These varieties of disordered structures are formed because carbon is able to exist in three hybridizations. Amorphous carbon presents deviations in both bonding distances and angles for the sp^2 as well as for the sp^3 configuration (Figure 1.11) due to a high concentration of dangling bonds [31].

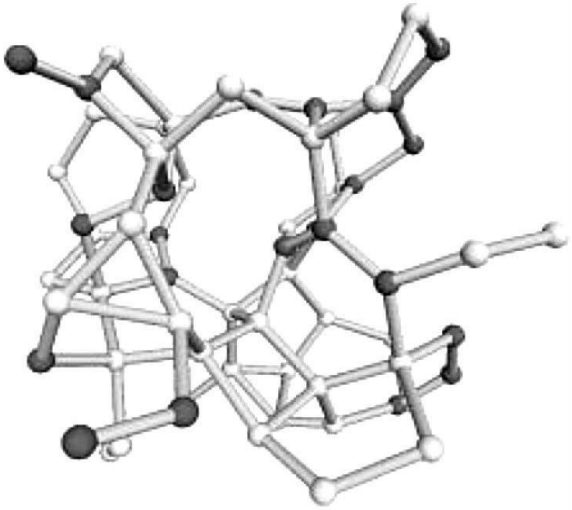

Figure 1.11. View of a-C network showing deviations in both bonding distances and angles for the sp^2 and sp^3 hybridized atoms [33].

These characteristics are inconsistent with any other allotrope of carbon. Two specific amorphous forms of carbon exist distinguished by their macroscopic and microscopic properties. These forms are graphite-like (*a*-C) and diamond-like (DLC) amorphous carbon. They are identified by the ratio of sp^2 to sp^3 hybridization contained in the material [34].

1. 2. 2. 4. 2. Glass-like Carbon

Glass-like carbon (GLC) is a very high isotropic carbon-based material. It is known that glassy carbon possesses exclusively sp^2 bonded atoms consisting in small graphite-like hexagonal layers with no true graphitic orientation between layers [35]. Glass-like carbon, often called glassy carbon or vitreous carbon, is a non-graphitizing carbon which combines glassy and ceramic properties with those of graphite. The most important properties are high temperature resistance, hardness, low density, low electrical resistance, low friction, low thermal resistance, extreme resistance to chemical attack and impermeability to gases and liquids.

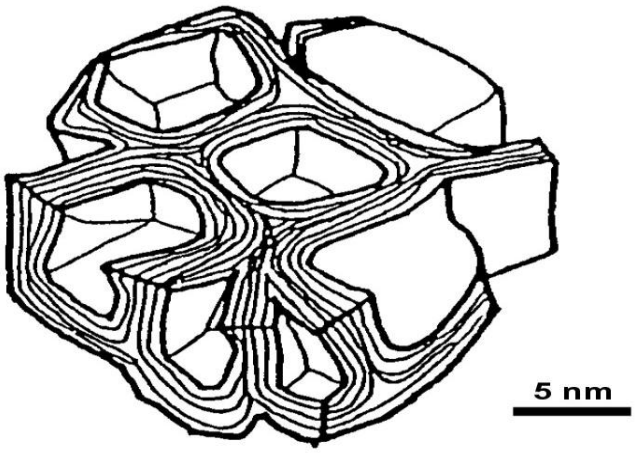

Figure 1.12. Coke Schematic diagram for the microstructure of the closed pore structure model for glassy carbon [36].

Glassy carbon is widely used as an electrode material in electrochemistry, as well as for high temperature crucibles and as a component of some prosthetic devices, and can be fabricated as different shapes, sizes and sections [37].

1. 2. 2. 4. 3. Activated Carbon

Activated carbon, also widely known as activated charcoal or activated coal is a form of carbon which has been processed to make it extremely porous and thus to have a very large surface area available for adsorption or chemical reactions. The word active is sometimes used in place of activated. Due to such high degree of micro porosity, just 1 gram of activated carbon has a surface area in excess of $500m^2$, as typically determined by nitrogen gas adsorption. Sufficient activation for useful applications may come solely from the high surface area, though further chemical treatment generally enhances the adsorbing properties of the material. Activated carbon is most commonly derived from charcoal [38].

Activated carbon is generally considered to exhibit a low affinity for water, which is an important property with respect to the adsorption of gases in the presence of moisture. Commercial activated carbon products are produced from organic materials that are rich in carbon, particularly coal, lignite, wood, nut shells, peat, pitches, and cokes .Activated carbons are produced and classified as granular, powdered, or shaped products. Activated carbon is a recyclable material that can be regenerated [39].

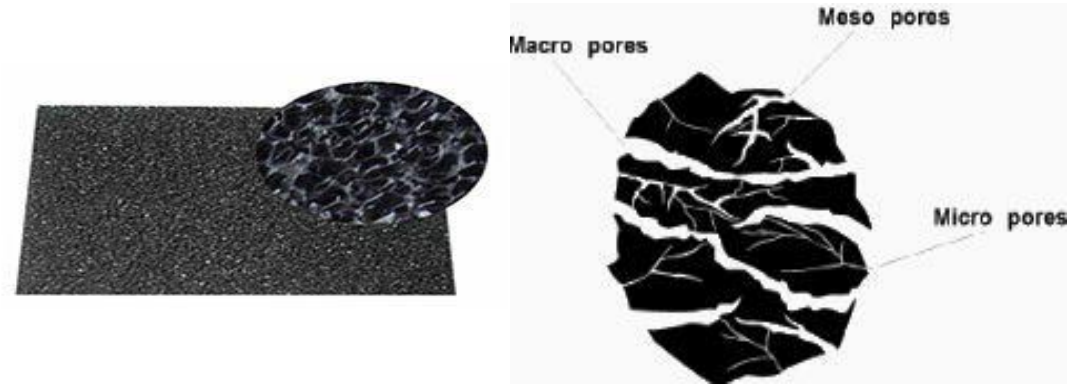

Figure 1.13. Powdered and Pore Structure of Activated Carbon

According to the IUPAC definition, pores can be distinguished in three groups with respect to their dimensions.

Macropores	Pores with diameters larger than 50 nm (500 Å)
Mesopores	Pores with diameters between 2 nm and 50 nm (20- 500 Å)
Micropores	Pores with diameters less than 2 nm (20 Å)

Table 1. Pore Sizes of Activated Carbon

Most activated carbons contain pores of different sizes; micropores, transitional mesopores and macropores. Therefore they are considered as adsorbents with wide variety of applications [40].

1. 2. 2. 5. Phase Diagram of Carbon

The large binding energy between atoms of carbon is reflected in the extremely high melting temperatures (~4000 K) of carbon allotropes. In addition, very high temperatures are required to transform one solid phase of carbon to another. The phase diagram of carbon reveals multiple crystallographic transitions in the solid phase. Initially, the diagram was traced knowing only graphite and diamond as allotropes of carbon. The experimental data accumulated in experiments done at high pressure and high temperature revealed that graphite could be transformed in diamond and diamond remained stable under ambient conditions [41,42]. In principle, it very slowly transforms back to the thermodynamically stable form of solid carbon, which is graphite. In the phase diagram proposed by F.P. Bundy (Figure 1.14), along with diamond and graphite, the hexagonal diamond and liquid carbon were emphasized.

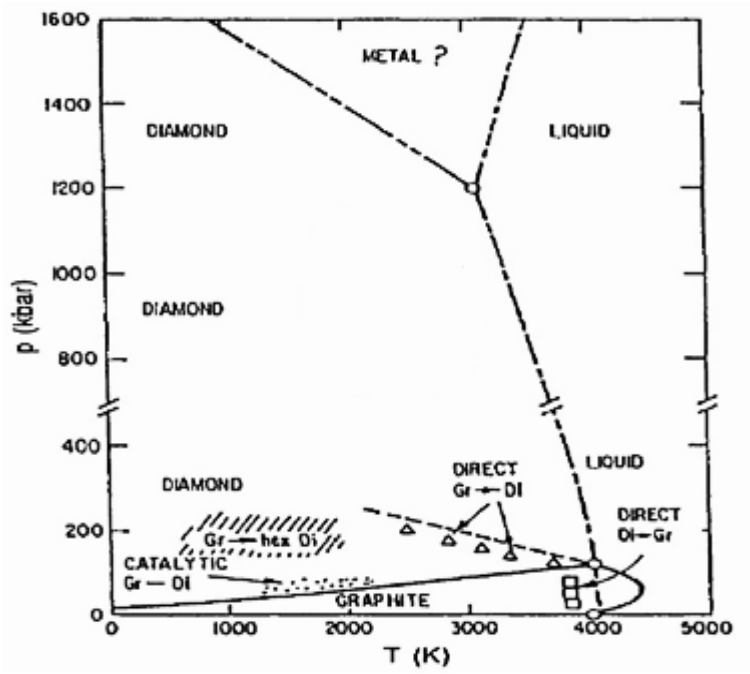

Figure 1.14. Phase diagram of carbon after F.P. Bundy

The liquid carbon phase at high pressures is still unexplored and is indicated in the diagram as metallic carbon (Figure 1.13). The investigation of new forms of carbon and of new synthesis procedures proved experimentally that carbon materials could be obtained at low pressure via CVD method. Unfortunately, low pressure experimental results and carbon structures such as carbyne or amorphous carbon (*a*-C) have not been localized on the phase diagram [43].

1. 2. 2. 6. Synthesis of Carbon Based Nanomaterials with Pyrolysis of Organic Materials

Pyrolysis is the chemical decomposition of organic materials by heating in the absence of oxygen or any other reagents [44]. The feedstock and processing influence pyrolysis production type and yield. Pyrolysis temperature, pressure, rate of temperature, gas and solid phase retention time and material size etc., are the main influence factors. Conventional pyrolysis consists of the slow, irreversible, thermal decomposition of the organic components of biomass, most of which are lignocellulosic polymers. Slow pyrolysis (hours-days) has traditionally been used for the production of charcoal. Short residence time pyrolysis (few seconds to a fraction of a second) of biomass (flash pyrolysis), at moderate temperatures (400–650^{o}C), has generally been used to obtain high yield of liquid products (up to 70% wt). Fast pyrolysis is characterized by high heating rates and rapid quenching of the liquid products, to terminate the secondary conversion of the products [45].

The specify mechanism and pathway are different by different components of feedstock and process parameter. According to the temperature of the process, pyrolysis can be described as the following steps:

a. 100 ^{o}C to 120 ^{o}C, Dry and water separation, there are no observation of the substance of the decomposition;
b. 250 ^{o}C within, minus oxygen desulfurization happen, can observe material breaks down, the structure of water and CO_2 separation;
c. 250 ^{o}C above, Polymer pyrolysis, hydrogen sulfide starts to split;
d. 340 ^{o}C, Aliphatic compounds starts to split, methane and other hydrocarbons is isolated;
e. 380 ^{o}C, Carburizing;
f. 400 ^{o}C, Carbon oxygen nitrogen compounds start decomposing;
g. 400 ^{o}C to 420 ^{o}C, Asphalt kind material into pyrolysis oil and pyrolysis tar;
h. 600 ^{o}C within, Asphalt kind material cracking into heat resistant material (gas phase, short chain carbohydrates, graphite);
i. 600 ^{o}C above, Olefins aromatic formation.

It is believed that as the reactions progress the carbon becomes less reactive and forms stable chemical structures and the volume of sludge will be much smaller [45].

The solid products include char which forms on surface of reacting particles and the residue after the sludge pyrolysis. Depending on temperature, the char fraction contains inorganic materials ashed to varying degrees, any unconverted organic solids and carbonaceous residues, produced on thermal decomposition of the organic components, in particularly lignin. The small particle size and high volatility of char, made in fast pyrolysis, cause it to be very flammable (autoignition temperature between 200 and 250°C), similar to powdered coal; hence, hot char must be properly handled. The ash content of the char is about 6–8 times greater than in

the original feed and as its alkali content is high it may cause slagging, deposition and corrosion problems in combustion [45]. Pyrolysis differs from other high-temperature processes like combustion and hydrolysis in that it usually does not involve reactions with oxygen, water, or any other reagents. In practice, it is not possible to achieve a completely oxygen-free atmosphere. Because some oxygen is present in any pyrolysis system, a small amount of oxidation occurs [46].

1. 2. 2. 7. Carbon Based Nanomaterials

Carbon based nanomaterials (CBNs) cover various types of nanostructured carbons. The most representative ones are nanodiamonds, fullerenes, nanotubes, nanofibres, nanosheets and graphene. Variations of these nanostructures are nanocones, nanorings, branched nanotubes, and nanofibres.

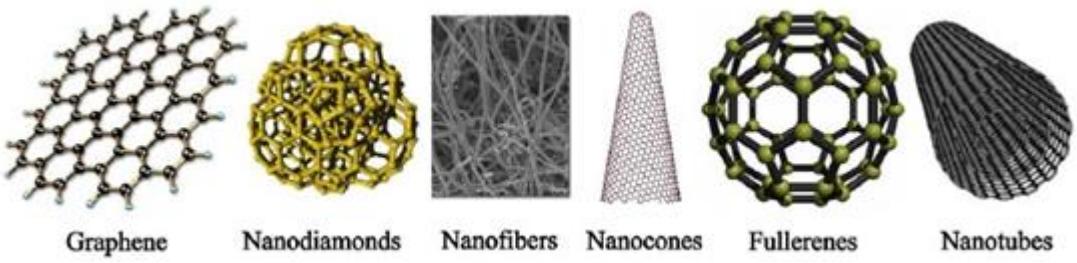

Figure 1.15. Phase Carbon Based Nanomaterials

By the early 1980s, although the majority of carbon based nanomaterials were almost unknown, carbon science was widely considered to be a mature discipline, unlikely to produce any major surprises. However, this situation changed in 1985 due to the synthesis of first all-carbon molecule, buckminsterfullerene. It was the discovery of Harry Kroto, Richard Smalley, and their colleagues, which led to the synthesis of carbon nanotubes and which made carbon science so fashionable [47].

1. 2. 2. 7. 1. Fullerenes

Fullerenes are a class of molecules composed entirely of carbon, in a spherical, ellipsoidal, or cylindrical arrangement. They are closed hollow cages consisting of carbon atoms interconnected in pentagonal and hexagonal rings. The smallest stable, and almost abundant fullerene is C_{60} (Figure 1.16), also called buckminsterfullerene. The next stable homologue is C_{70} (Figure 1.16) Spherical fullerenes are also called buckyballs, and cylindrical ones are called carbon nanotubes or buckytubes. Spherical fullerenes are zero-dimensional molecules since all dimensions are limited to nanoscale. The chemical formula of spherical fullerenes is C_n, where n represents the number of atoms in the molecule. Among the isolated stabile fullerenes are C_{60}, C_{70}, C_{76}, C_{80}, C_{84} and the series extends to gigantic fullerenes [48] and onion fullerenes [49].

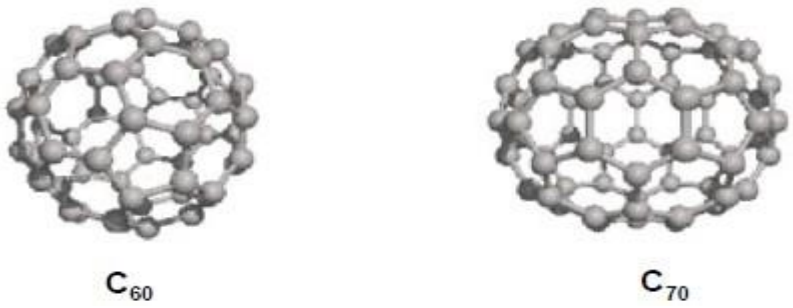

Figure 1.16. Chemical structures of the fullerenes C_{60} and C_{70}

1. 2. 2. 7. 2. Carbon Nanotubes

Carbon nanotubes (CNTs) are molecular-scale tubes of graphitic carbon. They discovered in 1991 by Iijima have diameters from fractions to tens of nanometers and lengths up to several micrometers [50]. CNTs can be considered as a graphene sheet in the shape of a cylinder capped by fullerene-like structures. Single-walled (SWCNTs) and multi-walled (MWCNTs) nanotubes are formed by seamless

roll up of single and multi layers of graphene lamella respectively. Their reported surface areas range from 150 to 1500 m^2 g^{-1}, which is a basis for serving as good sorbents [51].

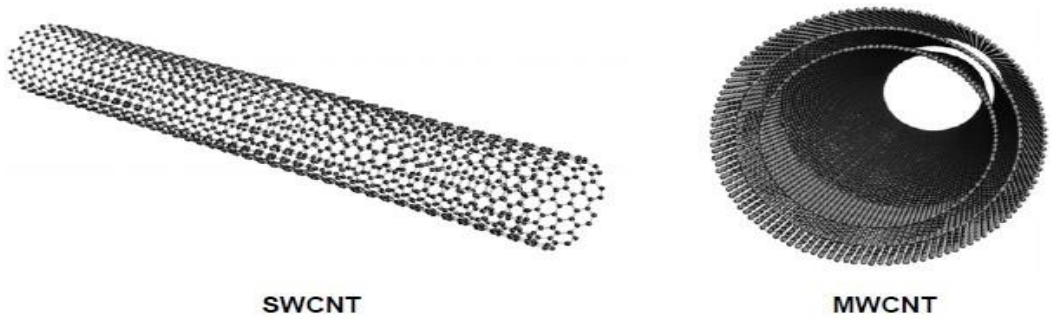

Figure 1.17. Schematic of a single-walled carbon nanotube (SWCNT) and a multi-walled carbon nanotube (MWCNT).

MWCNTs have more than one wall or concentric tubes and the inter-tube spacing is 0.34 nm, which corresponds to the interlayer distance of 0.35 nm in graphite [52]. While the diameter of CNTs is in the range of several hundred nanometers down to 0.3 nm [53], the length can be up to several centimeters [54]. CNTs can be produced by chemical vapor deposition (CVD), arc discharge and laser ablation techniques. Each method allows the synthesis of bulk amounts of CNT material consisting of entangled, bundled, and crystalline CNT structures [55].

1. 2. 2. 7. 3. Carbon Nanofibers

Carbon nanofibers are graphitic filamentous structures which differ from nanotubes in the orientation of the graphite monolayer planes. In CNTs, the graphite monolayer planes are parallel to the tube axis. In nanofibers, the graphite layers are arranged perpendicular to the fiber axis (stacked form) or at an angle to the axis (herringbone form) [16]. The structure of these nanofibers is illustrated in Figure 1.18.

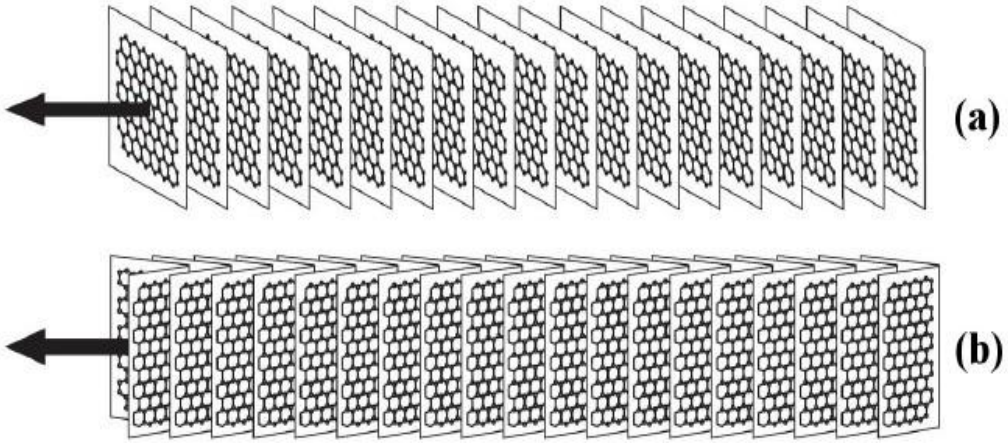

Figure 1.18. The structure of "stacked" (a) and "herringbone" (b) nanofibers (the arrow indicates the fiber axis) [16].

Carbon nanofibers are produced by catalytic exposure of gaseous hydrocarbons to high temperatures, similar to CNTs. The fiber structure is dictated by the chemical nature of the catalyst particle, the composition of the reactant gas, and the synthesis temperature. High strength combined with their superior stiffness has made carbon fibers an attractive material for high performance composite structures [56].

1. 2. 2. 7. 4. Graphenes

Graphenes represent the 2D carbon nanomaterials formed by one or several monolayers of graphite. Similar to the graphite structure, the sp^2-bonded carbon atoms are densely packed in a honeycomb crystal lattice with the bond length of about 0.142 nm. A single sheet is called a graphene sheet, while several graphene sheets, stacked with an interplanar spacing of 0.335 nm, are called few-layer graphene (FLG). Graphene is the basic structural element of the other carbon based nanomaterials, as it can be wrapped up to form 0D spherical fullerenes or rolled to form 1D nanotubes (Figure 1.19) [57].

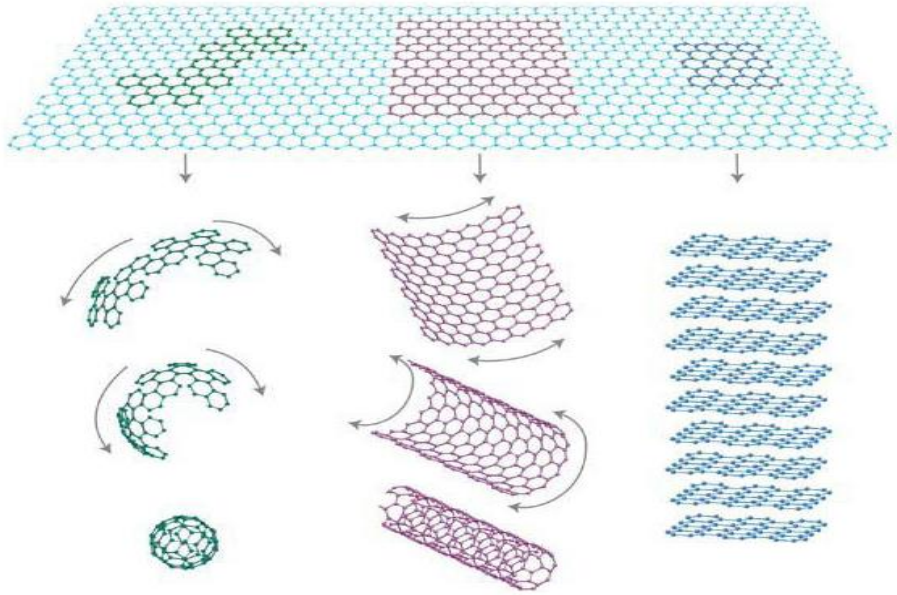

Figure 1.19. Graphene as a 2D building material for carbon materials of all other dimensionalities: 0D fullerenes, 1D nanotubes or 3D graphite.

Graphene has been studied theoretically for many years [58]. First method of graphene synthesis was reported in 1962 by P.Boehm. In this work, it was demonstrated the existence of monolayer of reduced graphene oxide flakes [59]. The produced graphene had low quality due to incomplete removal of various functional groups. Between 1990 and 2004, many efforts were made to create very thin films of graphite by mechanical exfoliation [60] but nothing less than several tens of layers were produced. In 2004, A. Geim and K. Novoselov obtained single-atom thick graphene from bulk graphite by using a process called micromechanical cleavage [61]. To date, different methods have been developed to produce single-layer or few-layer graphene such as mechanical exfoliation [60], oxidation of graphite [62], liquid-phase exfoliation [63, 64], by chemical vapour deposition [65, 66], thermal decomposition of silicon carbide [67, 68], and cutting open nanotubes [69]. Experimental results from electronic transport measurements show that graphene has remarkably high electron mobility at room temperature [70]. A single layer of

graphene has a high Young's modulus of more than 1 TPa [70] and is one of the stiffest known materials. It absorbs approximately 2.3% of white light demonstrating a very high opacity for an atomic monolayer [71]. The thermal conductivity of graphene was recently measured and exceeds the thermal conductivity for carbon nanotubes or diamond [72].

1. 2. 2. 7. 5. Carbon Nanosheets (CNSs)

Fullerenes, nanotubes, nanosheets, onions, nanofibers and other carbon nanostructures have attracted a great deal of interest in the last several years for a wide range of potential applications and especially in nanoelectronics, biomedical systems and polymer nanocomposites due to their outstanding mechanical, electrical and optical properties and their chemical and thermal stability. While the chemical and physical properties and the potential applications of fullerenes and carbon nanotubes have been studied, carbon nanosheets (CNSs), also an interesting carbon nanomaterial, have not been extensively studied [73].

Carbon is one of the abundant elements in nature and it also constitutes many nanoscaled materials with novel properties unobserved in the bulk materials due to the quantum size effect [74]. The key material in the synthesis of carbon nanomaterials is the carbon source that can provide the carbon species. In general, carbon-containing substances can potentially act as the carbon source as long as an appropriate synthesis technique is employed. The hydrocarbon gases have been widely used as the carbon sources because they have simple chemical structures which easily decompose to release the carbon species by means of catalyst-assisted or plasma-enhanced chemical vapour deposition (CVD) methods. Using the ultra-

high temperature arc-discharge method, even chemically stable graphite can also decompose and release carbon atoms for the formation of carbon nanomaterials [75].

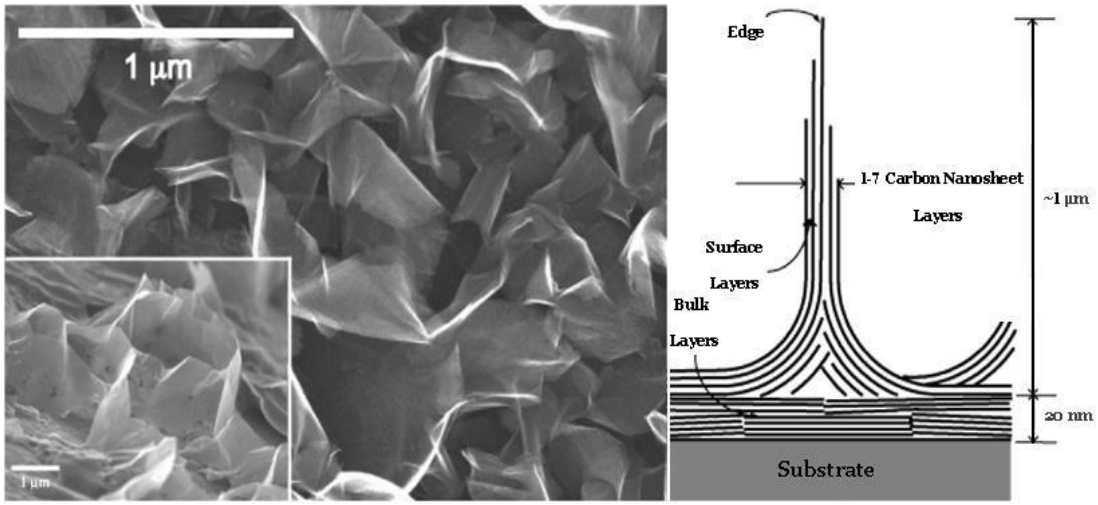

Figure 1.20. The SEM micrographs and Graphical drawing of the carbon nanosheets

Carbon sheets of a few nanometers thick (nanosheets) define a peculiar class of carbon materials with unique surface-to-volume ratio, smooth surface morphologies and thin edges, flexibility and elasticity, high thermal and chemical stability, and lightness. In this respect, carbon nanosheets are promising candidates for hydrogen storage materials, sensors, catalyst supports, fillers, templates, and substrates for further functionalization and single graphene production. In early studies, the particular carbon nanomaterials have been synthesized by :

1. Radio-frequency or microwave plasma-enhanced chemical vapour deposition (CVD),
2. Expansion of graphite,
3. Chemical reduction of exfoliated graphite oxide,
4. A solvothermal route or catalytic growth.

However, these preparative methods suffer (depending on the case) from the following drawbacks:

i. low yield or/and concurrent formation of other carbon morphologies, which limits extensive studies and development;

ii. the thickness of the sheets rarely falls below 10 nm;

iii. from a technical standpoint, they often require a sophisticated apparatus, controlled atmosphere, high temperature, flammable gaseous mixtures, gas flow adjustments, time-consuming steps, catalysts, or highly corrosive and potentially explosive chemicals; and

iv. poor surface functionality, which restricts further derivatization [76].

1. 2. 2. 7. 5. 1. Synthesis of Carbon Nanosheets from Betaines

Betaine, $(CH_3)_3N^+CH_2COO^-$, is an important zwitterionic organic compound widely distributed in nature [77]. It, a by-product of sugar beet processing, is found at a relatively high concentration in molasses, up to 8%. It is obtained by crystallization after chromatographic separation from molasses, either as anhydrous or monohydrate.

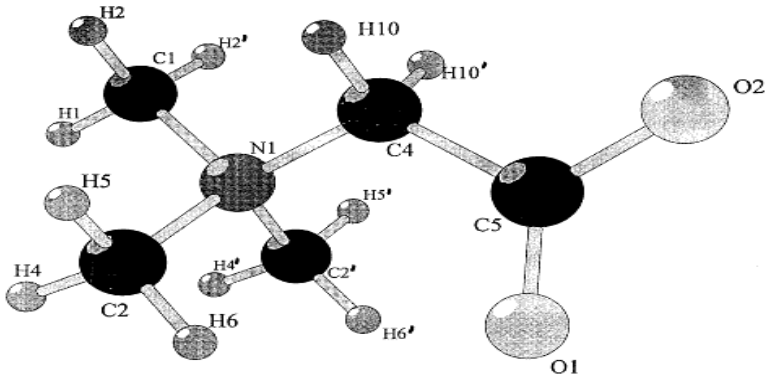

Figure 1.21. Atom labelling in the structure of anhydrous betaine [94].

Betaines are of importance in biological systems. They act as methyl transfer agents to complex lipids, and are accumulated under osmotic stress by different

organisms [78]. They are also known as osmoprotectors and osmoregulators [79]. Although the thermal decomposition of betaine has been studied in detail nonetheless, there is no information available on the structure and morphology of the residual carbon after pyrolysis. To that end, herein the pyrolytic formation of ultrathin carbon nanosheets is reported in air using betaine as a molecular precursor.

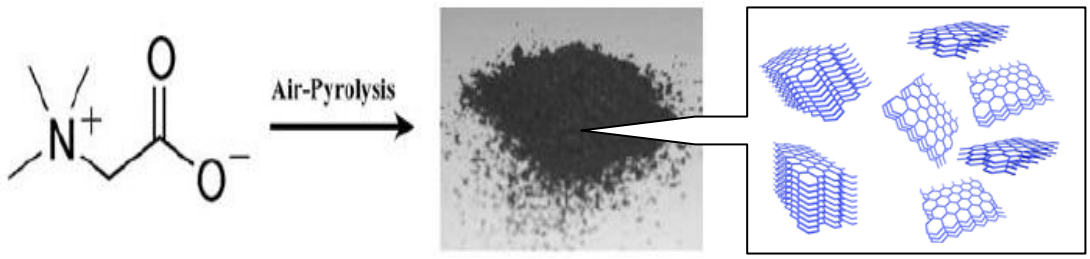

Figure 1.22. Solid-state pyrolysis of betaine in air results in bulk quantities of powder carbon nanosheets

This alternative yet paradox approach towards sheet-like carbons exhibits the following advantages:

i. it produces powder carbon nanosheets at fairly good yields;
ii. the thickness of the sheets is far less than 10 nm;
iii. the method is simple, safe, and inexpensive proceeding under normal conditions; and
iv. it directly introduces oxygen-containing functional groups in the solid,

Thus, providing active sites to the surface for further modification. Overall, the present method offers new possibilities for the cost-efficient production and processing of this kind of materials [77, 80].

1. 2. 2. 7. 5. 2. Properties of Carbon Nanosheets

Recently Carbon-based nanostructures and materials have become a popular subject of research due to their some unique properties such as thermal, mechanical, electrical, and optical properties. For example, the strong C–C bonds of graphene-based systems allow for excellent thermal conduction at room temperature and the conjugation of the sp^2 lattice enables extremely high electron mobility. However, the use of carbon nanostructures as a component in polymer composites has been limited by several factors, including the incompatibility with standard photolithography techniques, the high temperatures required for the nanostructure growth, and the presence of—or complication—of removing noncarbon species [81].

1. 2. 2. 7. 5. 2. 1. Thermal Properties of Carbon Nanosheets

A material's ability to conduct heat is rooted in its atomic structure, and knowledge of thermal properties can shed light on other materials' characteristics. The thermal properties of materials change when they are structured on a nanometre scale. At the same time, theoretical studies of heat conduction in two-dimensional (2D) and one-dimensional (1D) crystals have revealed exotic behaviour that leads to infinitely large intrinsic thermal conductivity. The thermal-conductivity divergence in 2D crystals means that unlike in bulk, the crystal anharmonicity alone is not sufficient for restoring thermal equilibrium, and one needs to either limit the system size or introduce disorder to have the physically meaningful finite value of thermal conductivity [82, 85].

Because nanosheets, like other carbon nanostructures, require a high growth temperature, growth of carbon nanosheets on temperature sensitive substrates is not a

viable option. Therefore, the ability to transfer easily the nanosheets and pattern them via standard photolithography techniques, without the use of a heat treatment step, greatly increases the potential of nanostructures in the various applications [81].

1. 2. 2. 7. 5. 2. 2. Magnetic Properties of Carbon Nanosheets

Carbon allotropes show a variety of magnetic properties ranging from diamagnetism to ferromagnetism and exhibit magnetic susceptibility in the range of $x = -(10^{-4}\text{-}10^{-7})$ emu/gOe, which indicates a diamagnetic nature. Exceptions to this include a variety of carbon nanostructures, such as amorphous carbon, activated carbon fibres, single-wall carbon nanohorns, nanoscale carbon tori and charred anthracenes [86]. Although the origin of this type of anomalous low magnetisation (compared to typical ferromagnetic materials) of organic materials has been assumed to be the result of magnetic impurities, recent studies have indicated that some organic materials exhibit low magnetisation as an intrinsic property due to a number of factors, such as the ferromagnetic interaction of spins [87] or the presence of defects.

Carbon nanosheets are 2-D graphite structures, characterised by their nanoscale thickness (few nm) and open geometry (open non-connected edges leading to the presence of edge inherited non-bonding states), are an allotrope of carbon which has attracted significant attention since its discovery [88]. Carbon nanosheets have been synthesised using RF plasma enhanced chemical vapour deposition (RF-PECVD) reliably on a variety of substrates and under a wide range of reaction parameters. While the magnetic properties of other carbon allotropes, such as fullerenes, nanohorns, nanotubes and nanofibres, have been widely studied, the properties of the 2-D nanosheet remain unexplored. It is known that the use of

inductively coupled plasma in RF-PECVD tends to favour the growth of carbon nanosheets over carbon nanotubes. This has been attributed to the plasma density of the inductively coupled plasma process, which provides higher concentration of activated carbon species and produces a larger electric field that, in turn, enhances the field-induced surface species migration [89].

1. 2. 2. 7. 5. 2. 3. Electrical Properties of Carbon Nanosheets

Graphene, an atomically thick allotrope of carbon with a two dimensional structure (carbon nanosheet), has received a great deal of attention. Most notably, properties such as an atomically controlled thickness, an electron mobility of 150,000 $cm^2\ V^{-1}s^{-1}$ under ambient conditions, a sheet resistance (Rs) of 30 $\Omega\ sq^{-1}$, and an optical transmittance of 97.5% have provided potential pathways for a wide range of applications [61]. In this respect, carbon nanosheets are promising candidates for hydrogen storage materials, catalyst supports, fillers, templates, and due to their electrical properties these may also be suited for electronic applications [90].

1. 2. 3. Aim of this work

The aim of this work can be ordered as follows:

- To synthesize phenylphthalazinium betaine in order to study its microscopic properties in which we could obtain due to both nitrogen and air pyrolysis.
- To synthesize new carbon nanosheet structures from phenylphthalazinium betaine and also investigate the structural properties or structural characterization of the carbon nanosheets.
- To provide low cost and facile synthesis of carbon nanosheet.

2. EXPERIMENTAL

2. 1. Synthesis of 2-phenylphthalazin-2-ium-4-olate (Betaine)

All stage of the synthesis of 2-phenylphthalazin-2-ium-4-olate(betaine) was carried out in Organic Chemistry Research Laboratory in A.I.B.U. Melting points were determined with Electrothermal 9200 apparatus. The purification analysis of compounds was made in t.l.c plate and they were observed as single spots on t.l.c (Ethyl acetate, Hexane as eluant). The solvents were primarily used and they were dried before using. The spectra of compounds were analyzed and saved with a Shimadzu Scientific Instrument Prestige-21 FT/IR and Shimadzu FT/IR-8400S and also compounds were made a KBr pellet for spectral analysis in Shimadzu FT/IR-8400S.

2. 1. 1. Mainly Used Solvents and Chemicals

2. 1. 1. 1. Chloroform ($CHCl_3$)

Drying agents were added to the commercially available solvent.

2. 1. 1. 2. Tetrahydrofuran (THF)

Solvent was stirred with CuCl about 3 hours, then filtered and distilled.

2. 1. 1. 3. Acetone ($(CH_3)_2CO$)

Solvent was refluxed with small quantity of $KMnO_4$ until violet color persists. Dried with anhydrous K_2SO_4 or $CaSO_4$, then filtered and distilled.

2. 1. 1. 4. Phthalic Anhydride ($C_6H_4(CO)_2O$)

Solid form phthalic anhydride was directly used from its commercial box.

2. 1. 1. 5. Phenylhydrazine ($C_6H_5NHNH_2$)

Phenylhydrazine has a liquid form which was directly used from its commercial bottle.

2. 1. 1. 6. Ethyl Alcohol (C_2H_5OH)

Ethyl Alcohol was purchased as a commercial and used without further purification unless stated otherwise.

2. 1. 2. Synthesis Stages of 2-phenylphthalazin-2-ium-4-olate (Betaine)

2. 1. 2. 1. Synthesis of 2-(2-phenylhydrazinecarbonyl)benzoic acid (1c)

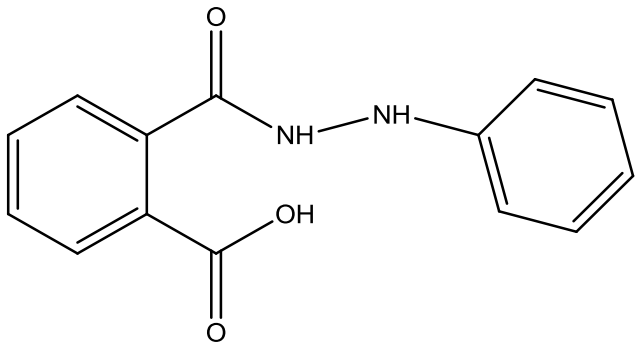

1c

Phenylhydrazine **1a** (2.10 g, 0.020 mol, 2.00 mL) in $CHCl_3$ (10 mL) was added to phthalic anhydride **1b** (2.96 g, 0.02 mol) in $CHCl_3$ (100 mL) and the mixture was kept at 20 °C for 3 h. Then, the color of mixture turned to pink and precipitation occurred. The precipitated 2-(2-phenylhydrazinecarbonyl)benzoic acid **1c** was filtered off as white crystals and air dried. The yield was 66% (3.384 g).

M.p. : Not specified (converted into imide)

R_f : 0.19 (EtOAc)

IR (KBr): *v* (cm^{-1}) : 3292, 1703, 1653, 1604

2. 1. 2. 2. Synthesis of 2-(phenylamino)isoindoline-1,3-dione (1d)

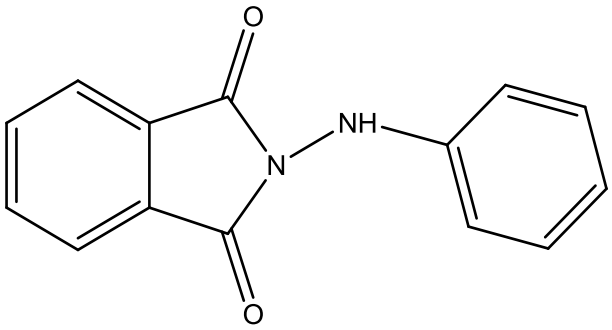

1d

2-(2-phenylhydrazinecarbonyl)benzoic acid **1c** (3.384 g, 0.013 mol) was heated at 160-170 °C in a sand bath with occasional stirring for 15 min to give 2-(phenylamino)isoindoline-1,3-dione **1d** as yellow powders. To purify the precipitated 2-(phenylamino)isoindoline-1,3-dione **1d ,** it was dissolved in 50 mL ethanol and it was kept in sand bath increasing temperature slowly at 80-90 °C. The yield was 65% (2.013 g).

M.p. : 178-180 ^oC

R_f : 0.60 (EtOAc-n-Hexane; 1:1)

IR(KBr): *v* (cm^{-1}) : 3317, 1782, 1705, 1597

2. 1. 2. 3. Synthesis of 3-hydroxy-2-(phenylamino)isoindolin-1-one (1e)

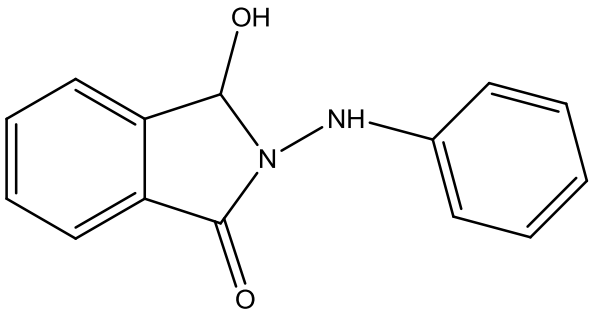

1e

$NaBH_4$ (0.1 g, 0.02 mole) in $[CH_2]_4O$ (3 mL) was added quickly and with vigorously stirring to 2-(phenylamino)isoindoline-1,3-dione **1d** (0.238 g, 0.001 mol) in THF (8 mL) and distilled water (0.50 mL) at 20 °C. After 2 hours, the excess of $NaBH_4$ was decomposed with a large excess of dry acetone (~10 mL). The solution was stirred for 0.5 h more, filtered, and evaporated under vacuum and an oily product **1e** was obtained. The yield was 72% (0.174 g).

M.p. : Not specified (Product was oily)

R_f : 0.37 (EtOAc-n-Hexane; 1:1)

IR(KBr): ν (cm^{-1}) : 3464, 1712, 1604

2. 1. 2. 4. Attempts to synthesize 2-phenylphthalazin-2-ium-4-olate (1f)

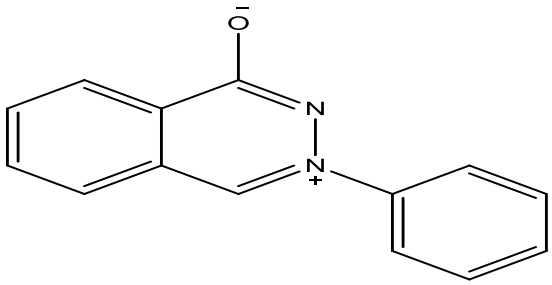

1f

The oily residue **1e** was heated at 130-140 °C for 30 min to give a solid which was dissolved in hot ethanol (15 mL). Then, diethyl ether about 50 mL was added to give a betaine **1f** as it was done for the preparations of 3-arylphthalazinium-1-olates [4]. The yield was 70% (0.160 g).

M.p. : 201-203 ^{o}C (from ethanol)

R_f : 0.04 (EtOAc)

IR(KBr): ν (cm^{-1}) : 1599, 1564

2. 2. Synthesis of Carbon Nanoheets From 2-phenylphthalazin-2-ium-4-olate (Betaine)

All the synthesis works and some investigations of carbon nanosheet from 2-phenylphthalazin-2-ium-4-olate(betaine) was carried out in Organic Chemistry Research Laboratory in A.I.B.U and Physics Department in Institute of Natural Sciences in A.I.B.U.

The chemical bondings of carbon nanosheet samples were analyzed and saved with a Shimadzu FT/IR-8400S and also carbon nanosheet samples were made a KBr pellet for spectral analysis in Shimadzu FT/IR-8400S.

The surface morphology and structures of carbon nanosheet samples were examined by scanning electron microscope (SEM, Jeal JSM-6390LW) operating at 20 kV so as to attain better surface image and resolution, respectively. The semi quantification elemental analysis was done using the IXRF Systems Model 550i Energy Dispersive X-Ray Spectrometer (SEM-EDS) in order to determine the weight percentage of major and minor elements present in the carbon nanosheet samples. Carbon nanosheet samples were coated with gold using COXEM KIC-1A Ion Coater before SEM analysis. Gold coating was made with 4 mA current at 220 sec.

The phase purity and the crystalline phase was identified by using a Rigaku Multiflex diffractometer (XRD). It was run 38 kV/28 mA with a scan speed of 5.00 deg/min in a 2θ range from 20° to 80° with Cu Kα radiation (λ = 1.5418 Å).

Thermal gravimetric analysis (TG/DTA) of carbon nanosheet sample was realized by using a Exstar6000 TG/DTA6300 thermal analyzer from 20 °C to 500 °C at a heating rate of 10 °C/min in an N_2 atmosphere.

2. 2. 1. Mainly Used Equipments and Chemicals

2. 2. 1. 1. Ring Stand and Clamps

A stand was used to support some types of clamps such as a ring clamp or flask clamp.

2. 2. 1. 2. Bunsen Burner

A bunsen burner was used to produce a open gas flame. It provided enough heat for the synthesis of carbon nanosheets.

2. 2. 1. 3. Thermometer

A thermometer was used to measure the reaction temperature.

2. 2. 1. 4. One- and Two-Neck Round Bottomed Flasks

These flasks were made of glass for chemical inertness and samples were put into them to realize reactions.

2. 2. 1. 5. Sand Bath

A sand bath was used to provide even heating for one- and two-round bottomed flasks during the chemical reaction.

2. 2. 1. 6. Tripod Stand

A tripod stand was used to put under the sand bath so as to get heat from the bunsen burner.

2. 2. 1. 7. Condenser

A condenser was utilized to remove the nitrogen gas atmosphere from the medium safely.

2. 2. 1. 8. Nitrogen Gas (High Purity)

An inert gas does not undergo chemical reactions with many substances. The noble gases, argon and nitrogen are some examples of inert gases. So, nitrogen gas

was used to generate an inert gas atmosphere for the synthesis of carbon nanosheets from 2-phenylphthalazin-2-ium-4-olate (Betaine). This gas was stored into the tensile steel nitrogen gas tube.

The properties of nitrogen into the tensile steel tube:

N_2, % Vol. : > 99.999

O_2, ppm : < 5

H_2O, ppm : < 4

2. 2. 1. 9. 2-phenylphthalazin-2-ium-4-olate (Betaine)

2-phenylphthalazin-2-ium-4-olate is obtained (or synthesized) from 1,3-Dipolar cycloaddition reaction of phthalic anhydride and phenyl hydrazine.

2. 2. 2. Synthesis of Carbon Nanosheets From 2-phenylphthalazin-2-ium-4-olate (Betaine) in an Air Pyrolysis

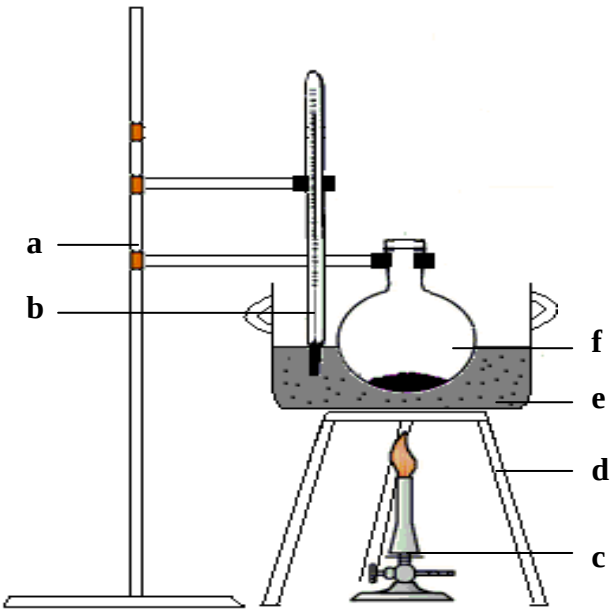

a. Ring Stand and Clamps

b. Thermometer

c. Bunsen Burner

d. Tripod Stand

e. Sand Bath

f. One-Neck Round Bottomed Flask

Figure 2.1. The air pyrolysis system for the synthesis of carbon nanosheets from 2-phenylphthalazin-2-ium-4-olate (Betaine)

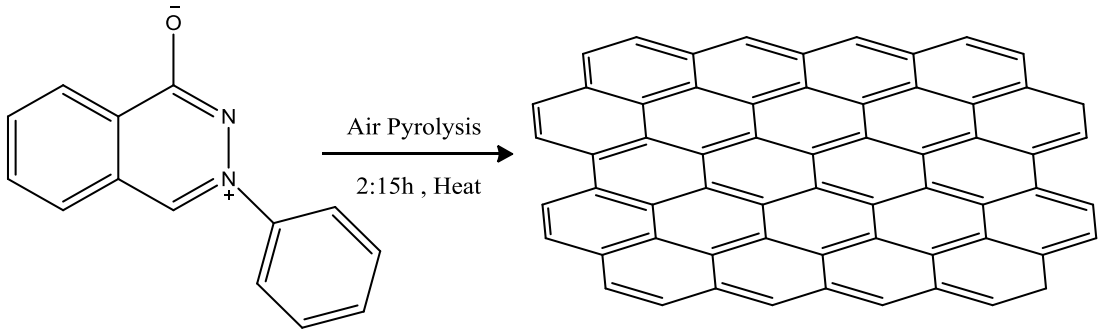

1f **1g**

Figure 2.2. Solid-state pyrolysis reaction of 2-phenylphthalazin-2-ium-4-olate in air results to synthesize the powder carbon nanosheets

0.50 g of 2-phenylphthalazin-2-ium-4-olate (Betaine) was calcined in air at 400 °C [93, 97], 500 °C, 350 °C, and 300 °C for 2:15 h at a heating rate of 7 °C min^{-1} to afford a lightweight, black-brown powder at 2% yield containing exclusively carbon nanosheets.

2. 2. 3. Synthesis of Carbon Nanosheets From 2-phenylphthalazin-2-ium-4-olate (Betaine) in a Nitrogen Gas Atmosphere (Inert Gas Atmosphere)

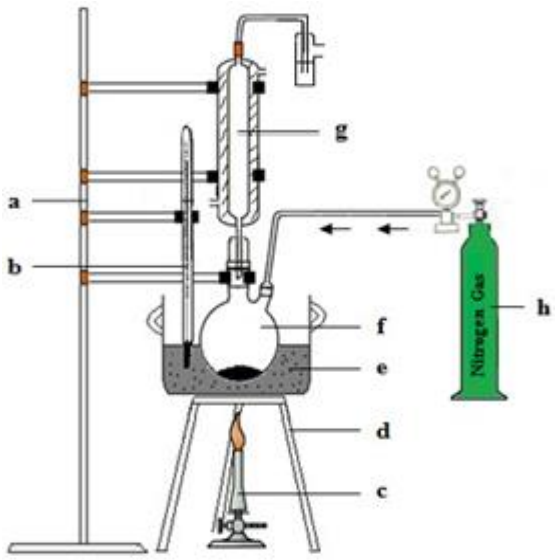

a. Ring Stand and Clamps

b. Thermometer

c. Bunsen Burner

d. Tripod Stand

e. Sand Bath

f. Two-Neck Round Bottomed Flask

g. Condenser

h. Nitrogen Gas (High Purity)

Figure 2.3. The pyrolysis system for the synthesis of carbon nanosheets from 2-phenylphthalazin-2-ium-4-olate (Betaine) in N_2 gas atmosphere.

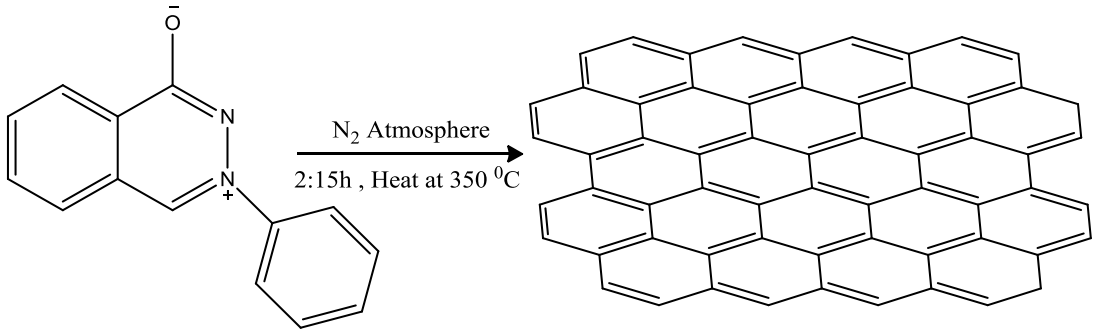

1f **1g**

Figure 2.4. Solid-state pyrolysis reaction of 2-phenylphthalazin-2-ium-4-olate in N_2 gas atmosphere results to synthesize the powder carbon nanosheets

0.50 g of 2-phenylphthalazin-2-ium-4-olate (Betaine) was heated to afford a lightweight, black-brown carbon nanosheet powder in N_2 gas atmosphere at 350 °C for 2 hours 15 minutes at a heating rate of 7 °C min^{-1} .

3. RESULTS AND DISCUSSION

This work includes firstly the synthesis of 2-phenylphthazin-2-ium-4-olate (betaine) from the reaction of phthalic anhydride and phenylhydrazine starting materials. Secondly, it contains the studies of synthesis of carbon nanosheets from 2-phenylphthazin-2-ium-4-olate in an air pyrolysis at four different temperatures (300°C, 350°C, 400°C and 500°C) and in nitrogen (N_2) gas atmosphere at 350°C. Also, it covers the surface morphology properties of carbon nanosheets in an air pyrolysis and in nitrogen (N_2) gas atmosphere. The synthesis methods of 2-phenylphthazin-2-ium-4-olate (betaine) and carbon nanosheets were talked about in detail in the experimental part.

3. 1. Synthesis of 2-phenylphthazin-2-ium-4-olate (Betaine)

Betaine, $(CH_3)_3N^+CH_2COO^-$, is an important zwitterionic organic compound widely distributed in nature [77]. The presence of ring confined positive and negative charges in a heterocyclic conjugated system gives rise to an interesting class of molecules known as mesomeric betaines (MB) [91]. From a structural point of view, the MB are molecules that can exclusively be represented by dipolar canonical formulae in which the charges are delocalized within the π-electron system [92]. Heterocyclic mesomeric betaines have been broadly classified into two types; conjugated heterocyclic mesomeric betaines which are associated with 1,3-dipoles and cross-conjugated heterocyclic mesomeric betaines which are associated with 1,4-dipoles [93]. Mesomeric betaines constitute a unique class of 1,3-dipoles which

have long been known to be extremely important intermediates in cycloaddition reactions for the construction of a number of natural products and new heterocyclic compounds. Their utility derives from the fact that most act as 1,3-dipoles and lead to heteropolycycles by one-step reactions with dipolarophiles [94].

In this work, the synthesis of 2-phenylphthazin-2-ium-4-olate (betaine) was tried to do in four reaction steps which were explained in modified method of Lund by Katritzky [4].

In the first step of the synthesis of 2-phenylphthazin-2-ium-4-olate (betaine), 2-(2-phenylhydrazinecarbonyl)benzoic acid **1c** was precipitated as white crystals by reacting phthalic anhydride **1a** and phenylhydrazine **1b** in THF. Afterthat, the solid 2-(2-phenylhydrazinecarbonyl)benzoic acid was heated at 160-170°C to get corresponding 2-(phenylamino)isoindoline-1,3-dione **1d** structure. Afterwards, 2-(phenylamino)isoindoline-1,3-dione was reduced by using sodium borohydride, $NaBH_4$ in THF and 3-hydroxy-2-(phenylamino)isoindolin-1-one **1e** as an oily product was obtained in the $NaBH_4$ reduction of 2-(phenylamino)isoindoline-1,3-dione. Finally, formation of solid 2-phenylphthazin-2-ium-4-olate (betaine) **1f** was occurred by heating 3-hydroxy-2-(phenylamino)isoindolin-1-one at 130-140°C for hours.

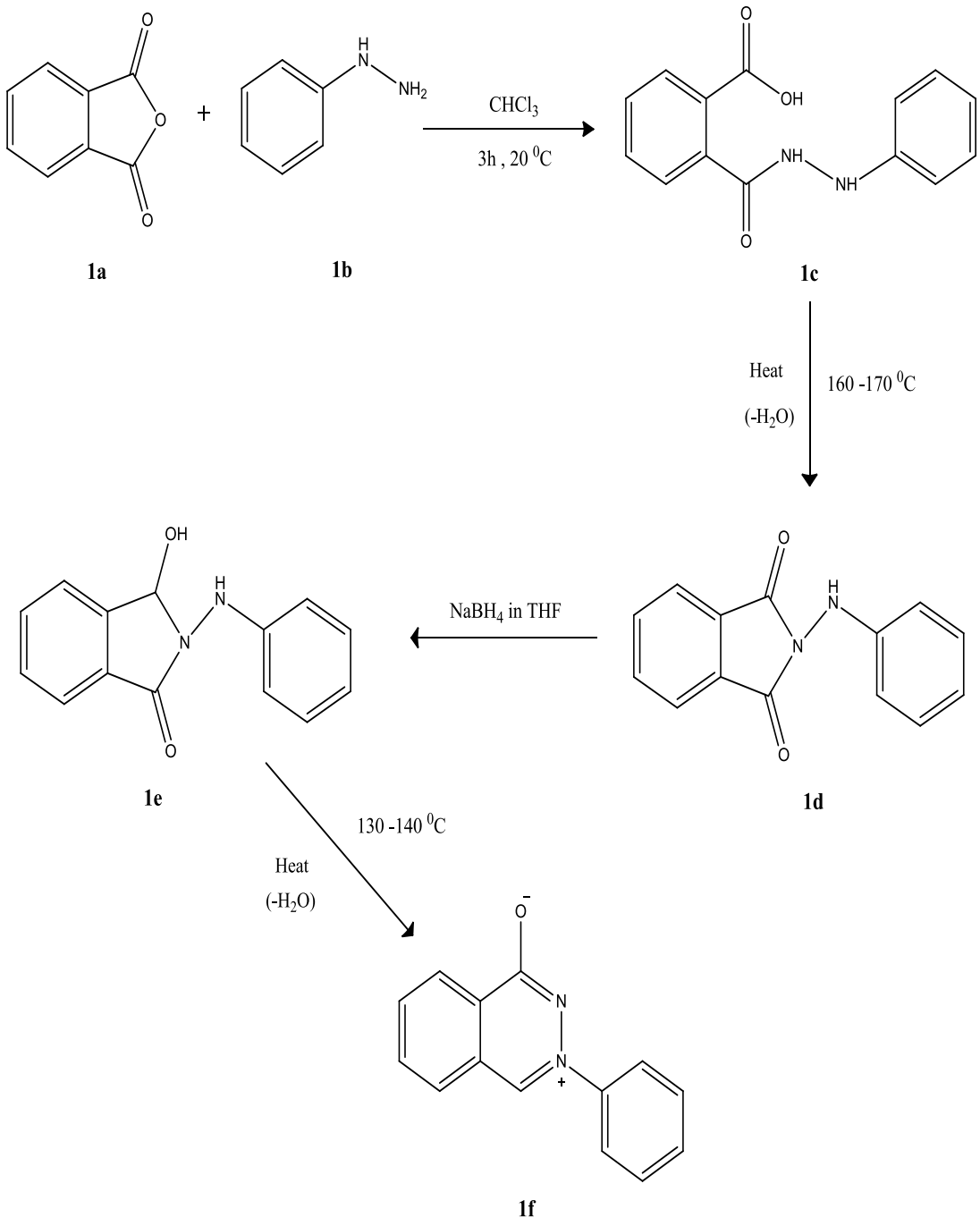

Figure 3.1. The schematic representation of the synthesis of 2-phenylphthazin-2-ium-4-olate (betaine) 1f

During the work, the synthesis of 2-(2-phenylhydrazinecarbonyl)benzoic acid was always obtained very easily and successfully. Afterthat, the conversion of 2-(phenylamino)isoindoline-1,3-dione was achieved from 2-(2-phenylhydrazine-

carbonyl)benzoic acid to heat enough temperature. When we heated 2-(2-phenylhydrazinecarbonyl)benzoic acid in sand bath, firstly we got some brown-red liquid material and we added ethanol on this material up to observation of yellow solid, which was called 2-(phenylamino)isoindoline-1,3-dione. In this step, ethanol was used to provide for the purification and crystallization of 2-(phenylamino) isoindoline-1,3-dione. Afterwards, the reduction of 2-(phenylamino)isoindoline-1,3-dione was performed with $NaBH_4$ in THF. At the end of $NaBH_4$ reduction, the large excess of dry acetone was used to decompose the excess of $NaBH_4$ and then excess of dry acetone was evaporated under vacuum. At the end of vacuum, 3-hydroxy-2-(phenylamino)isoindolin-1-one, which was an oily residue, was obtained. But, there is an important point to be considered in here that if the excess dry acetone was not evaporated totally under vacuum, the yield of related betaine would be very low to convert it. Moreover, it had sometimes caused the deterioration of chemical structure of betaine. So, we did not carry out the conversion of 2-phenylphthazin-2-ium-4-olate (betaine) from 3-hydroxy-2-(phenylamino) isoindolin-1-one in a cycloaddition reaction. To sum up, we heated the oily residue to the specified temperature in the experimental section, the conversion of 2-phenylphthazin-2-ium-4-olate (betaine) was achieved by obtaining significant amount and, again ethanol was used to provide for the purification and crystallization of betaine. And so, we investigated the characterization of chemical bonds for 2-(2-phenylhydrazine- carbonyl)benzoic acid, 2-(phenylamino)isoindoline-1,3-dione, 3-hydroxy-2-(phenylamino)isoindolin-1-one, 2-phenylphthazin-2-ium-4-olate (betaine) by using FT/IR. When we compared the IR spectra of these compounds, we used to the corresponding spectra of those compounds given by Katritzky and his co-workers[4].

As for the result of FT/IR spectroscopy analysis, first of all, the 2-(2-phenylhydrazinecarbonyl)benzoic acid **1c** structure is explained by the i.r. absorbtions for aromatic stretching band [*v* (KBr) (C=C) 1604 cm^{-1}], amide groups [*v* (KBr) (C=O) 1653 cm^{-1}], α,β-unsaturated carboxylic acid groups [*v* (KBr) (C=O) 1703 cm^{-1}] and NH stretching [*v* (KBr) (NH) 3292 cm^{-1}] **(Fig. 3.2)**. Second of all, the 2-(phenylamino)isoindoline-1,3-dione **1d** structure demonstrates an aromatic stretching band [*v* (KBr) (C=C) 1597 cm^{-1}], a strong carbonyl band and a shoulder [*v* (KBr) (C=O) 1705 and 1782 cm^{-1}] and NH stretching [*v* (KBr) (NH) 3317 cm^{-1}] **(Fig. 3.3)**. Third of all, the 3-hydroxy-2-(phenylamino)isoindolin-1-one **1e** structure is associated with i.r. absorbtions for aromatic stretching band [*v* (KBr) (C=C) 1604 cm^{-1}], five membered lactam carbonyl [*v* (KBr) (C=O) 1712 cm^{-1}] and OH band [*v* (KBr) (OH) 3464-3200 cm^{-1}] **(Fig. 3.4)**. Finally, the 2-phenylphthazin-2-ium-4-olate (betaine) **1f** structure indicates C^{+}-O^{-} band [*v* (KBr) (C^{+}-O^{-}) 1564 cm^{-1}] and an aromatic stretching band [*v* (KBr) (C=C) 1599 cm^{-1}] **(Fig. 3.5)**.

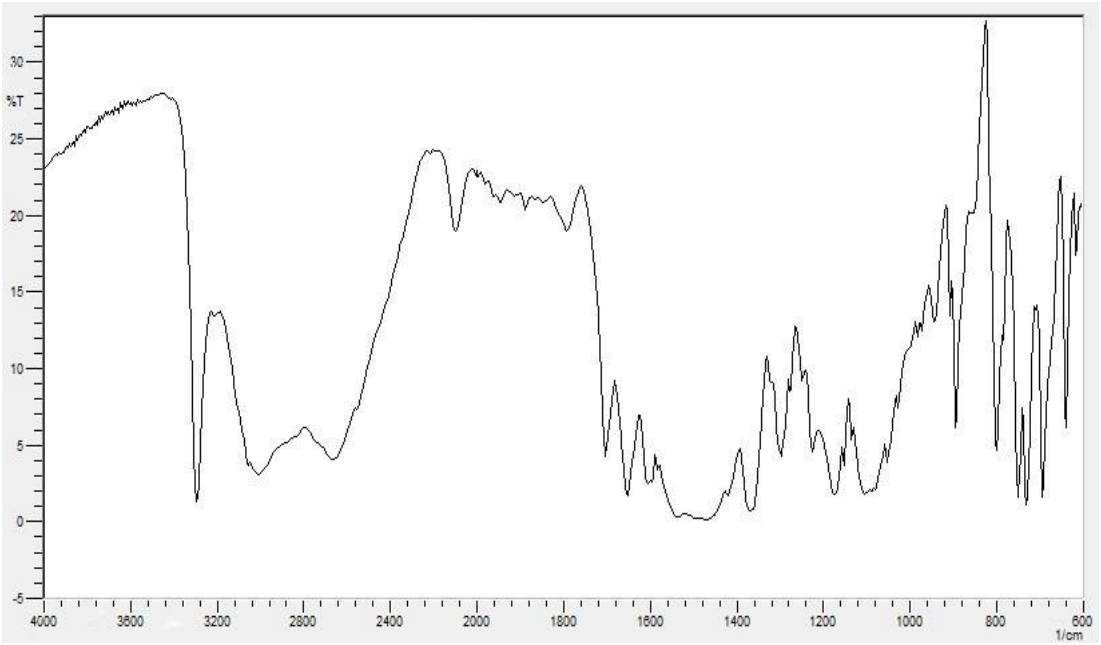

Figure 3.2. The IR spectrum of 2-(2-phenylhydrazinecarbonyl)benzoic acid, 1c (KBr)

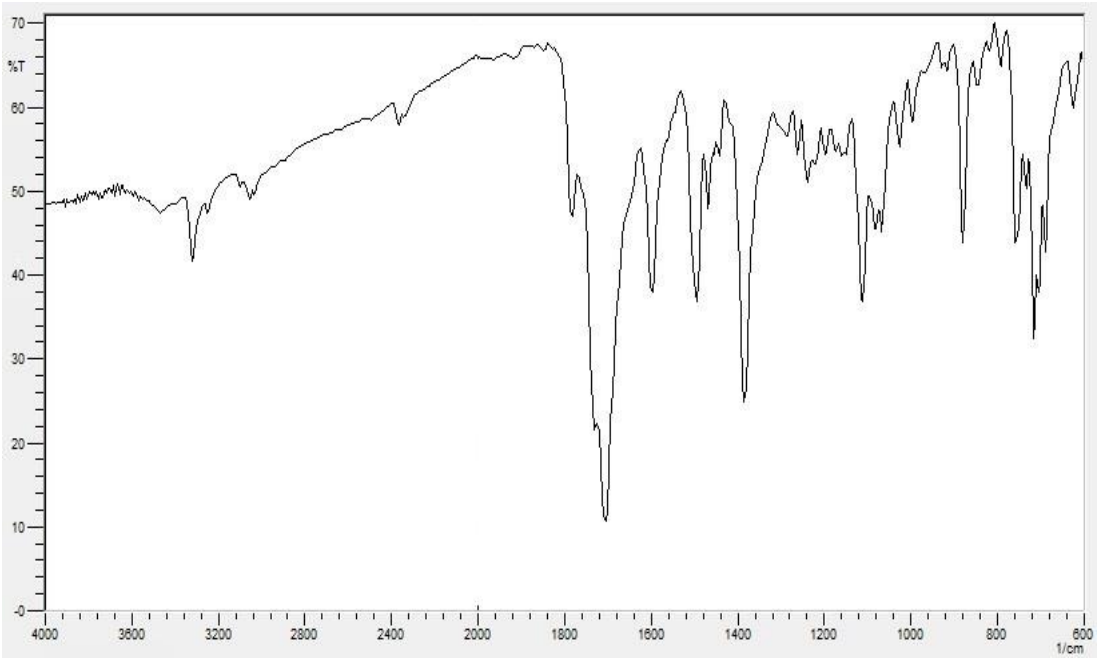

Figure 3.3. The IR spectrum of 2-(phenylamino)isoindoline-1,3-dione, 1d (KBr)

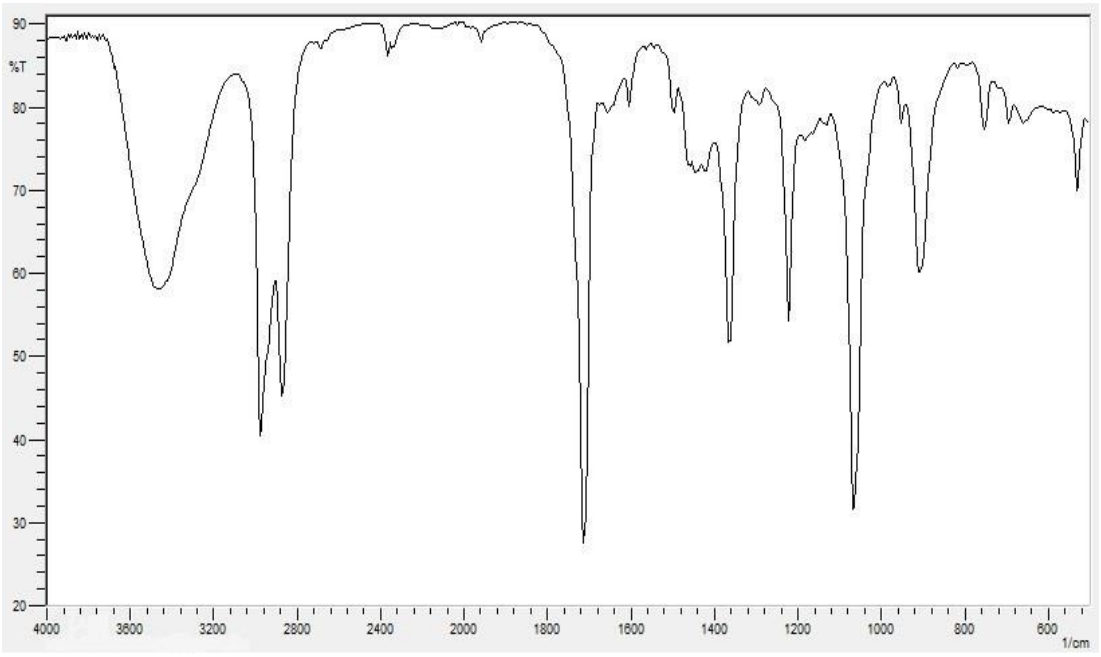

Figure 3.4. The IR spectrum of 3-hydroxy-2-(phenylamino)isoindolin-1-one, 1e (KBr)

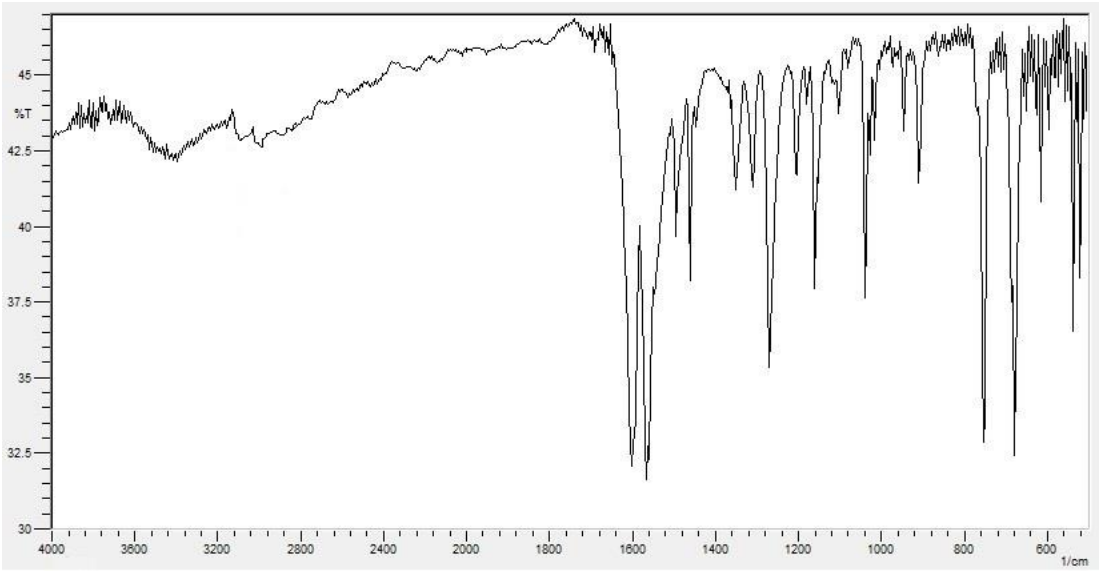

Figure 3.5. The IR spectrum of the 2-phenylphthazin-2-ium-4-olate (betaine), 1f (KBr)

3. 2. Synthesis of Carbon Nanosheets

Carbon nanostructures are currently under intense investigation for their exceptional electronic and mechanical properties. These properties result from the unique qualities of covalent sp^2-bonded carbon constrained to small dimensions and small numbers of atoms [95]. Two-dimensional (2D) materials are some of the most fascinating research targets nowadays. Graphene is an ideal system as a two-dimensional crystalline sheet of carbon atoms, for its infinite number of repetitive elements and long-range order. Graphene is an exciting two dimensional (2-D) monolayer carbon sheet [96]. Carbon sheets of a few nanometers thick (nanosheets) define a peculiar class of carbon materials with unique surface-to-volume ratio, smooth surface morphologies and thin edges, flexibility and elasticity, high thermal and chemical stability, and lightness [76]. Different from graphene, which consists

of a single layer of graphite sheet, carbon nanosheets (CNSs) are 2D carbon nanostructures a few nanometers thick [97]. In the synthesis of carbon nanosheets, aromatic compounds have an inherent tendency to form graphite-like structures because of their typical molecular structures comprised of hexagonal rings [98].

Most nanostructures derive their extraordinary configurations from topological defects in graphene sheets, and the energetically driven need to eliminate dangling bonds by folding in on themselves. Nanotubes, nano-onions, nanocones, and fullerenes fall into this category. Carbon nanosheets, however, preserve the graphene layers as relatively isolated structures despite their sometimes extensive topological defects. These structures hold promise for field emission and catalysis due to their sharp edges, upright orientation, and high surface area [95].

In this work, the synthesis of carbon nanosheets was tried to do with nitrogen (N_2) gas atmosphere and the air pyrolysis which were explained by Vasilios Georgakilas in the corresponding article [76]. However, anhydrous betaine (Sigma) was calcined only 400°C in an air pyrolysis in this method. Different from this method, we calcined 2-phenylphthazin-2-ium-4-olate (betaine) with air at four different temperatures (300°C, 350°C, 400°C and 500°C) and in nitrogen (N_2) gas atmosphere at 350°C. In other words, meaning of methods was the same; the temperature and medium were different. Moreover, we used to the combination of Scanning Electron Microscopy, FT/IR Spectroscopy and X-Ray Diffractometer to execute the characterization of carbon nanoheets.

3. 2. 1. The Studies of Synthesis of Carbon Nanosheets at 300°C in Air Pyrolysis

In this study, 2-phenylphthazin-2-ium-4-olate (betaine) was heated at 300°C with air pyrolysis for 2h, and 15min. The heating rate was 5 °C/min to get black-brown powder. Before the reaction took place, we had noted some important points and observations. At 150°C, the color change began from yellow to brown without melting. Betaine was completely melted and it had even brown color between 200°C and 205°C. Then, some gas evolution carried out significantly until the temperature reached 250°C. After that, we observed an unknown yellow-cottony material on the surface of black-brown powder, which can be known as carbon nanosheets, between 255°C and 285°C. This unknown material cannot contact with the black-brown powder. We collected it easily by using spatula in the reaction medium and later, we investigated the structure of this unknown material to decide that it was an untransformed or degraded material. Between 250°C and 300°C, some gas evolution and some bubbles on the surface of black-brown powder occurred and as a result, we obtained a black-brown powder in sufficient quantity. We examined to get information about the chemical bonds, structure and surface morphology of black-brown powder by using FT/IR Spectroscopy, X-Ray Diffractometer and Scanning Electron Microscopy (SEM).

In the result of FT/IR spectroscopy analysis, the peak at 1651 cm^{-1} can be ascribed for an aromatic stretching C=C band and it is skeletal vibration of carbon nanosheets. Because, when we analyzed the FT/IR spectrum, we observed that there is no information about the other functional groups and vibrations such as carbonyl group of amide, tertiary amine, C=N double bond, and C^{+}-O^{-} band. **(Fig. 3.6)**

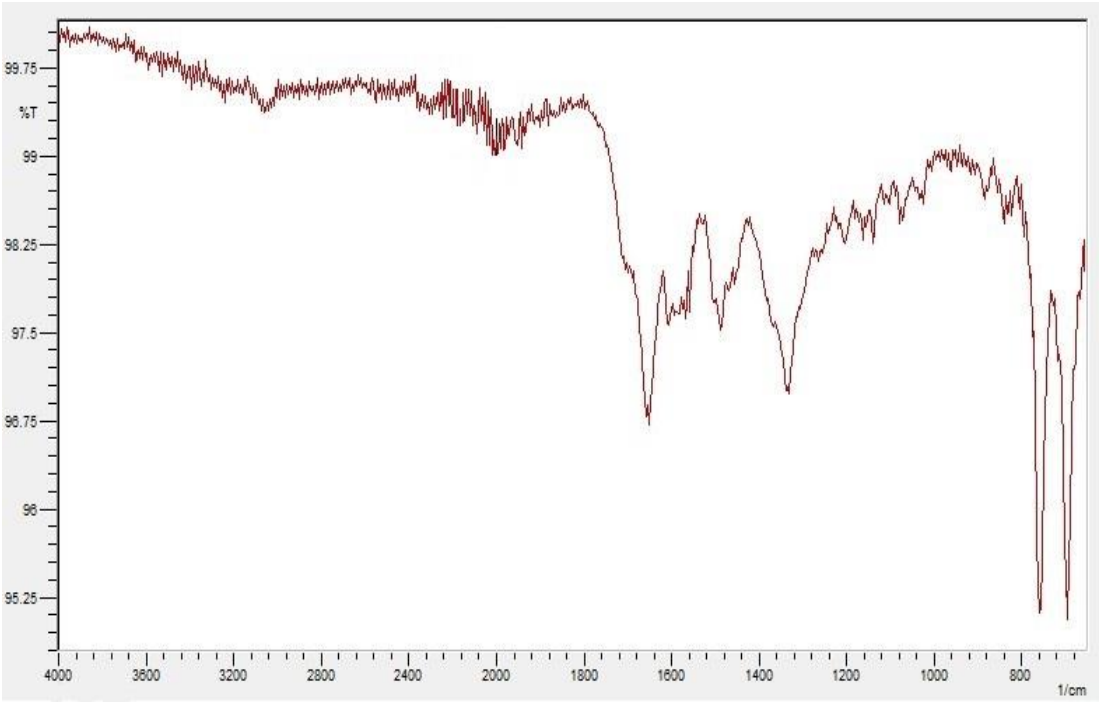

Figure 3.6. The IR spectrum of Carbon Nanosheet sample at 300 °C (KBr)

Fig. 3.7 shows the XRD pattern of carbon nanosheet sample at 300 °C. There are three main peaks in this diffraction pattern. The first peak is a broad and weak at 2θ = 6.40°. Because of the typical diffraction peak of graphene oxide (GO), it is possible to denote the presence of inter-few-layered graphene with defects. The second one is a strong and very broad peak at 2θ = 21.52° for the plane (002), corresponding to a d-spacing of 4.1259 nm. It indicates a lower degree of crystallization and the existence of some defects in the carbon nanosheet line. The third and final one is a very broad and weak peak at about 44.20°, corresponding to a d-spacing of 2.0474 nm. It is stated that the graphitization of the structure is not complete and it has a lower the degree of long-range order than that of bulk graphite. The results of XRD pattern are coherent with the SEM results of this product given below.

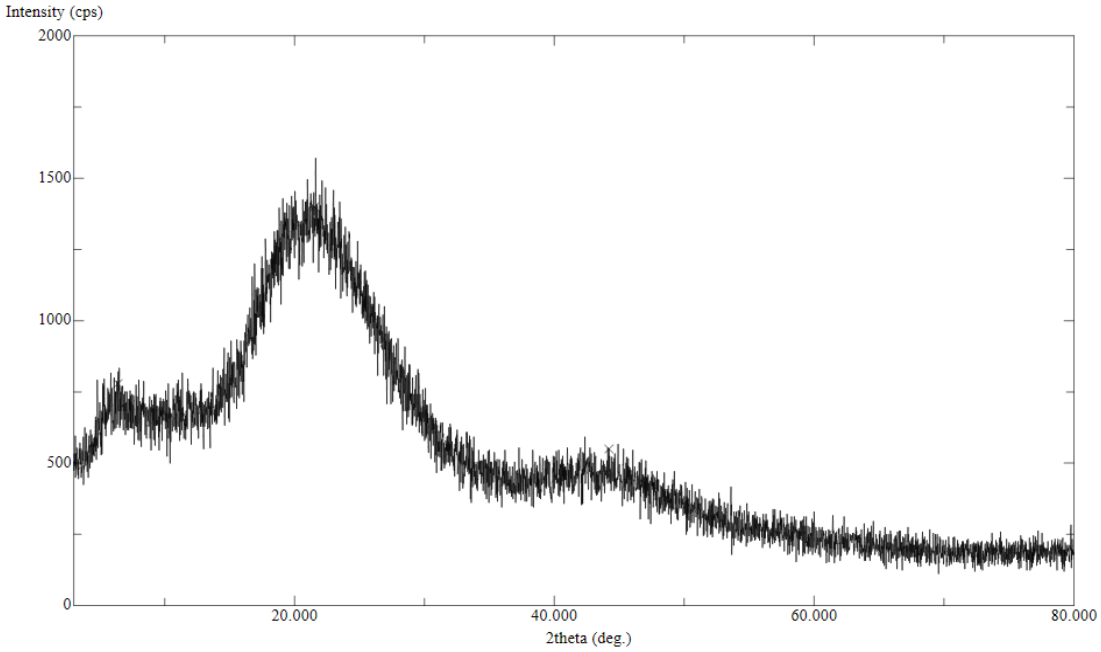

Figure 3.7. The XRD pattern of Carbon Nanosheet sample at 300 °C

The groundwork of carbon nanosheets consists of plenty of graphene layers and the formation of carbon nanosheets starts to approach the graphene layers each other by getting heat energy. Then, when the distance of graphene layers closes completely, they begin to leave from their groundwork slowly and vertical surface layers or sheets, which are called carbon nanosheets, perpendicular to the groundwork are obtained in angles between 50° and 90°. These sheets can be found regularly or irregularly on the groundwork. **(Fig. 3.8)**

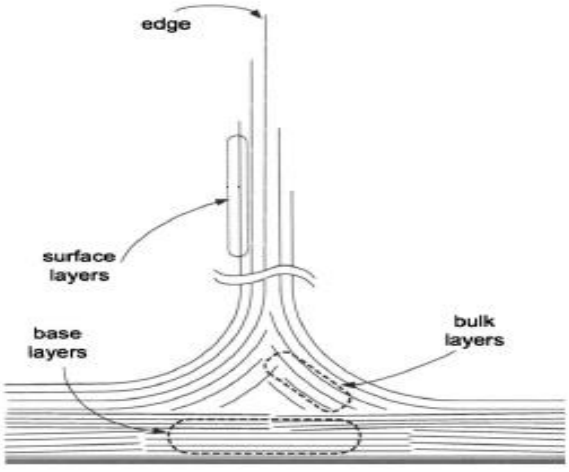

Figure 3.8. A Schematic Diagram of idealized Carbon Nanosheets

The SEM micrographs of carbon nanosheet sample at 300°C **(Fig. 3.9)** showed that the product comprises of a large number of bulk layers on the groundwork. In addition, they have many folds and they are unlike well-separated with each other. Moreover, there is a uniform thickness along the entire plane and a smooth, especially dense surface. Also, when we compared to our micrographs with idealized carbon nanosheets structure, we can say that the distance of graphene layers closed wholly and there were only bulk layers on the surface of the product, nothing else such as sharp edges and vertical surface layers. To summarize, micrograph results demonstrate that the formation of CNSs is the initial stage at this temperature.

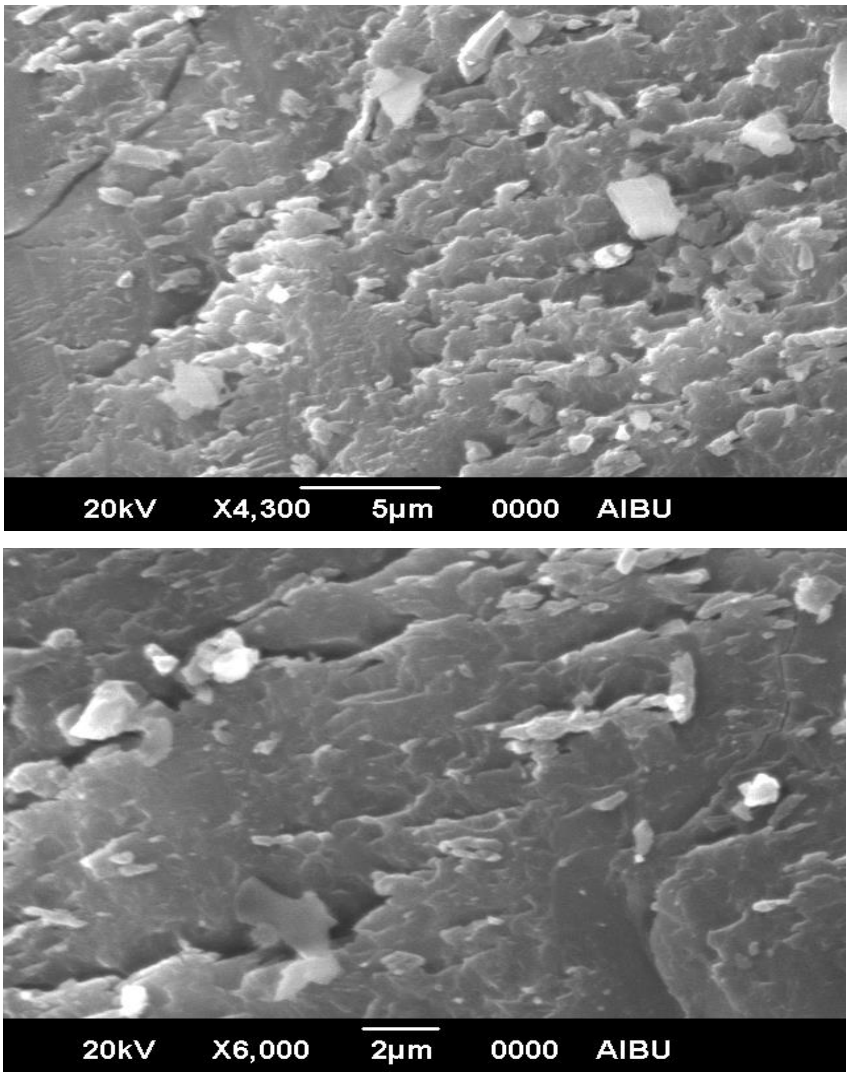

Figure 3.9. The SEM Micrographs of Carbon Nanosheet sample at 300 °C

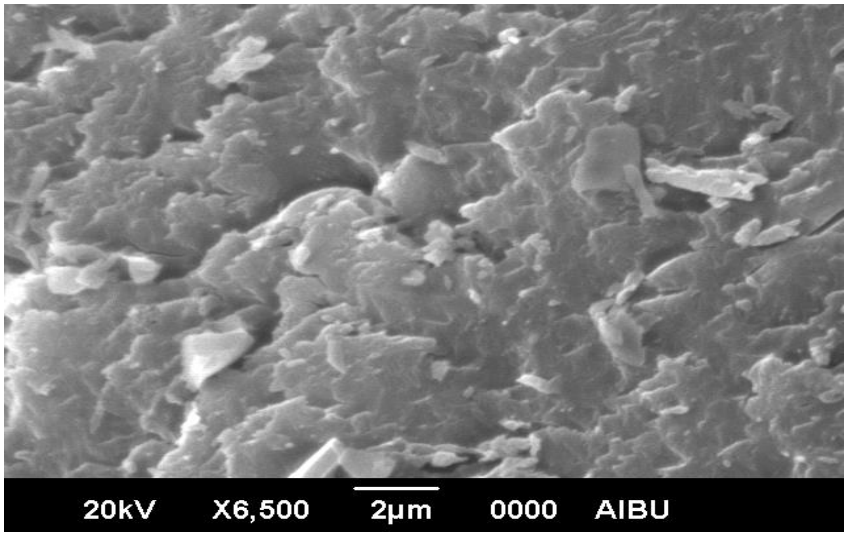

Figure 3.9. The SEM Micrographs of Carbon Nanosheet sample at 300 °C (continued)

EDS makes use of the X-Ray spectrum emitted by a solid sample bombarded with a focused beam of electrons to obtain a localized chemical analysis [84]. In other words, EDS are used to make the chemical analysis in the surface area of a specific location, not whole sample.

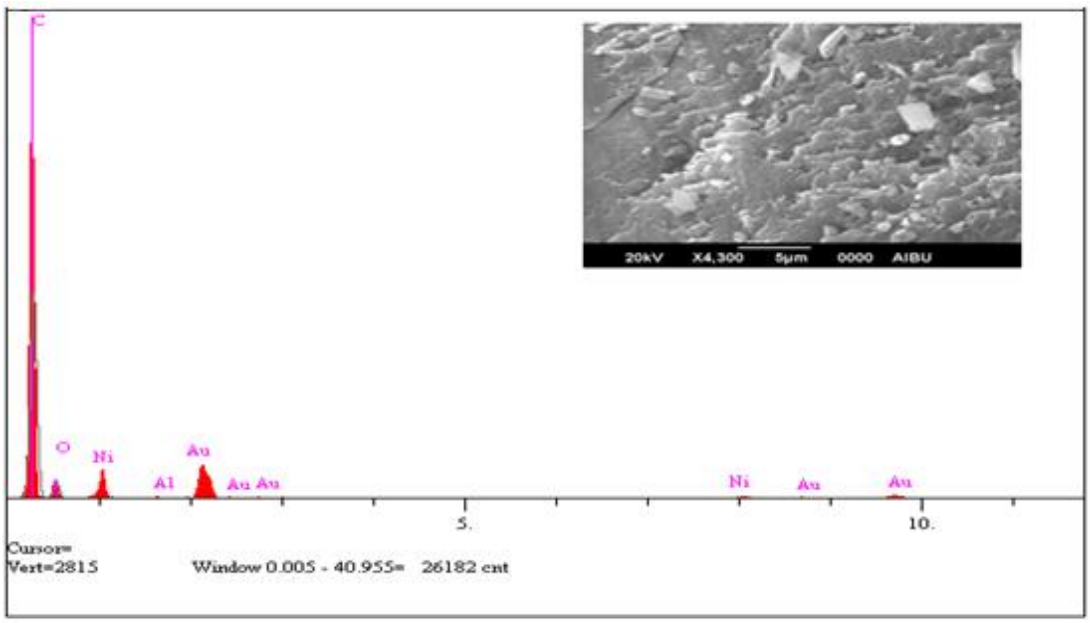

Figure 3.10. The SEM Image and Corresponding EDS Spectrum of Carbon Nanosheet sample at 300 °C

In the EDS spectrum, we saw that there were five different elements (C, O, Al, Au, and Ni) and we know that Ni, Al and Au come from coating material of the product. When we consider the FT/IR spectrum of the product, there was only an aromatic stretching C=C band and it indicates that there must be only carbon atoms in the product. It may be in associations with the fact that oxygen element appears in the EDS spectrum of the product because of the graphene oxide defects in moist air atmosphere. If the oxygen element came from the structure of product, we should see corresponding characteristic peak of it such as hydroxyl, carbonyl group in the FT/IR spectrum or another different element in the EDS spectrum such as nitrogen element. **(Fig. 3.10)**

3. 2. 2. The Studies of Synthesis of Carbon Nanosheets at 350°C in Air Pyrolysis

In the study of the synthesis of CNSs, 2-phenylphthazin-2-ium-4-olate (betaine) was heated at 350°C with air pyrolysis for 2h, 15min; a heating rate of 6 °C/min to obtain black-brown powder. While the pyrolysis of betaine was occurring at this temperature, we noted considerable points and observations of the reaction. First of all, the color change of betaine began from yellow to brown without melting at 175°C. It had brown color completely at 195°C and was started to melt between 200°C and 204°C. Later on, until the temperature reached 260°C, some gas evolution and crackling sound from the compound carried out significantly. Between 260°C and 290°C, we observed the same yellow-cottony material on the surface of product as in the studies of synthesis of CNSs at 300°C. They are in contact with each other at this temperature range. Afterwards, the surface contact of them with the each other

was cut off spontaneously. Between 300°C and 350°C, gas evolution from the product continued by increasing and the color of it was darker than at the beginning of it. Finally, black-brown powder could be from the pyrolysis of betaine. The investigation of the black-brown powder was made by the analysis of Scanning Electron Microscopy, FT/IR Spectroscopy and X-Ray Diffractometer to determine whether the synthesis of CNSs carried out correctly or not.

In the FT/IR spectra of the synthesis of CNSs at 350 °C **(Fig. 3.11)**, the peak at 1643 cm^{-1} indicates a strong aromatic stretching band [*v* (KBr) (C=C) 1643 cm^{-1}] and there is no another substantial vibrations in the FT/IR spectra of the product such as carbonyl, hydroxyl, amide and amine groups. Consequently, when we consider on this FT/IR spectra, we can say that this strong aromatic stretching vibration is based on vibration of the product and it have supported to our considered carbon nanosheet structure **1g**.

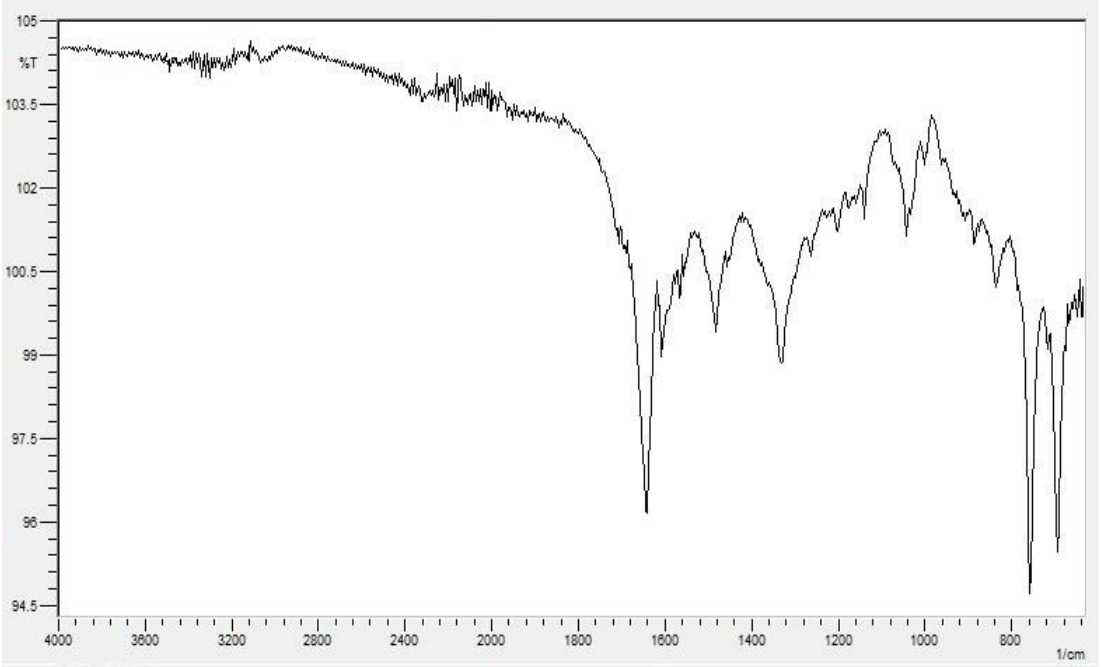

Figure 3.11. The IR spectrum of Carbon Nanosheet sample at 350 °C (KBr)

In the XRD pattern of carbon nanosheet sample at 350 °C (**Fig. 3.12**), there are two important broad peaks. The first peak is a very broad and strong at a diffraction angle (2θ) of 21.38° for the plane (002) and the interlayer spacing is computed to be about 4.1526 nm. This result defines the lower degree of crystallization and some defects. The formation of unknown yellow-cottony material led to these surface defects between carbon nanosheets. Also, It may be in associations with the fact that it shows the existence of regions of expanded stacking of more corrugated in the existing at the edge areas in agreement with the SEM results. The second broad peak at a diffraction angle (2θ) of 44.40° XRD pattern denotes that the graphitization of the structure does not occur entirely and the corresponding interlayer d-spacing is calculated to be a 2.0386 nm.

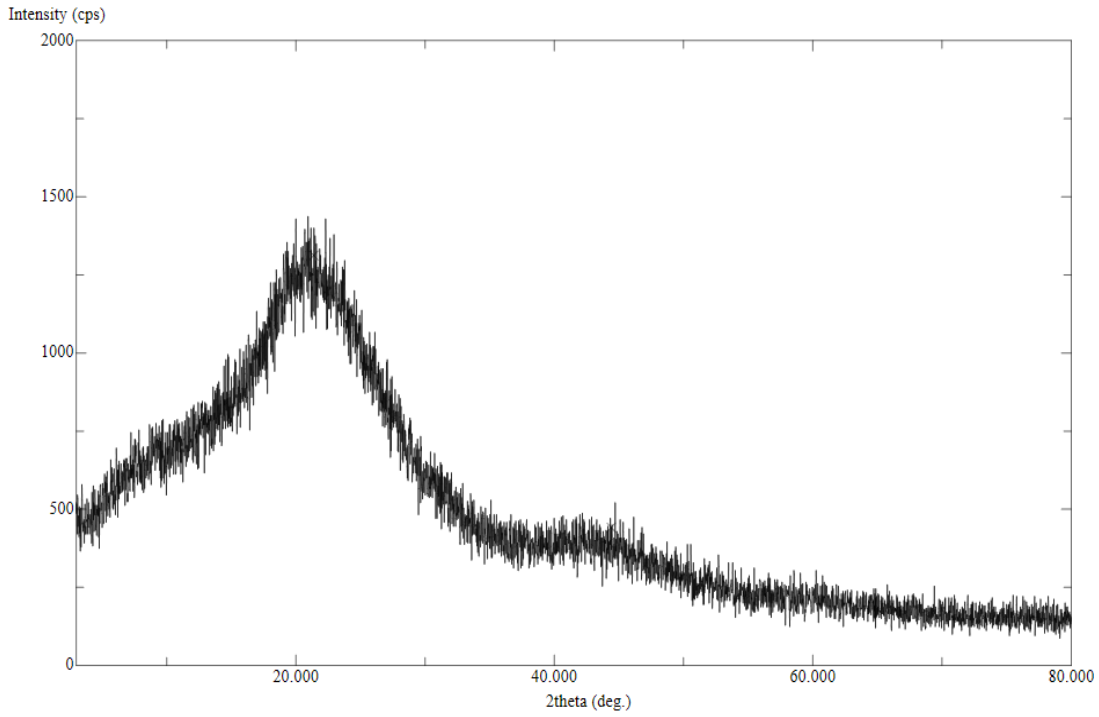

Figure 3.12. The XRD pattern of Carbon Nanosheet sample at 350 °C

According to the results of the SEM micrographs at 350 °C, **Fig. 3.13(a)–(e)** demonstrate that there are large quantity of flexible thin nanosheets or layers with uniform thickness along the translucent surface and we observe well-ordered multilayered graphene layers and we cannot see any impurities such as degraded material, carbon spheres, carbon nanotubes and other types of carbon nanostructures. The graphene layers of the product on the groundwork are so close to each other and they have sharp edges, vertical layers and many corrugated. Also, they have been placed interlaced with each other in a large surface area and have a vertical orientation with respect to the groundwork and unfortunately, it is not possible to provide the information about the height of layers or sheets in these SEM micrographs. Especially in **Fig. 3.13(c, d),** the carbon nanosheets or layers are spread on the translucent surface in a highly ordered and dense manner.

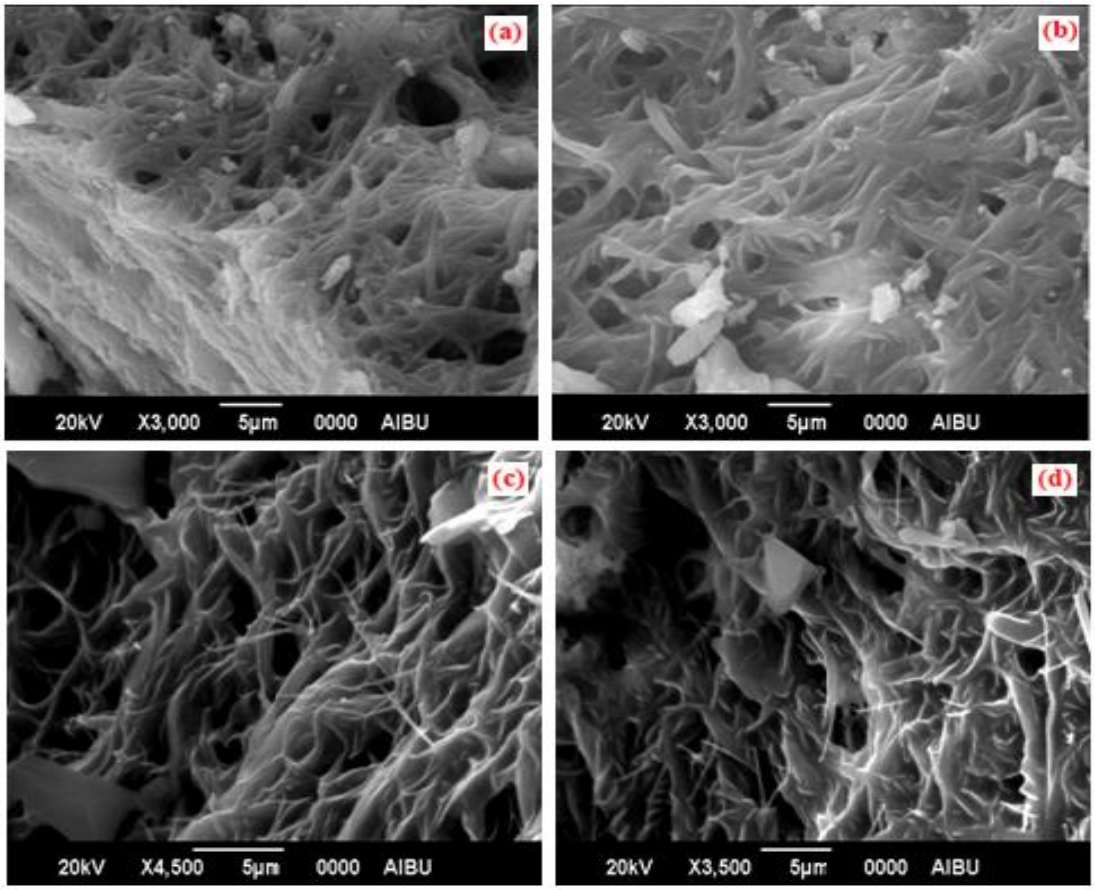

Figure 3.13. The SEM Micrographs of Carbon Nanosheet sample at 350 °C

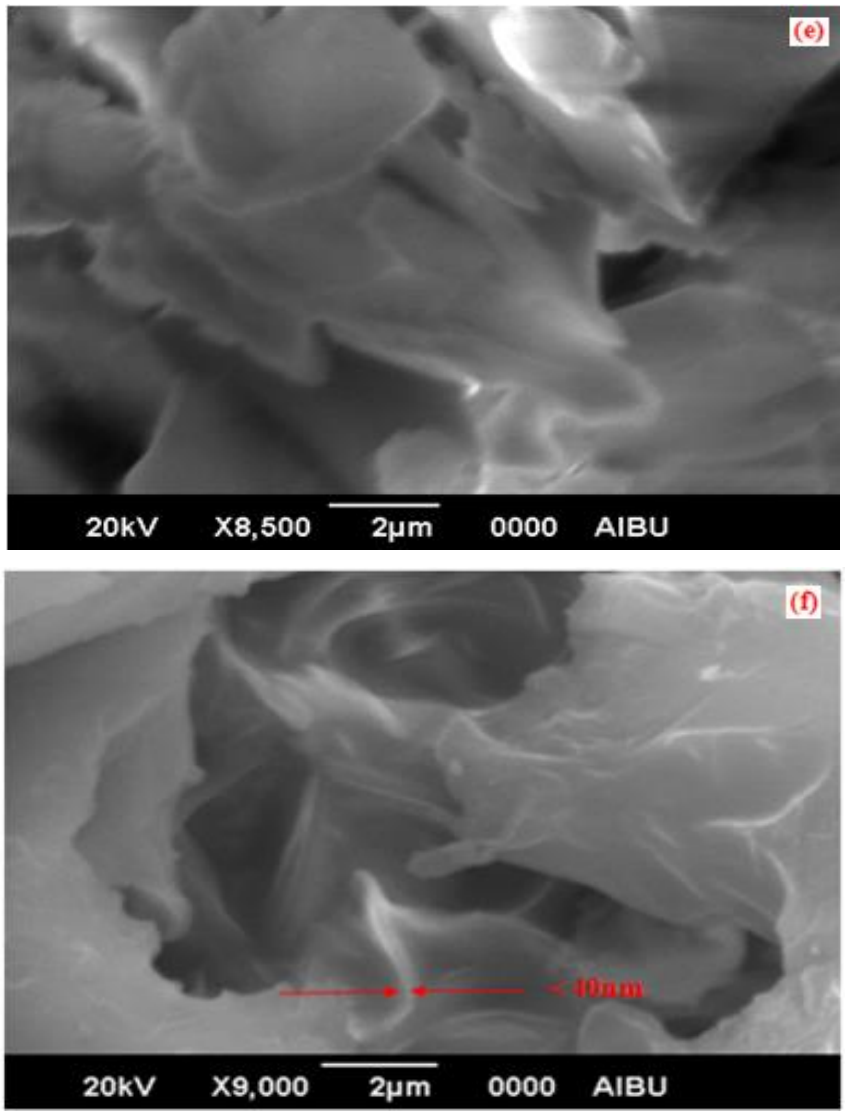

Figure 3.13. The SEM Micrographs of Carbon Nanosheet sample at 350 °C (Continued)

Fig. 3.13(f) shows that the carbon nanosheets seem uniform, translucent and thicknesses of them are less than < 40 nm. Moreover, when we investigate these nanosheets individually, we can say that because of transparent, the thickness of individual nanosheets can be thinner in a few nanometers. Finally, The SEM micrographs of carbon nanosheets sample at 350°C indicate that the formation of CNSs was carried out successfully.

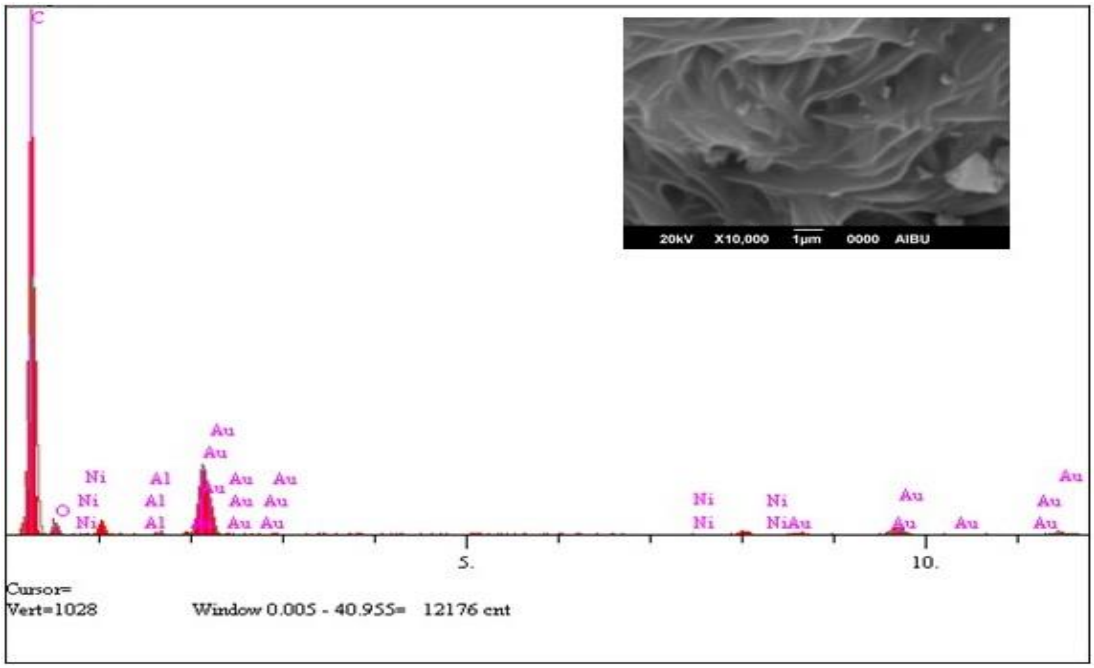

Figure 3.14. The SEM Image and Corresponding EDS Spectrum of Carbon Nanosheet sample at 350 °C

As shown in **Fig. 3.14,** Ni, Al and Au elements can be found on the surface of coating material and the component element of CNSs is carbon and the amount of carbon on the surface of CNSs is the percentage of 83.64. There is an important amount of oxygen (16.36 %) on the surface. It may be in associations with the fact that because of moist air medium, oxygen is seen in EDS spectrum of CNSs sample at 350 °C.

3. 2. 3. The Unknown Yellow-Cottony Material

This unknown material was found as a yellow cottony shape in the wall of reaction flask without contacting with the surface of CNSs. It was collected easily by using spatula in the reaction medium. Then, it was placed between the lam and lamella into the sand bath and was heated again at 350°C to understand that it was an untransformed or degraded material. Therefore, heating of it at 350°C was carried

out without air pyrolysis for 2h, 15min, a heating rate of 5 °C/min. At a result of the reaction, there was no change on the physical structure of this material such as color and shape. So, we applied some chemical analysis such as Scanning Electron Microscopy, FT/IR Spectroscopy and X-Ray Diffractometer in order to determine whether the material was an untransformed or degraded material.

The formation of the structure of carbon nanosheets can be defined with four different layers. These are base layer, which is called groundwork, bulk layer, surface layer and sharp edges. These properties or structures indicates us whether it is the carbon nanosheets or not. According to the results of the SEM micrographs of this material, the product is composed of large amount of nanograss. They have located irregularly on the surface of the material. **(Fig. 3.15)**

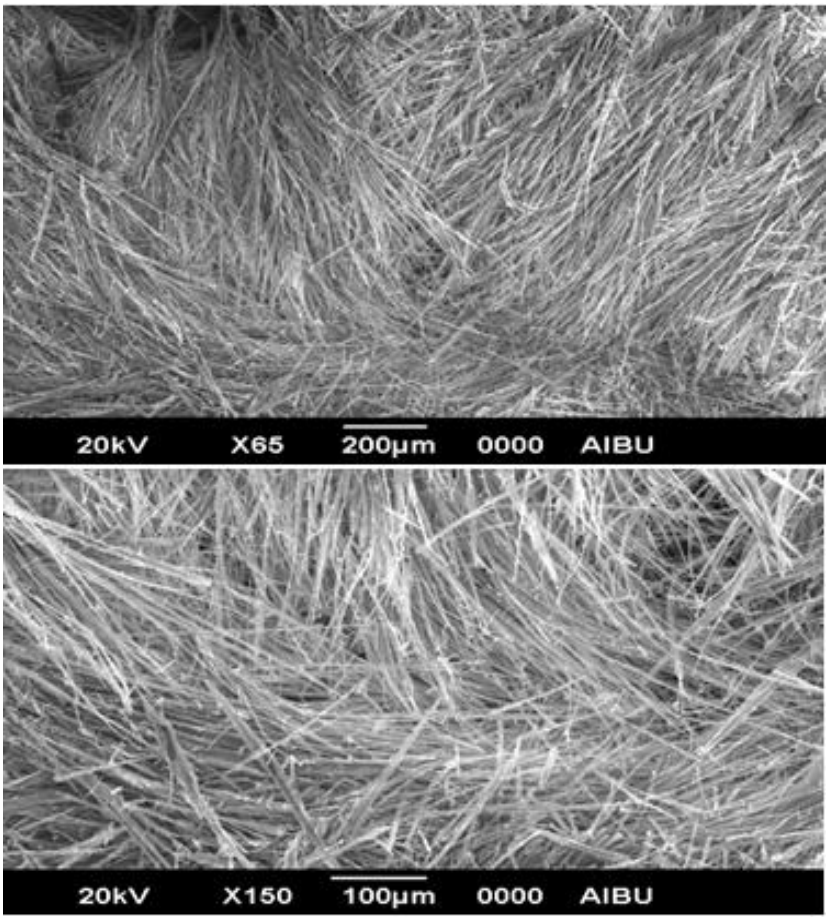

Figure 3.15. The SEM Micrographs of Unknown Yellow-Cottony Material

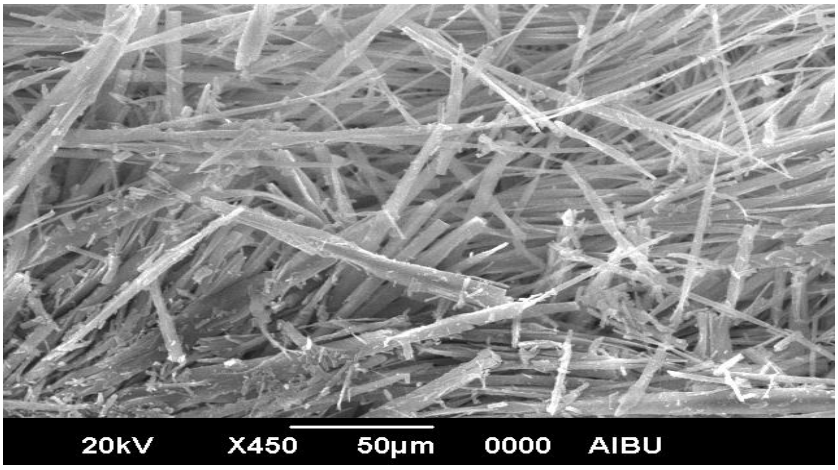

Figure 3.15. The SEM Micrographs of Unknown Yellow-Cottony Material (Continued)

According to the Cletus Nunes article about the betaines [101], we determined to the corresponding peaks about the 2-phenylphthazin-2-ium-4-olate (betaine) on the XRD pattern. There are five characteristic sharp peaks for betaine at the diffracion angles (2θ) of 15.20°, 17.06°, 18.64°, 24.84° and 26.14°. The other sharp peaks are related to the by-product as a result of the synthesis of 2-phenylphthazin-2-ium-4-olate (betaine).

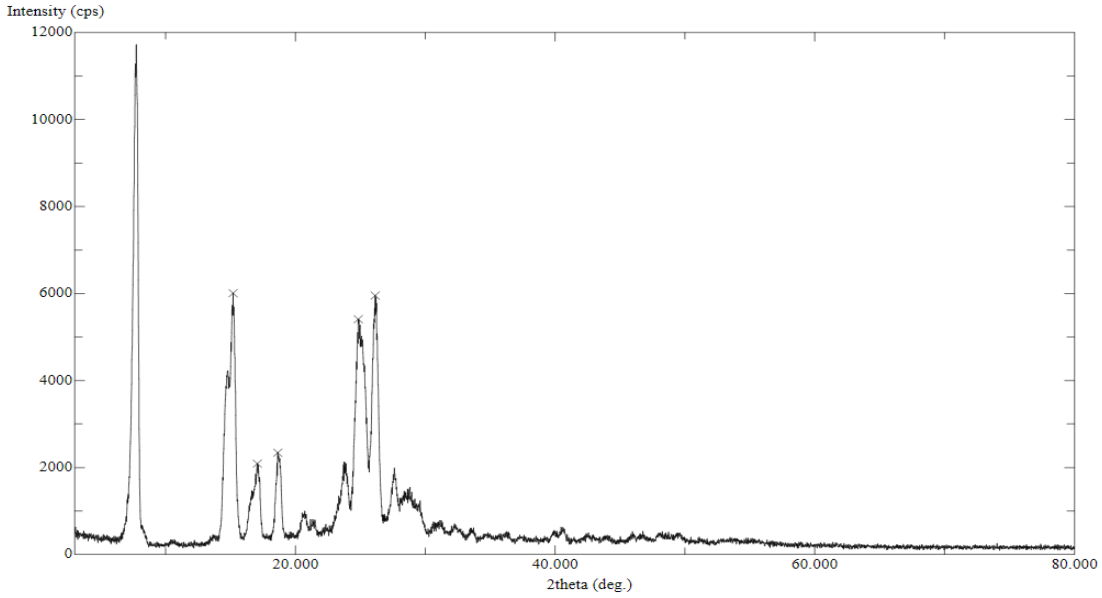

Figure 3.16. The XRD pattern of 2-phenylphthazin-2-ium-4-olate (betaine)

Additionally, the comparing of the XRD patterns of unknown yellow-cottony material and 2-phenylphthazin-2-ium-4-olate (betaine) **(Fig. 3.17)** was used to provide the complementary evidence. Whereas the XRD pattern for unknown yellow-cottony material shows the high intensity sharp peak at 2θ value of 9.30, we cannot observe any characteristic sharp peak for 2-phenylphthazin-2-ium-4-olate (betaine) at diffraction angle (2θ) between 0° and 10.00°. Moreover, the XRD pattern indicates that both of them have some sharp peaks at different diffraction angles (2θ) between 15.00° and 30.00°. In brief, when we compare all the diffraction angle of these materials, we exactly say that the XRD pattern of unknown yellow-cottony material is not the same with the XRD pattern of 2-phenylphthazin-2-ium-4-olate (betaine).

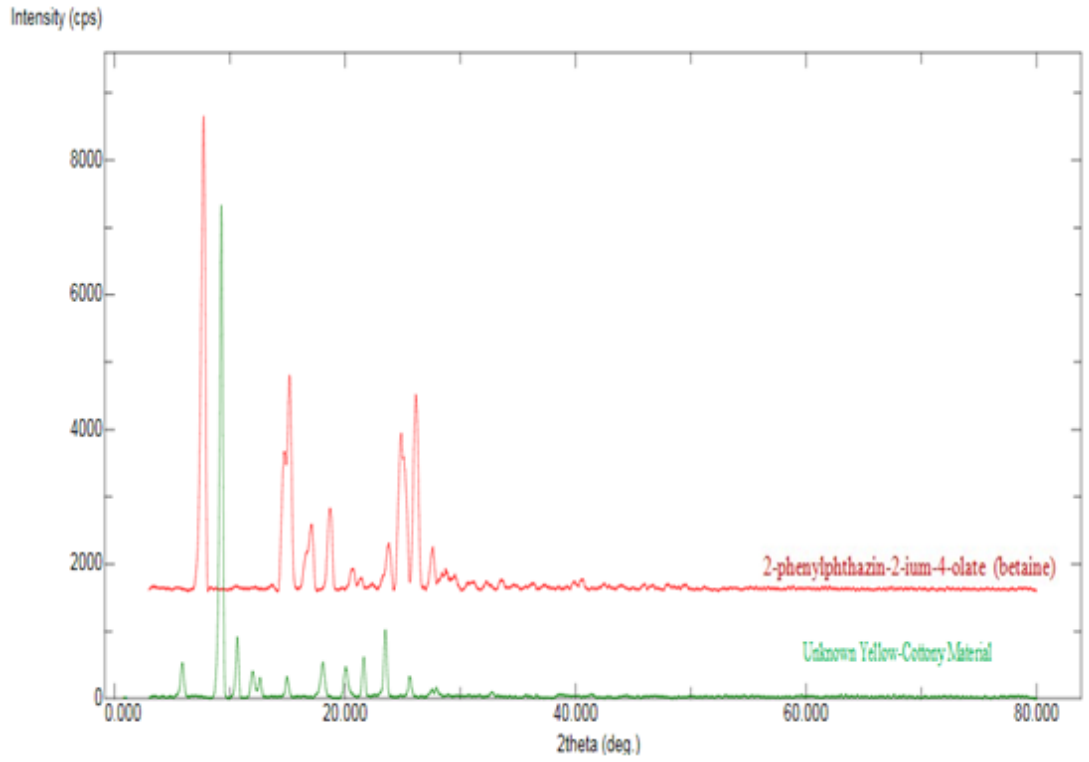

Figure 3.17. The XRD patterns of Unknown Yellow-Cottony Material and 2-phenylphthazin-2-ium-4-olate (betaine)

FT/IR spectrum gives general information about what functional groups are present, but not always. it is not possible to learn the whole structure of the molecule with only IR spectrum. So, we should have the mass spectrum and NMR spectrum of that matter to determine the molecular structure. At present, we have FT/IR spectrum of this unknown material to understand what type of functional groups are present in the molecule, not to determine the structure of the material. Detailed information of structure of this material is not important for us. In the FT/IR spectra of the unknown yellow-cottony material **(Fig. 3.18)**, there are no substantial vibrations between 1700-4000 cm^{-1} such as carbonyl, hydroxyl, and amide groups. The peak at1639 cm^{-1} can be important to this material, It may indicate a strong C=C stretching band.

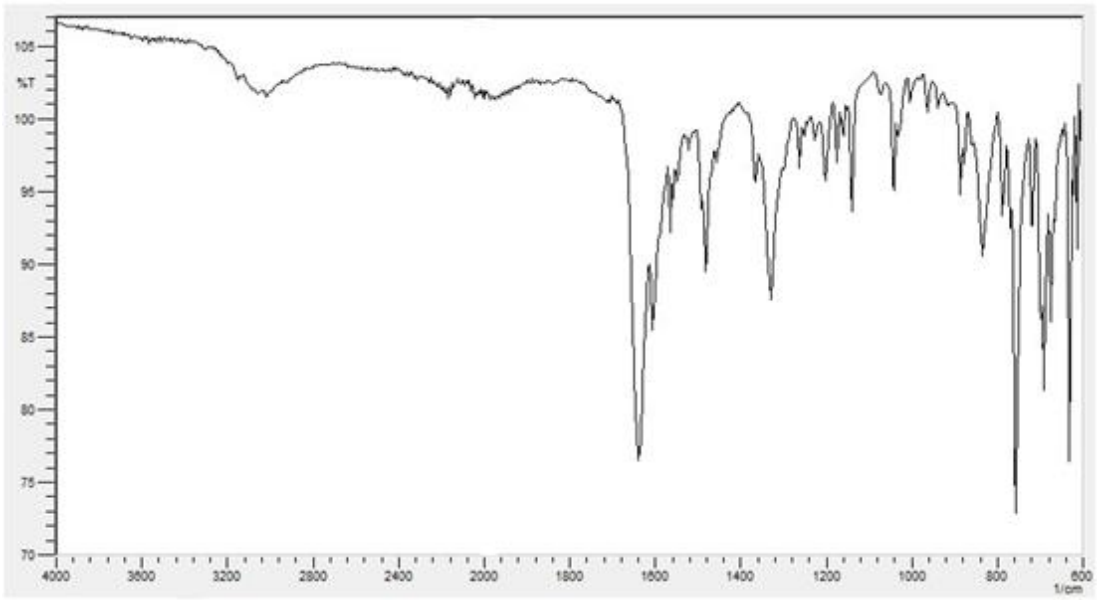

Figure 3.18. The IR spectrum of Unknown Yellow-Cottony Material (KBr)

As the result of these informations (SEM micrographs, FT/IR spectrum and XRD diffraction patterns), it does not have any properties of betaine or carbon nanosheets. We exactly say that it is not an untransformed material. It is a degraded material and also it is composed of the free radicals in the reaction medium as a result of pyrolysis.

3. 2. 4. The Studies of Synthesis of Carbon Nanosheets at 400°C in Air Pyrolysis

In this work, 2-phenylphthazin-2-ium-4-olate (betaine) was calcined at 400°C with air pyrolysis for 2h, 15min. The heating rate was 5 °C/min to get black-brown powder. While the reaction was taking place, we observed some significant developments in the reaction and we noted these observations. Firstly, the color change of betaine began from yellow to brown without melting at 180°C. It was started to melt slowly and had brown color completely at 195°C. After that, it was totally melted between 202°C and 205°C. Until the temperature reached from 205°C to 250°C, the high amount of gas evolution was seen and some crackling sound from the compound was heard. There was no important changing between 250°C and 300°C. The degraded material, which was called unknown yellow cottony material previously, was started to form at 300°C. It was collected in the wall of reaction flask without contacting with the surface of product between 300°C and 350°C. Then, the color of the degraded material turned from yellow to brown completely by burning with heat at 355°C. Finally, sufficient amount of black powder was synthesized with air pyrolysis at 400°C and the chemical analysis of it was made with FT/IR Spectroscopy, Scanning Electron Microscopy (SEM) and X-Ray Diffractometer.

FT/IR spectrum of carbon nanosheet sample at 400 °C recorded form its KBr pellet is shown in **Figure 3.19**. There is no important vibration peak between 1700-4000 cm^{-1} for this product. The peak at 1651 cm^{-1} is the characteristic vibration. It attributes an aromatic C=C stretching band.

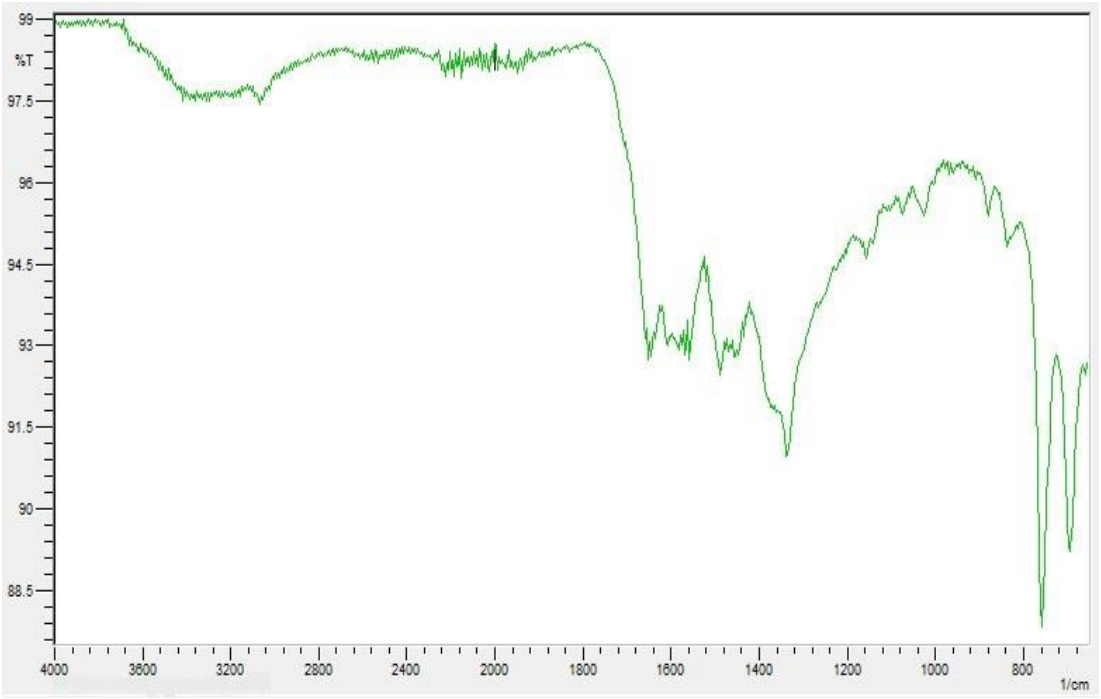

Figure 3.19. The IR spectrum of Carbon Nanosheet sample at 400 °C (KBr)

The XRD pattern of carbon nanosheet sample at 400 °C is shown in **Fig. 3.20**. There are three observed peaks, which approve the crystalline nature of the product, in the XRD pattern. The observed broad peak at 9.38° is indicative of the inter-few-layered graphene, corresponding to a d-spacing of 9.4207 nm. It looks like the characteristic diffraction peak of graphene oxide. The other observed peak is a strong and very broad peak at a diffraction angle (2θ) of 23.12° for the plane (002), corresponding to a d-spacing of 3.8438 nm. It signifies a lower degree of crystallization and the presence of some graphene-sheet line defects. The final broad peak on the XRD pattern is observed at a high diffraction angle (2θ) of 44.04° and the interlayer spacing is calculated to be a 2.0545 nm. It specifies that there is an uncompleted graphitization structure and it has a lower the degree of long-range order than that of normal graphite. The results of XRD diffraction pattern have been supported with the SEM results of this product given below.

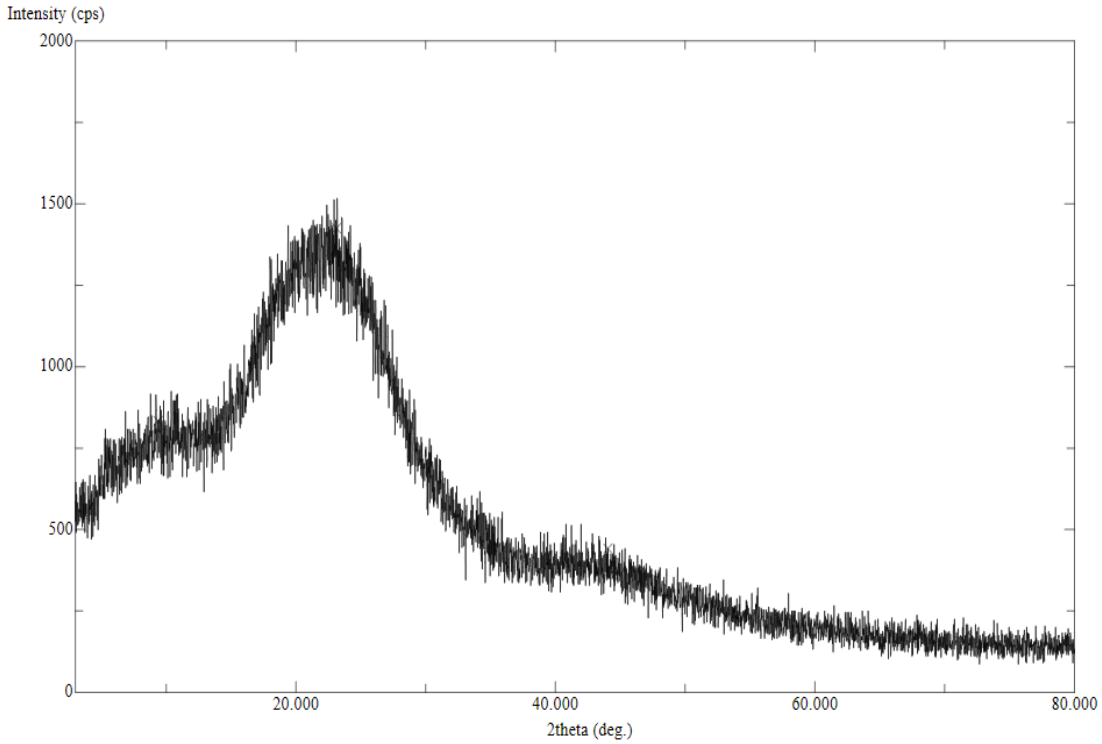

Figure 3.20. The XRD pattern of Carbon Nanosheet sample at 400 °C

Fig. 3.21 shows the surface morphology of the heat treated sample of carbon nanosheets at 400 °C. There are several flexible nanosheet layers on the surface of the product. The layers are overlapped with each other to the groundwork and show many irregularities and are not continuous. When we examine the SEM micrographs of this product in detail, we say that there are no any impurities such as degraded material, carbon spheres, carbon rods and other types of carbon nanostructures. Also, these micrographs show that the formation of CNSs was carried out successfully on the graphene layers. However, these sheets broke off from their roots because of the high heat energy. In accordance with the SEM micrographs, this temperature is too high for the formation of carbon nanosheets on the groundwork of graphene layers.

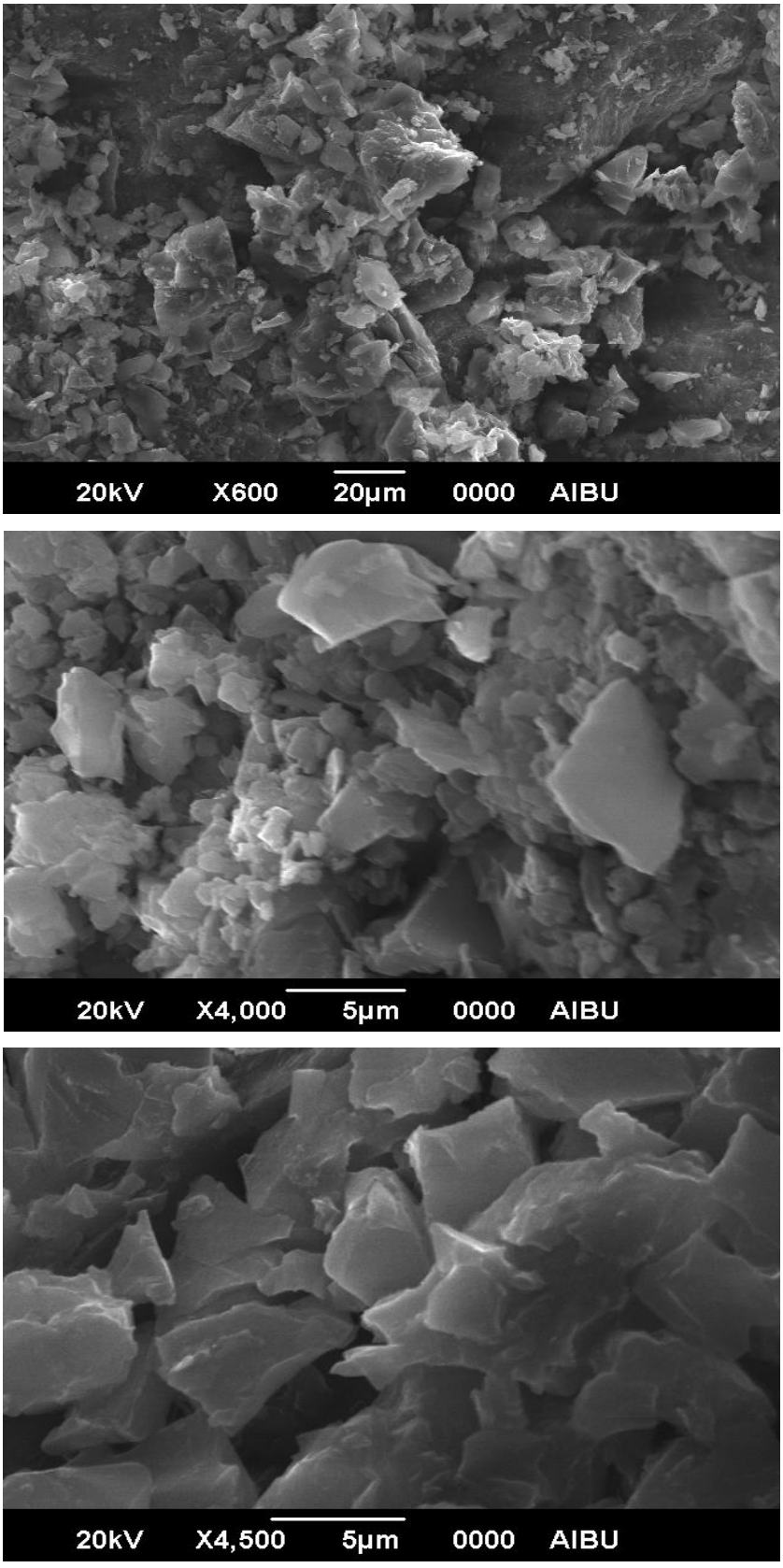

Figure 3.21. The SEM Micrographs of Carbon Nanosheet sample at 400 °C

The EDS spectrum of the heat treated sample of carbon nanosheets at 400 °C was shown in **Figure. 3.22**. Carbon, which is the based element of CNSs, is found the percentage of 74.96 on the surface of the product. Also, there is an important amount of oxygen (25.04 %) on the surface. In my opinion, oxygen element was held on to the surface of the product because of high heat energy in the air pyrolysis.

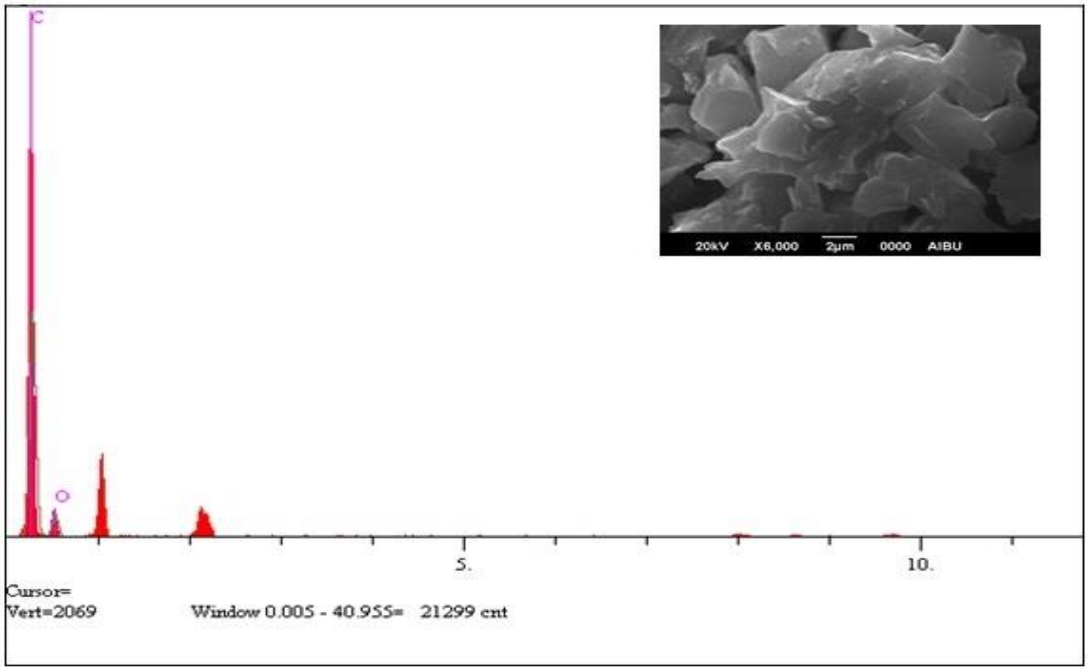

Figure 3.22. The SEM Image and Corresponding EDS Spectrum of Carbon Nanosheet sample at 400 °C

3. 2. 5. The Studies of Synthesis of Carbon Nanosheets at 500°C in Air Pyrolysis

In the study of the synthesis of CNSs at 500°C was executed by heating 2-phenylphthazin-2-ium-4-olate (betaine) with air pyrolysis for 2h, 15min; a heating rate of 5 °C/min to get black-brown powder. When the reaction took place, we had noted some important points and observations. At first, the color of betaine turned from yellow to brown without melting at 175°C. It had entirely brown color at 196°C and was melted between 201°C and 205°C. We saw the high amount of gas

evolution and heard some crackling sound from the compound when the temperature reached from 205°C to 260°C. Until the temperature reached at 300°C, gas evolution from the product continued by increasing and the color of product was darker than at the beginning of it. At 300°C, the formation of degraded material occurred on the surface of the product. Then, the color of the degraded material started to turn from yellow to brown at 315°C and it had dark brown color completely at 360°C. There was no important changing between 360°C and 500°C. Finally, the black powder sample of CNSs could be gotten from the pyrolysis of betaine and the chemical analysis of the product was made by using Scanning Electron Microscopy, FT/IR Spectroscopy and Thermal Gravimetric (TG/DTA) Analyzer.

FT/IR Spectroscopy is useful in determining chemical structure because energy that corresponds to specific values allows us to identify various functional groups within a molecule. An IR spectrum usually extends from radiation around 4000 cm^{-1} to 600 cm^{-1} and can be split into the functional group region and the fingerprint region. The fingerprint region is different for each molecule just like a fingerprint is different for each person [100].

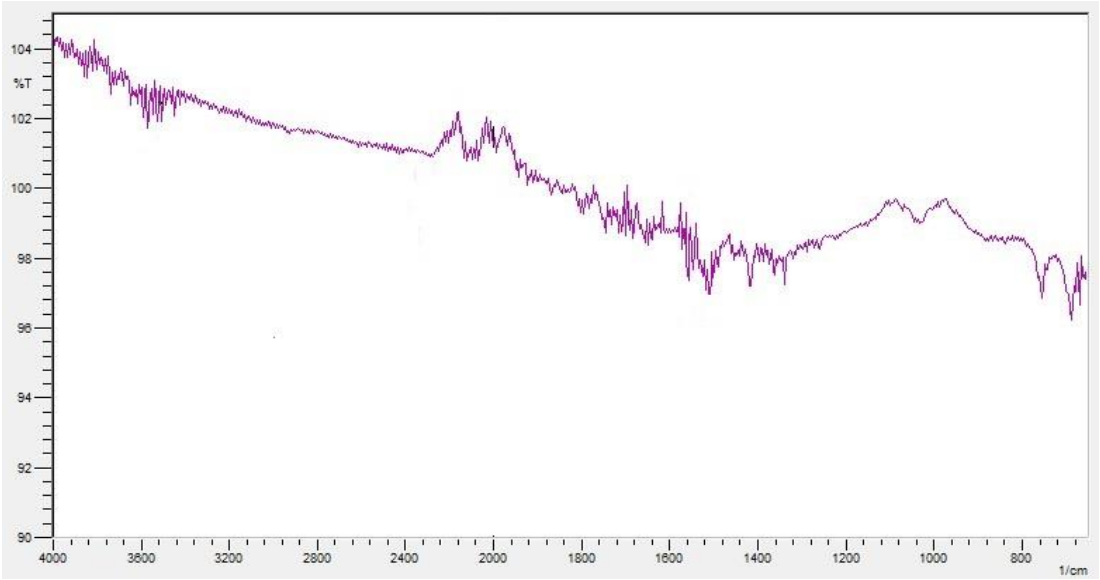

Figure 3.23. The IR spectrum of Carbon Nanosheet sample at 500 °C (KBr)

In the FT/IR spectrum of carbon nanosheet sample at 500°C **(Fig. 3.23)** shows that there are no any stretching or bending vibrations in the functional group region and fingerprint region. It indicates that the structure of the betaine was damaged at this temperature. As a result, the formation of CNSs has not actualized.

Fig. 3.24 has provided some information about the surface morphology of carbon nanosheet sample at 500 °C. Ideal carbon nanosheet formation is carried out with base, bulk, surface layers and sharp edges. There are not found any data related to these layers in the SEM micrographs. They demonstrate clearly disruption of carbon nanosheets on the surface of the product. Also, we have seen some interesting situations on the surface morphology of the product. For instance, we obtained the formation of nanograss like structures as a result of these disruptions. They are so close to each other along the entire plane and a smooth. Consequently, it indicates that they are organized in a highly ordered on the surface of the product.

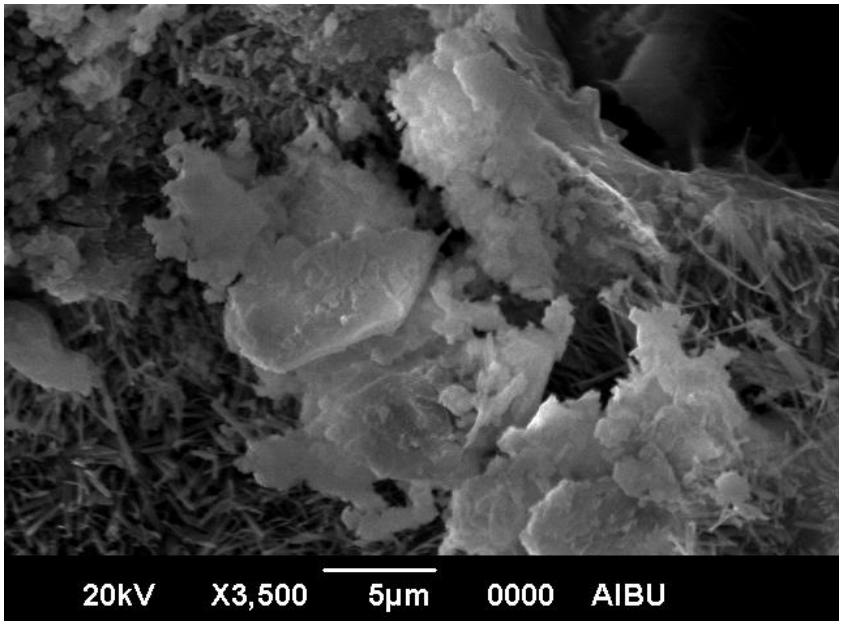

Figure 3.24. The SEM Micrographs of Carbon Nanosheet sample at 500 °C

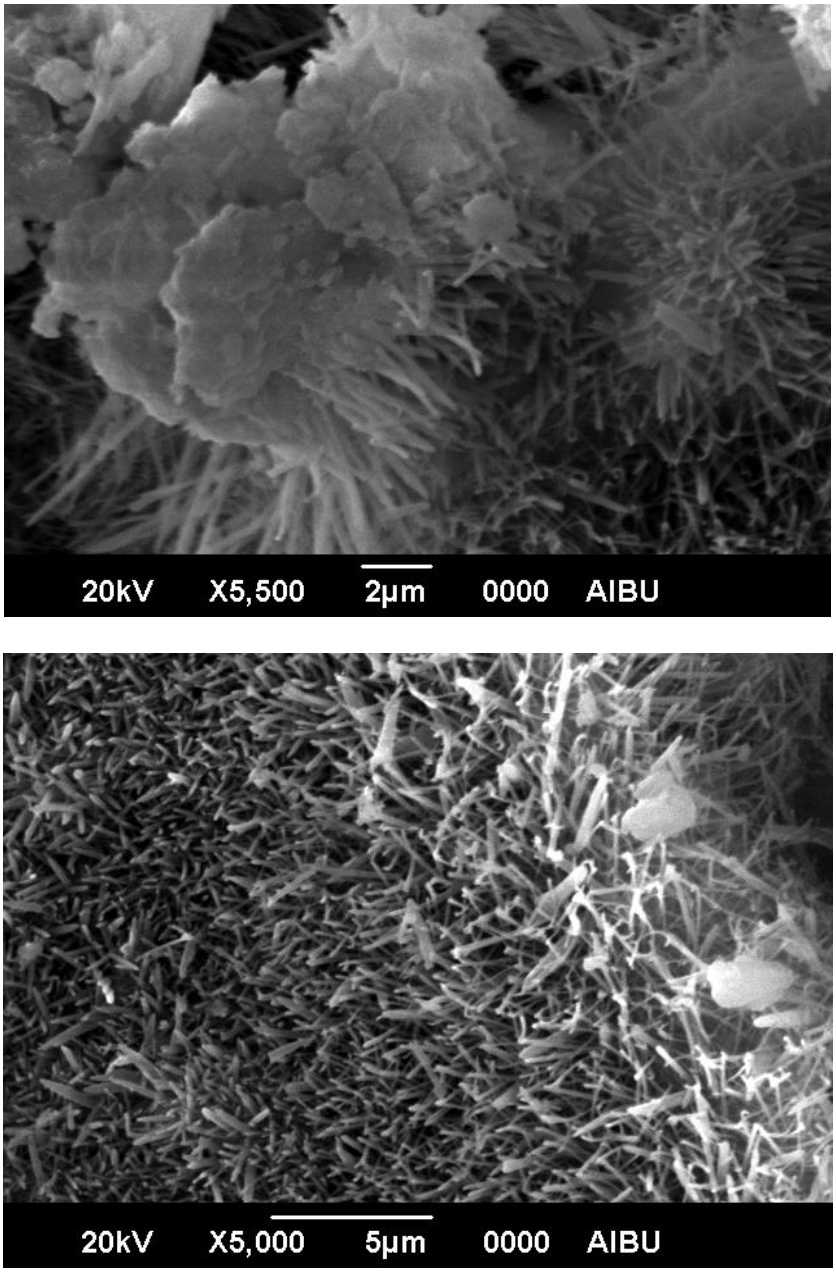

Figure 3.24. The SEM Micrographs of Carbon Nanosheet sample at 500 °C (Continued)

When we consider the combination of SEM micrographs and FT/IR spectrum results, we can say that there is no any carbon nanosheet structure. It deteriorated fully at this temperature. This idea has been supported with TG/DTA analysis.

The thermal gravimetric (TG/DTA) analysis of carbon nanosheet sample at 500°C was shown at below in **Figure 3.25**. This analysis was carried out in the temperature range 20-500°C purging with N_2 gas, a heating rate of 10°C/min. The first mass decomposition of the molecule takes place with a net loss of 5.1% between 20-100°C. It could be arrogated to the decomposition CO group and some CN group. The following mass loss occurs between 100-350°C with a net loss of 3.0% with respect to the decomposition of CH group on the aromatic rings. To sum up, the 9.7% mass loss could be attributed to the separation of phenyl hydrazine structure totally.

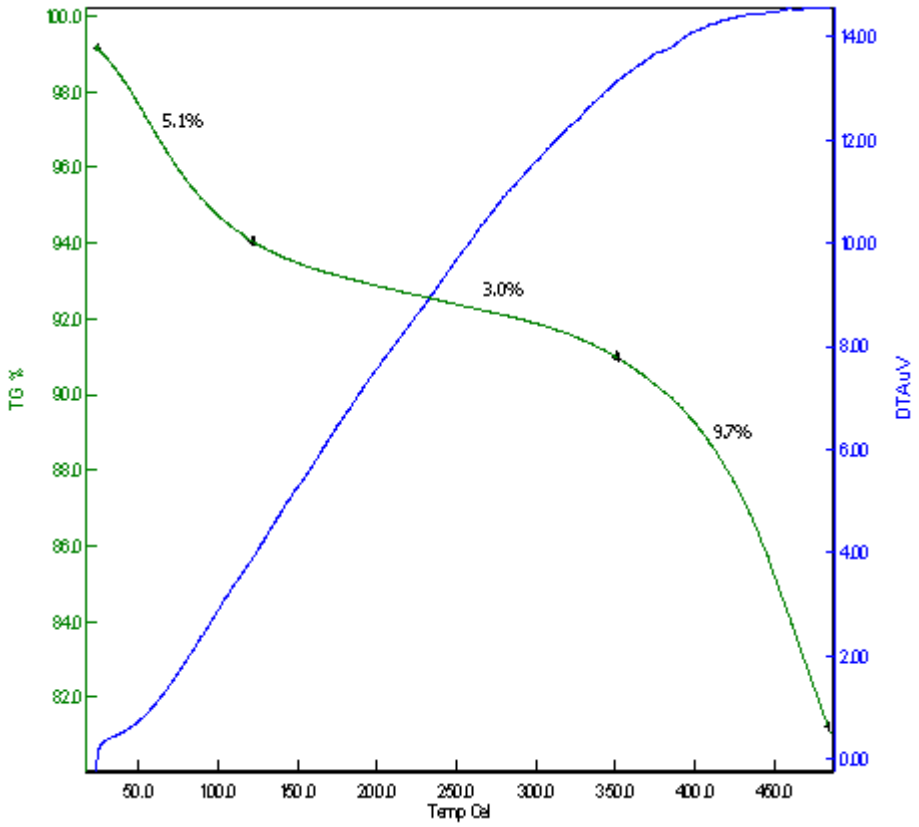

Figure 3.25. The TGA/DTA curve of Carbon Nanosheet sample at 20-500 °C

3. 2. 6. The Studies of Synthesis of Carbon Nanosheets at 350°C in N_2 Gas Atmosphere Pyrolysis

In this experiment, 2-phenylphthazin-2-ium-4-olate (betaine) was heated at 350°C with the pyrolysis in nitrogen gas atmosphere for 2h, 10min. The heating rate was 5 °C/min to get black-brown powder. While the reaction was taking place, we wrote down all the points and observations about the reaction. Before the pyrolysis, we passed 0.1 bar pressurized high purity nitrogen gas for approximately 4 minutes from the reaction medium. There was not any color change in the substance until the temperature attained at 190°C. At this temperature, the color change began from yellow to brown without melting. Betaine had brown color entirely at 201°C and started to melt at 203°C. When the temperature reached from 203°C to 300°C, the color of product was darker than at the beginning of it. There was no change such as the color and the phase of matter between 300°C and 350°C. After that, we observed small amount of degraded material (yellow - cottony) on the small part of the surface of black-brown at 350°C. To summarize, we obtained a black-brown powder as a result of pyrolysis and the chemical analysis of the product was made using FT/IR Spectroscopy, X-Ray Diffractometer and Scanning Electron Microscopy (SEM).

In the FT/IR spectrum of carbon nanosheet sample at 350 °C **(Fig. 3.26)** in N_2 gas atmosphere, the peak at 1643 cm^{-1} can be attributed for an aromatic stretching C=C band and it can be shown the skeletal vibration of product. Because, there is not any important peak(s) in the functional group region of FT/IR spectrum.

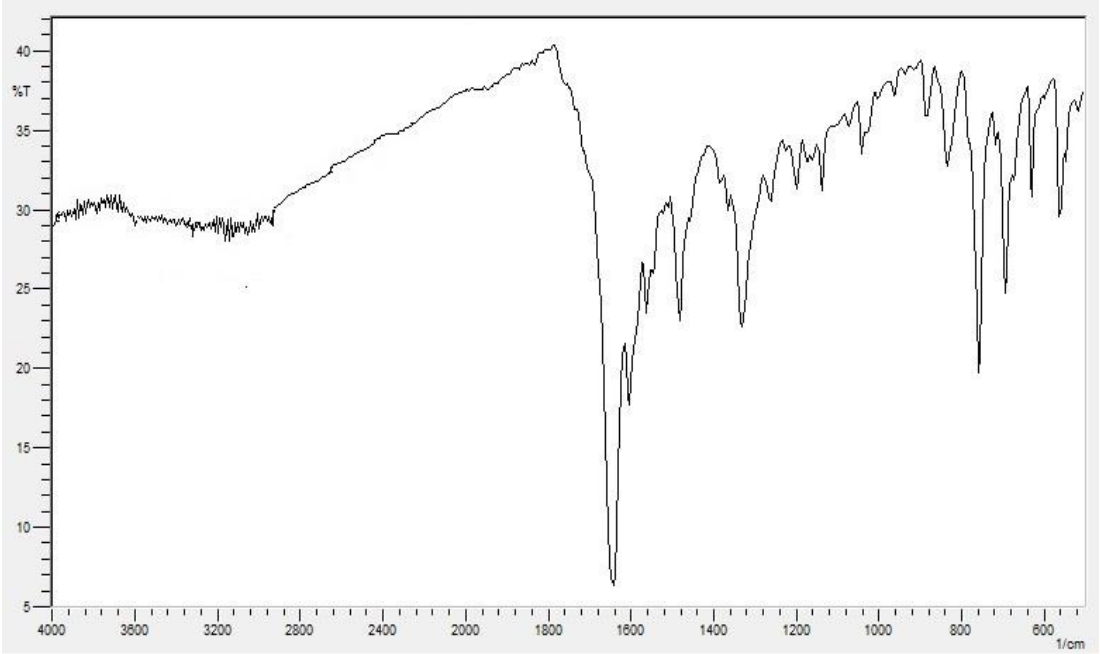

Figure 3.26. The IR spectrum of Carbon Nanosheet sample at 350 °C in N_2 gas atmosphere (KBr)

Fig. 3.27 demonstrates the XRD pattern of carbon nanosheet sample at 350 °C in the pyrolysis of N_2 gas atmosphere. There are two main points or peaks in the XRD pattern. The first peak has been found at a diffraction angle (2θ) of 21.16° for the plane (002) and the corresponding interlayer d-spacing is calculated to be a 4.1952 nm. It shows a very broad and strong intensity property and it means that the degree of crystallization is low because of some defects in the carbon nanosheet line. Furthermore, it explains the existence of regions of expanded stacking in the existing at the edge areas in settlement with the SEM results. The second peak is a rather weak and very broad peak at 2θ of 42.58° and the corresponding d-spacing between planes is calculated to be a 2.1215 nm. When we compare the crystal structure of the product against that of bulk graphite, we can say that it has a lower the degree of long-range order. It indicates that the graphitization of the structure is not complete.

In addition to these peaks, there is another very broad peak at 2θ = 9.44°, corresponding to a d-spacing of 9.3610 nm. It may occur on account of diffraction by the presence of the small amount of inter-few-layered graphene such as the typical diffraction peak of graphene oxide.

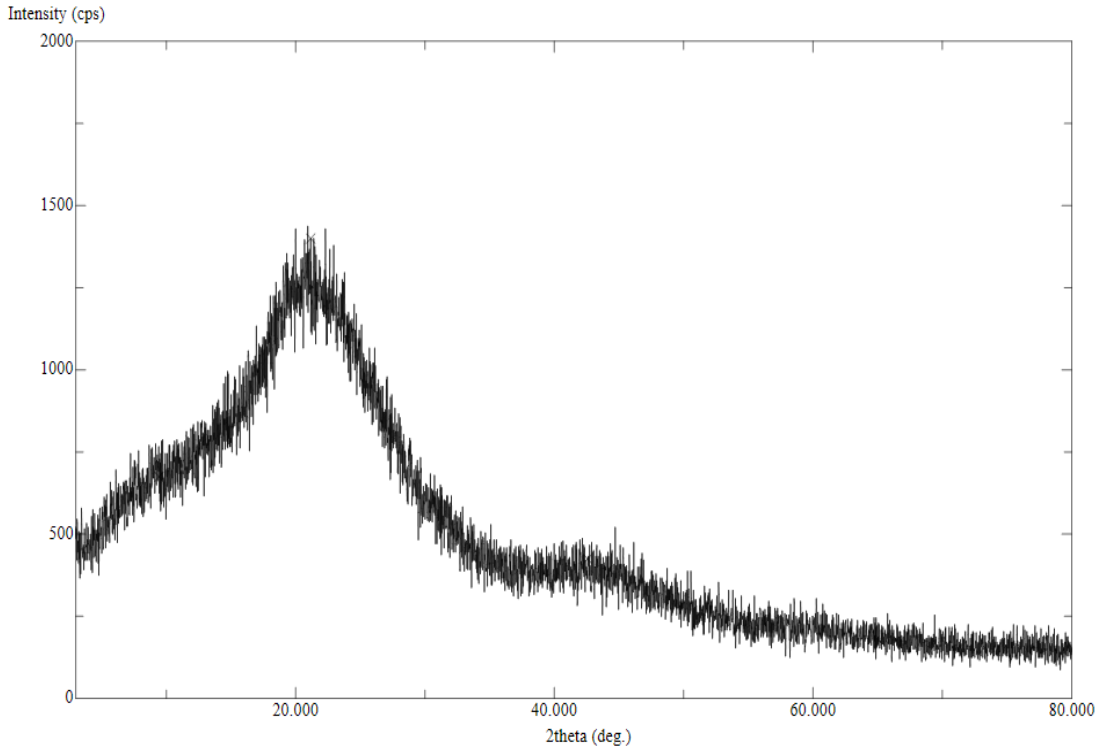

Figure 3.27. The XRD pattern of Carbon Nanosheet sample at 350 °C in N_2 gas atmosphere

Additionally, **Fig. 3.28** shows the comparison of the degraded material + carbon nanosheet sample mixture and simple degraded material in the XRD pattern. Both of them have showed the sharp peaks at the same diffraction angles (2θ). However, some peaks have the elliptical tops in the XRD pattern of the mixture of degraded material and carbon nanosheet sample at 350°C in N_2 gas atmosphere because of special broad peaks of carbon nanosheets.

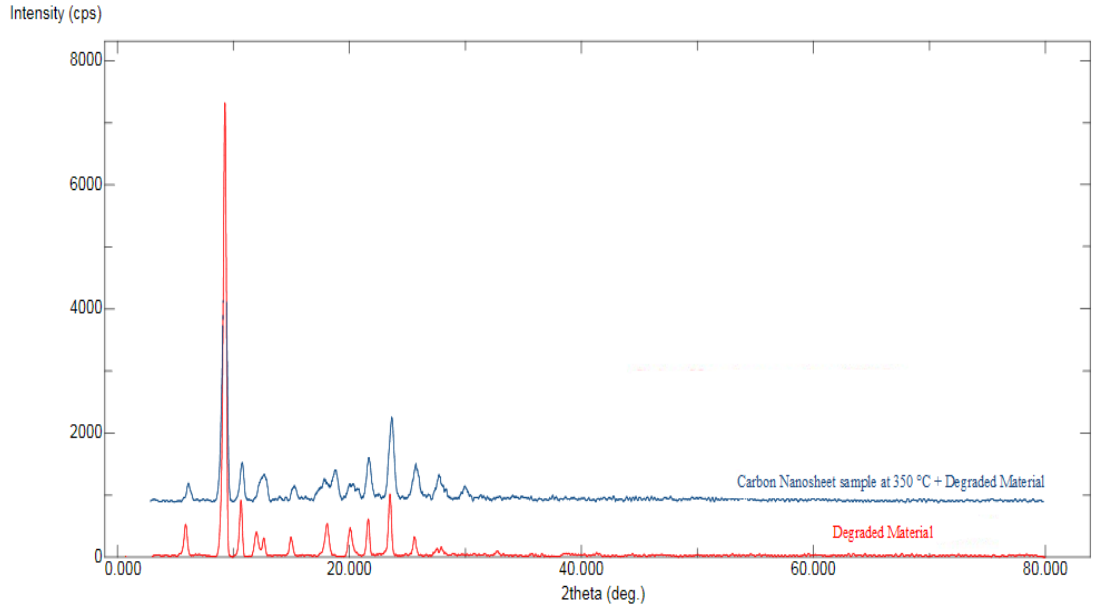

Figure 3.28. The XRD patterns of (a) the mixture of degraded material and carbon nanosheet sample at 350 °C in N_2 gas atmosphere (b) the degraded material.

Fig. 3.29 has given some information about the surface morphology of carbon nanosheet sample at 350 °C in the pyrolysis of N_2 gas atmosphere. It is clear to the SEM micrographs that there are a large number of vertical surface layers, which are called carbon nanosheets, on the groundwork of the product. It has an opaque structure because of irregular dense nanosheets morphology. In other words, the carbon nanosheets are not aligned in a highly ordered and there is no smooth nanosheet formation along the entire plane. In addition, they are overlapped with the each other. So, some defects have occurred on the surface morphology of the product. This information has supported with the XRD pattern at diffraction angles of 21.16° and 42.58°. Also, as a result of the examination of the SEM micrographs, there has not been seen other types carbon nanostructures such as carbon spheres, carbon nanorods carbon nanograss.

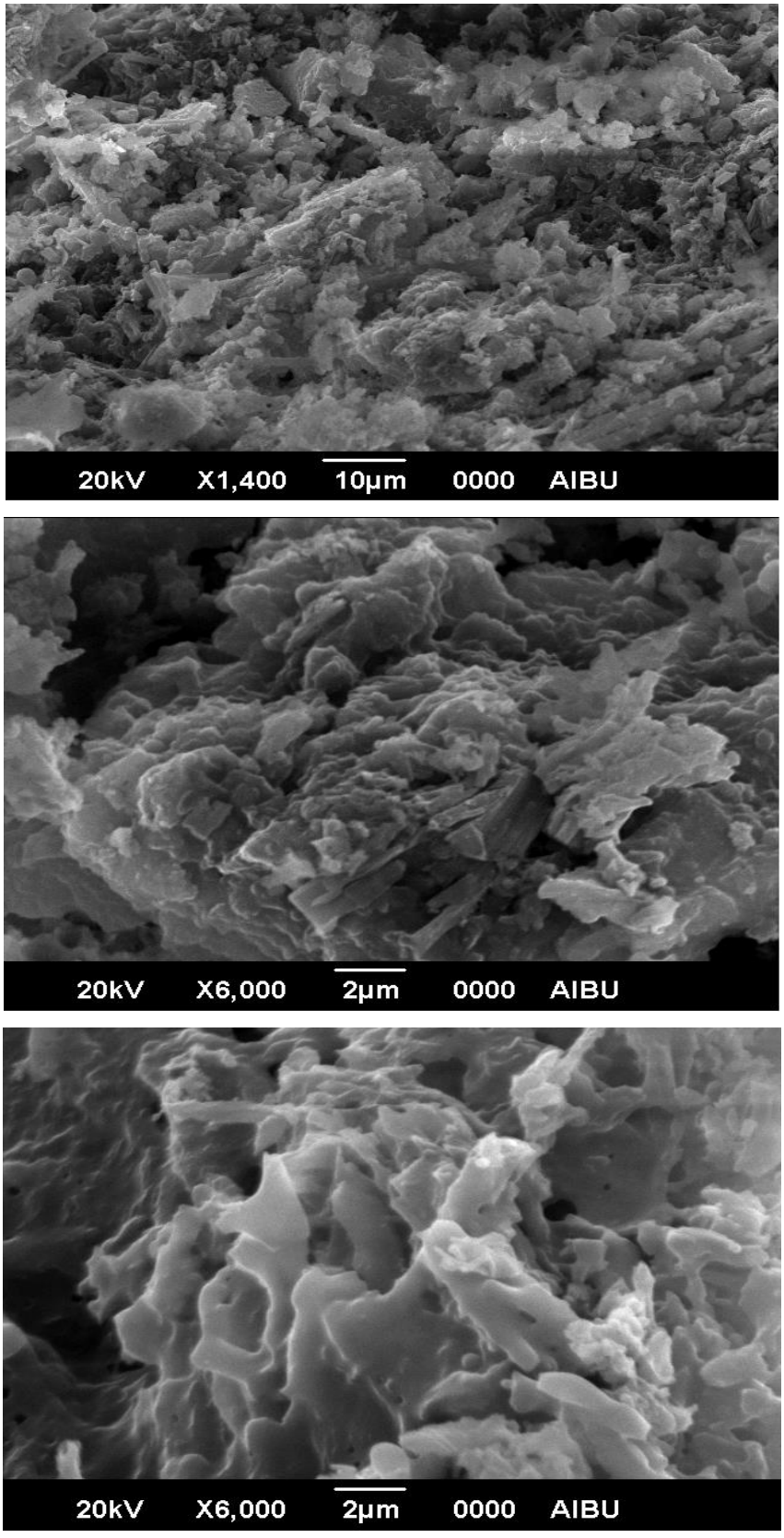

Figure 3.29. The SEM Micrographs of Carbon Nanosheet sample at 350 °C in N_2 gas atmosphere

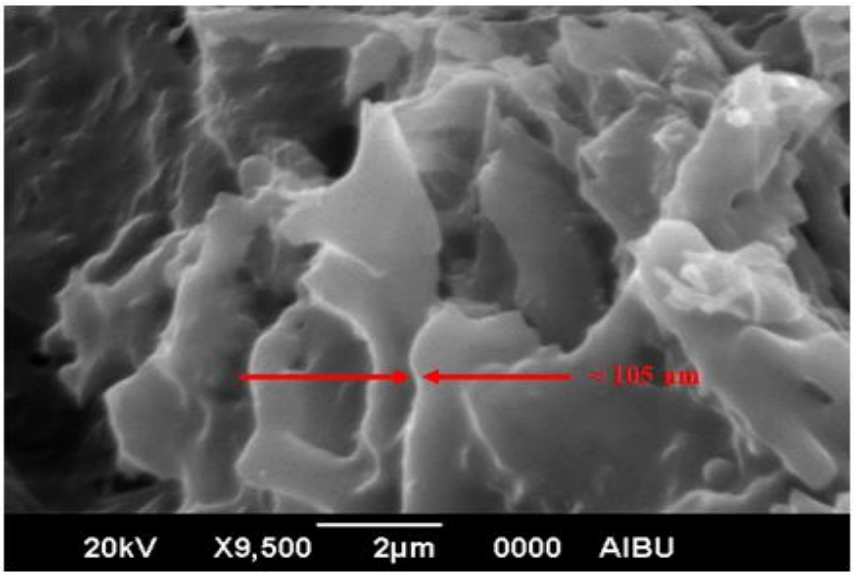

Figure 3.29. The SEM Micrographs of Carbon Nanosheet sample at 350 °C in N_2 gas atmosphere (Continued)

The last SEM micrograph in **Fig. 3.29** shows that the thickness of carbon is approximately 105 nm. In addition, when we examine these nanosheets individually, we cannot get the information about the height of layers or sheets in these SEM micrographs because of the irregular formation of carbon nanosheets. As a result, the SEM micrographs display that the formation of CNSs has been achieved on the graphene layers with some defects.

4. CONCLUSIONS

In this research, we can infer the following main points:

To begin with, we tried to do the synthesis of 2-phenylphthazin-2-ium-4-olate, which can be called azomethine type betaine, by starting with phthalic anhydride and phenylhydrazine When we compared the results of our azomethine imine with the characteristic results in the corresponding article [4], it was clearly stated that both of them showed the same characteristic properties.

Afterthat, we carried out some investigations about the synthesis of carbon nanosheets form the betaine. Carbon nanosheet structures possess a temperature-dependent and atmosphere-dependent such as air pyrolysis and the pyrolysis of inert (N_2) atmosphere. So, this study based on these criteria.

The synthesis of carbon nanosheets was studied by using this betaine with air pyrolysis at four different temperatures (300°C, 350°C, 400°C and 500°C). According to the combination of FT/IR, SEM and XRD results, Carbon nanosheets had slowly started to occur the temperature at 300°C. The results at 350°C demonstrated that there was some graphitization defects in carbon nanosheet lines.

However, the formation of CNSs was carried out successfully as it is seen from the surface morphology. The study done at 400°C especially indicated that carbon nanosheets could not resist to the high heat energy. So, these sheets seem to be broken off from their roots and they accumulated on top of each other. At last, the

results of 500°C sample have showed evidently the deterioration of chemical structure of the product.

In addition to these works, betaine was also studied at 350°C with the pyrolysis under nitrogen gas atmosphere to compare with the air pyrolysis results at the same temperature. In this work, the formation of CNSs was successfully executed again with respect to the surface morphology.

Consequently, we can clearly state that there are some differences on the pyrolytic synthesis of carbon nanosheets at 350°C between nitrogen gas atmosphere and air pyrolysis. These differences can be expressed as follows: Whereas the carbon nanosheets have been found regularly, dense and uniform on the surface of the product as the results of the air pyrolysis, The CNSs layers indicate many irregularities and are not continuous in the pyrolysis of nitrogen gas atmosphere.

It can be concluded that anneling process performed at 350°C in air atmosphere is found to be the best condition for the industrial and technological applications.

REFERENCES

1. R. K. Parashar; Reaction mechanisms in organic synthesis, A John Wiley and Sons Inc., United Kingdom, 313, (2009).

2. R. Huisgen; Angewandte Chemie International Edition, Vol. 2, No. 10, 565-632, (1963).

3. R. Huisgen; Adventure playground of mechanisms and novel reactions: in the series ‘’Profiles, Pathways and Dreams’’, American Chemical Society, Washington DC, (1994).

4. A. R. Katritzky, N. Dennis, M. Ramaiah; Journal of Chemical Society, Perkin Transactions 1, 2281, (1976).

5. A. P. Alivisatos; Semiconductor clusters, nanocrystals and quantum dots, American Association for the Advancement of Science, New Series, Vol. 271, No. 5251, 933-937, (1996).

6. F. Gu, L. Zhang, B. A. Teply, N. Mann, A. Wang, A. F. Radovic-Moreno, R. Langer, O. C. Farakhzad; Precise engineering of targeted nanoparticles by using self-assembled biointegrated black polymers, Proceedings of the National Academy of Sciences, United States of America, 2586-2591, (2008).

7. W. S. Jonathan, R. T. David, J. W. Karl; Core concepts in supramolecular chemistry, A John Wiley and Sons Inc., 229, (2007).

8. E. Roston; The carbon age: how life’s core element has become civilization’s greatest threat, Walker & Company, United States of America, (2009).

9. P. Harris; On charcoal, Interdisciplinary Science Reviews, Vol. 24, No. 4, 301-306, (1999).

10. M. Faraday; The chemical history of a candle, Collier Books, New York, (1962).

11. Y. Gogotsi; Carbon nanomaterials, CRC Press, (2006).

12. H. O. Pierson; Handbook of carbon, graphite, diamonds and fullerenes: processing, properties and applications, William Andrew, (1995).

13. R. P. Feynman; Engineering and Science, 23, (1960).

14. R. C. Haddon, R. E. Palmer, H. W. Kroto, P. A. Sermon; The fullerenes: powerful carbon-based electron acceptors, Philosophical Transactions: Physical Sciences and Engineering, Vol. 343, 53-62, (1993).

15. R. B. Heimann; Carbon allotropes: a suggested classification scheme based on valence orbital hybridization, Carbon, Vol. 35, No. 10, 1654-1658, (1997).

16. G. Messina, S. Santangelo; Carbon: the future material for advanced technology applications, Springer, (2006).

17. L. Itzhaki, E. Altus, H. Basch, S. Hoz; Harder than diamond: determining the cross-sectional area and young's modulus of molecular rods, Angewandte Chemie International Edition, Vol. 44, Issue 45, 7432-7435, (2005).

18. B. T. Kelly; Physics of graphite, Springer, (1981).

19. IUPAC Compendium of Chemical Terminology, 2nd Edition, (1997).

20. D. Chung; Review: Graphite, Journal of Materials Science, Vol. 37, No. 8, 1475-1489, (2002).

21. C. Cousins; Formal elasticity of four carbon allotropes: I. the inner elastic constants, internal strain tensors, and zone-centre optic mode frequencies and their pressure dependences, Journal of Physics Condensed Matter, Vol. 14, 5091-5113, (2002).

22. L. Samuelson, I. P. Batra, C. Roetti; A comparison of electronic properties of various modifications of graphite, Solid State Communications, Vol. 33, 817-820, (1980).

23. S. Flandrois and B. Simon; Carbon materials for lithium-ion rechargeable batteries, Carbon, Vol. 37, Issue 2, 165-180, (1999).

24. S. Y. Boey, D. J. Bacon; Deformation of polycrystalline graphite under pressure, Carbon, Vol. 24, Issue 5, 557-564, (1986).

25. L. Wei, P. K. Kuo, R. L. Thomas, T. Anthony, W. Banholzer; Thermal conductivity of isotopically modified single crystal diamond, Physical Review Letters, Vol. 70, No. 24, 3764–3767, (1993).

26. M. Werner and R. Locher; Growth and application of undoped and doped diamond films, Reports on Progress in Physics, Vol. 61, 1665-1710, (1998).

27. B. T. Kelly; Physics of graphite, Springer, (1981).

28. P. John, N. Polwart, C. E. Troupe, and J. I. B. Wilson; The oxidation of (100) textured diamond, Diamond and Related Materials, Vol. 11, Issue 3, 861-866, (2002).

29. C. Cousins; Elasticity of carbon allotropes: I. Optimization and subsequent modification of an anhormonic keating model for cubic diamond, Physical Review B – Condensed Matter and Materials Physics, Vol. 67, 241013-241071, (2003).

30. L. Itzhaki, E. Altus, H. Basch, S. Hoz; Harder than diamond: determining the cross-sectional area and young's modulus of molecular rods, Angewandte Chemie International Edition, Vol. 44, Issue 45, 7432-7435, (2005).

31. S. Elliot; Physics of Amorphous Materials, 2nd Edition, Longman, (1990).

32. M. Terrones, H. Terrones; The carbon nanocosmos: novel materials for the twenty-first century, Philosophical Transactions of the Royal Society A, Vol. 361**,** No. 1813, 2789-2806, (2003).

33. N. A. Marks, D. R. McKenzie, B. A. Pailthorpe, M. Bernasconi, and M. Parrinello; Microscopic Structure of tetrahedral amorphous carbon, Physical Review Letters, Vol. 76, Issue 5, 768, (1996).

34. J. Robertson; Diamond-like amorphous carbon, Materials Science and Engineering: R: Reports, Vol. 37, Issues 4-6, 129-281, (2002).

35. P. J. F. Harris; Fullerene-related structure of commercial glassy carbons, Philosophical Magazine, Vol. 84, No. 29, 3159–3167, (2004).

36. A. Yoshida, Y. Kaburagi, and Y. Hishiyama; Microtexture and magneto-resistance of glass-like carbons, Carbon, Vol. 29, Issue 8, 1107-1111, (1991).

37. Recommended terminology for the description of carbon as a solid (IUPAC Recommendations), 67, 490, (1995).

38. Activated Charcoal Specialists; Properties of Activated Carbon, CPL Caron Link, accessed 2008-05-02.

39. Kirk-Othmer; Encyclopedia of chemical technology, A John Wiley and Sons Inc., (2003).

40. R. F. Reinoso, M. J. M. Martinez, M. M. Sabio; A comparison of the porous texture of two CO_2 activated botanic materials, Carbon, Vol. 23, 19-24. (1985).

41. F. P. Bundy; The P, T phase and reaction diagram for elemental carbon, Journal of Geophysical Research, Vol. 85, Issue B12, 6930-6936, (1979).

42. F. P. Bundy, W. A. Bassett, M. S. Weathers, R. J. Hemley, H. U. Mao, and A. F. Goncharov; The pressure-temperature phase and transformation diagram for carbon, updated through 1994, Carbon, Vol. 34, Issue 2, 141-153, (1996).

43. F. Bundy; Solid state physics under pressure: recent advances with anvil devices, edited by S. Minomura, Kluwer Academic Publishers, (1985).

44. I. Fonts, A. Juan, G. Gea, M. B. Murilla, J. L. Sa'nchez; Sewage sludge pyrolysis in fluidized product bed: influence of operational conditions on the product distribution, Industrial & Engineering Chemistry Research, Vol. 47, 5376-5385, (2008).

45. D. Vamluka; Bio-oil, solid and gaseous biofuels from biomass pyrolysis processes – an overview, International Journal of Energy Research, Vol. 35, 835-862, (2011).

46. InnoFireWood's Website; Burning of Wood, accessed on 2010-02-06.

47. H. W. Kroto, J. R. Heath, S. C. O'Brien, R. F. Curl, and R. E. Smalley; C_{60}: Buckminsterfullerene, Nature, Vol. 318, No. 6042, 162-163, (1985).

48. H. W. Kroto and K. McKay; The formation of quasi-icosahedral spiral shell carbon particles, Nature, Vol. 331, 328-331, (1988).

49. D. Ugarte; Curling and closure of graphitic networks under electron-beam irradiation, Nature, Vol. 359, No. 6397, 707-709, (1992).

50. D. S. Iijima; Helical microtubules of graphitic carbon, Nature, Vol. 354, 56–58, (1991).

51. C. M. Hussain, S. Mitra; Micropreconcentration units based on carbon nanotubes (CNT), Analytical and Bioanalytical Chemistry, Vol. 399, 75–89, (2011).

52. H. Dai; Carbon nanotubes: opportunities and challenges, Surface Science, Vol. 500, No. 1-3, 218-241, (2002).

53. X. Zhao, Y. Liu, S. Inoue, T. Suzuki, R. O. Jones, and Y. Ando; Smallest carbon nanotube is 3Å in diameter, Physical Review Letters, Vol. 92, No. 12, 125502, (2004).

54. Q. Wen, R. Zhang, W. Qian, Y. Wang, P. Tan, J. Nie, and F. Wei; Growing 20 cm long DWNTs/TWNTs at a rapid growth rate, chemistry of materials, Vol. 22, 1294-1296, (2010).

55. L. Brand, M. Gierlings, A. Hoffknecht, V. Wagner, A. Zweck; Kohlenstoff-Nanoröhren–Technologieanalyse, Zukünftige Technologien Consulting der VDI Technologiezentrum GmbH, Düsseldorf, (2009).

56. P. Morgan; Carbon fibers and their composites, CRC Press, (2005).

57. A. K. Geim and K.S. Novoselov; The rise of graphene, Nature Materials, Vol. 6, No. 3, 183-191, (2007).

58. P. R. Wallace; The band theory of graphite, Physical Review, Vol. 71, No. 9, 622, (1947).

59. H. P. Boehm, A. Clauss, G. O. Fischer, and U. Hofmann; Das adsorptions-verhalten sehr dunner kohlenstoff-folien, Zeitschrift Fur Anorganische Und Allgemeine Chemie, Vol. 316, Issue 3-4, 119-127, (1962).

60. A. K. Geim and P. Kim; Carbon Wonderland, Scientific American, Vol. 298, No. 4, 90-97, (2008).

61. K. S. Novoselov, A. K. Geim, S. V. Morozov, D. Jiang, Y. Zhang, S. V. Dubonos, I. V. Grigorieva, and A. A. Firsov; Electric field effect in atomically thin carbon films, Science, Vol. 306, No. 5696, 666-669, (2004).

62. D. A. Dikin, S. Stankovich, E. J. Zimney, R. D. Piner, G. H. B. Dommett, G. Evmenenko, S. T. Nguyen, and R. S. Ruoff; Preparation and characterization of graphene oxide paper, Nature, Vol. 448, No. 7152, 457-460, (2007).

63. Y. Hernandez, V. Nicolosi, M. Lotya, F. M. Blighe, Z. Sun, S. De, T. McGovernI, B. Holland, M. Byrne, Y. K. Gun'Ko, J. J. Boland, P. Niraj, G. Duesberg, S. Krishnamurthy, R. Goodhue, J. Hutchison, V. Scardaci, A. C. Ferrari, and J. N. Coleman; High-yield production of graphene by liquid-phase exfoliation of graphite, Nat Nano, Vol. 3, 563-568, (2008).

64. M. Lotya, Y. Hernandez, P. J. King, R. J. Smith, V. Nicolosi, L. S. Karlsson, F. M. Blighe, S. De, Z. Wang, I. T. McGovern, G. S. Duesberg, and J. N. Coleman; Liquid phase production of graphene by exfoliation of graphite in surfactant/water solutions, Journal of the American Chemical Society, Vol. 131, 3611-3620, (2009).

65. A. Reina, X. Jia, J. Ho, D. Nezich, H. Son, V. Bulovic, M. S. Dresselhaus, and J. Kong; Large area, few-layer graphene films on arbitrary substrates by chemical vapour deposition, Nano Letters, Vol. 9, No. 1, 30-35, (2009).

66. C. Di, D. Wei, G. Yu, Y. Liu, Y. Guo, and D. Zhu; Patterned graphene as source/drain electrodes for bottom-contact organic field-effect transistors, Advanced Materials, Vol. 20, No. 17, 3289-3293, (2008).

67. C. Berger, Z. Song, X. Li, X. Wu, N. Brown, C. Naud, D. Mayou, T. Li, J. Hass, A. N. Marchenkov, E. H. Conrad, P. N. First, and W. A. de Heer; Electronic confinement and coherence in patterned epitaxial graphene, Science, Vol. 312, 1191-1196, (2006).

68. H. Huang, W. Chen, S. Chen, and A. T. S. Wee; Bottom-up growth of epitaxial graphene on 6H-SiC(0001), ACS Nano, Vol. 2, No. 9, 2513-2518, (2008).

69. L. Jiao, X. Wang, G. Diankov, H. Wang, and H. Dai; Facile synthesis of high quality graphene nanoribbons, Nat Nano, Vol. 5, No. 5, 321-325, (2010).

70. C. Lee, X. Wei, J. W. Kysar, and J. Hone; Measurement of the elastic properties and intrinsic strength of monolayer graphene, Science, Vol. 321, 385- 388, (2008).

71. A. B. Kuzmenko, E. van Heumen, F. Carbone, and D. van der Marel; Universal optical conductance of graphite, Physical Review Letters, Vol. 100, No. 11, 117401, (2008).

72. A. A. Balandin, S. Ghosh, W. Bao, I. Calizo, D. Teweldebrhan, F. Miao, and C.N. Lau; Superior thermal conductivity of single-layer graphene, Nano Letters, Vol. 8, No. 3, 902-907, (2008).

73. V. Georgakilas; Chemical functionalization of ultrathin carbon nanosheets, Fullerenes, Nanotubes and Carbon Nanostructures, Vol. 18, No. 1, 87-95 (2010).

74. J. L. Qi, X. Wang, H. W. Tian, Y. S. Peng, C. Liu, W. T. Zheng; Syntheses of carbon nanomaterials by radio frequency plasma enhanced chemical vapor deposition, Journal of Alloys and Compounds, Vol.486, Issues 1-2, 265–272, (2009).

75. Yu-Ting Huang, Yi-Wei Lin, Chih-Ming Chen; Characterization of carbon nanomaterials synthesized from thermal decomposition of paper phenolic board, Materials Chemistry and Physics, Vol. 127, Issues 1-2, 397–404, (2011).

76. A. B. Bourlinos, T. A. Steriotis, R. Zbori, V. Georgakilas, A. Stubos; Direct synthesis of carbon nanosheets by the solid-state pyrolysis of betaine, Journal of Material Science, Vol. 44, 1407–1411, (2009).

77. M. Viertorinne, J. Valkonen, I Pitkanen, M. Mathlouthi, J. Nurmi; Journal of Molecular Structure, Vol.477, 23-29, (1999).

78. I. R. Booth, B. Pourkomailian, D. McLaggan, S. P. Koo; Mechanisms controlling compatible solute accumulation: a consideration of the genetics and physiology of bacterial osmoregulation, in: P. Fito, A. Mulet (Eds.), Water in Foods, Elsevier, London, 381–397, (1994).

79. S. Cayley, B. A. Lewis, M. T. Record; Origins of the osmoprotective properties of betaine and proline in escherichia coli K-12, Journal of Bacteriology, Vol. 174, No. 5, 1586–1595, (1992).

80. J. Suuronen, I. Pitkanen, H. Halttunen, R. Moilanen; Formation of the main gas compounds during thermal analysis and pyrolysis: betaine and betaine monohydrate, Journal of Thermal Analysis and Calorimetry, Vol. 69, 359-369, (2002).

81. R. Quinlan, A. Javier, E. E. Foos, L. Buckley, M. Zhu , K. Hou, E. Widenkvist, M. Drees, U. Jansson, B. Holloway; Transfer of carbon nanosheet films to nongrowth, zero thermal budget substrates, Journal of Vacuum Science & Technology B, Vol. 29, 030602, (2011).

82. S. Lepri, R. Livi, and A. Politi; Thermal conduction in classical low-dimensional lattices, Physics Reports, Vol. 377, No. 1, 1–80, (2003).

83. G. Basile, C. Bernardin, and S. Olla; Momentum conversion model with anomalous thermal conductivity in low dimensional system, Physical Review Letters, Vol. 96, 204303–204304, (2006).

84. C. W. Chang, D. Okawa, H. Garcia, A. Majumdar, and A. Zettl; Breakdown of fourier's law in nanotube thermal conductors, Physical Review Letters, Vol. 101, 075903–075904, (2008).

85. O. Narayan, and S. Ramaswamy; Anomalous heat conduction in one dimensional momentum-conserving systems, Physical Review Letters, Vol. 89, 200601–200604, (2002).

86. A. V. Rode, E. G. Gamaly, A. G. Christy, J. FitzGerald, S. T. Hyde, R. G. Elliman, B. Luther-Davies, A. I. Veinger, J. Androulakis and J. Giapintzakis; Journal of Magnetism and Magnetic Materials, Vol. 290, 298, (2005).

87. A. A. Ovchinnikov and V. N. Spector; Organic Ferromagnets: New Results, Synthetic Metals B, Vol. 27, 615, (1988).

88. J. Wang, M. Zhu, R. A. Outlaw, X. Zhao, D. M. Manos and B. C. Holloway; Synthesis of carbon nanosheets by inductively coupled radio-frequency plasma enhanced chemical vapor deposition, Carbon, Vol. 42, No. 14, 2867, (2004).

89. B. P. C. Rao, R. Maheswaran, S. Ramaswamy, O. Mahapatra, C. Gopalakrishnan and D. J. Thiruvadigal; Fullerenes Nanotubes and Carbon Nanostructures, Full. Nano. Carb. Nano, Vol.17, 625-635, (2009).

90. M. Baikousia, K. Dimosa, A. B. Bourlinos, R. Zboril, I. Papadas, Y. Deligiannakis, M. A. Karakassides; Surface decoration of carbon nanosheets with amino-functionalized organosilica nanoparticles, Applied Surface Science, Vol. 258, 3703–3709, (2012).

91. A. Schmidt; Advances in Heterocyclic Chemistry, Vol. 85, 67, (2003).

92. E. Fischer, E. Besthorn; Ueber die Hydrazinverbindungen, Liebigs Annalen der Chemie, Vol. 212, 316, (1882).

93. W. D. Ollis, S. P. Stanforth, C. A. Ramsden; Heterocyclic mesomeric betaines, Tetrahedron, Vol. 41, 2239-2329, (1985).

94. N. Sakai, M. Funabashi, T. Hamada, S. Minakata, I. Ryu, and M. Komatsu; Synthesis of mesomeric betaines containing a pyrrolo- or imidazotriaziniumolate system and their cycloaddition with acetylenic dipolarophiles leading to triazocinone derivatives, Tetrahedron, Vol. 55, Issue 48, 13703-13724, (1999).

95. B. L. French, J. J. Wang, M. Y. Zhu, and B. C. Holloway; Structural characterization of carbon nanosheets via x-ray scattering, Journal of Applied Physics, Vol. 97, Issue 12, 114317, (2005).

96. J. Sakamoto, J. Heijst, O. Lukin, A. D. Schlueter; Two-Dimensional Polymers: Exploring Uncharted Territories of Polymer Science, Angewandte Chemie International Edition, Vol.48, No. 6, 1030-1069, (2009).

97. Q. Kuang, S. Xie, Z. Jiang, X. Zhang, Z. Xie, R. Huang, et al; Low temperature solvothermal synthesis of crumpled carbon nanosheets, Carbon, Vol. 42, 1737–1741, (2004).

98. L. Yu, Y. Lv, Y. Zhao, Z. Chen; Scalable preparation of carbon nanotubes by thermal decomposition of phenol with carbon utilizing rate, Materials Letters, Vol.64, 2145–2147, (2010).

99. J. C. Russ; Fundamentals of Energy Dispersive X-Ray Analysis, Butterworths, London, (1984).

100. Y. Bruice; Organic Chemistry fourth edition, Academic Internet Publishers, Upper Saddle River, New Jersey, 526-527, (2007).

101. C. Nunes**,** J. Han, D. C. Monkhouse, R. Suryanarayanan; Preformulation Studies to Meet the Challenges in the Manufacture of Betaine Solid Dosage Form, Journal of Pharmaceutical Sciences, Vol. 93, Issue 1, 38-47, (2004).